ABSTRACT

CARRELL, SOPHIA NOEL. Dorsoventral Patterning of the *Drosophila melanogaster* Embryo by the Dorsal/NF-κB Signaling Pathway. (Under the direction of Dr. Gregory T. Reeves).

During the first few hours of *Drosophila* embryogenesis, two major signaling pathways dictate dorsal-ventral (DV) axis patterning. On the ventral side of the embryo, the transcription factor Dorsal, homologous to NF-κB, is present in a nuclear gradient, with highest concentration at the ventral midline and a steady decay to about 40% of the embryo's circumference. The Dorsal gradient is initialized via Toll signaling, which phosphorylates the inhibitor protein Cactus (homologous to IκB), marking it for degradation. Free of Cactus, Dorsal enters the nuclei and activates expression of target genes in a concentration-dependent manner. On the dorsal side of the embryo, BMP signaling through the Dorsal target gene Dpp dictates gene placement. While the Dorsal signaling pathway has been well-studied in developing *Drosophila* embryos, little is known about how the Dorsal gradient (1) maintains robustness in the face of perturbations, (2) interacts with the BMP pathway, or (3) forms globally after Toll signaling initialization.

Our studies rely on careful handling of *Drosophila* embryos; therefore, we designed a method for imaging the DV cross-section of both live and fixed embryos, which can be found in Chapter 2. Following image collection, we conducted quantitative analysis to extract data about gene borders and the Dorsal gradient itself, which was modeled as a Gaussian.

Our curiosity was initially piqued when it was discovered that embryos receiving a half genetic dose of Dorsal have gradients that are shorter, flatter, and wider than wild type. These differences point to the existence of Dorsal gradient regulation in circumstances

in which protein levels are compromised. We propose that feedback loops through the inhibitor protein Cactus (Chapter 3) or BMP signaling (Chapter 4) could be responsible for this regulation. In Chapter 3, we discuss how the *cactus* and *dorsal* dosage affects the Dorsal gradient, finding that decreasing either leads to a widened gradient. Our results from the dosage study provided a foundation for Chapter 4, in which we discuss how the BMP signaling network can alter the Dorsal gradient. When we overexpressed BMP signaling cofactors, we found that the width of the Dorsal gradient expanded significantly. Such interactions between the NF-κB and BMP signaling pathways may be necessary to ensure robust gene expression in the developing *Drosophila* embryo.

In Chapter 5, we discuss how Dorsal's robustness in the face of genetic and environmental perturbation may also be due to its method of gradient formation: shuttling via its inhibitor Cactus. We had observed that Dorsal accumulates on the ventral side of the embryo, apparently defying Fickian diffusion. We propose that, instead of free Dorsal, Dorsal/Cactus complex is the primary diffusive species in the developing embryo. Since Toll signaling acts as a sink, Dorsal/Cactus complex will diffuse towards the ventral midline, depositing free Dorsal. When we slowed diffusion of the Dorsal/Cactus complex, we found that the Dorsal gradient widened, in line with our expectations and contrary to what would be expected (gradient narrowing) in a system in which free Dorsal is the primary diffusive species.

Our analysis of DV patterning in the early *Drosophila* embryo has greatly expanded the body of knowledge available on the subject. In addition to its contribution to the

Drosophila community, this work has the potential to inform research concerning a variety of signaling pathways in a variety of organisms.

Dorsoventral Patterning of the *Drosophila melanogaster* Embryo by the Dorsal/NF-κB Signaling Pathway

by

Sophia Noel Carrell

A dissertation submitted to the Graduate Faculty of
North Carolina State University
in partial fulfillment of the
requirements for the degree of
Doctor of Philosophy

Chemical Engineering

Raleigh, North Carolina
2016

APPROVED BY:

Dr. Robert Kelly	Dr. Chase Beisel
Dr. Jason Haugh	Dr. Gregory Reeves Committee Chair

DEDICATION

To my family, friends, and mentors,

without whom none of this would have been possible

“If I have seen further, it is by standing on the shoulders of giants”

–Isaac Newton

BIOGRAPHY

Sophia (Sophie) Carrell was born in Lafayette, IN in 1989. In 1993, she moved with her parents and two younger sisters to Oklahoma City, where she attended kindergarten. In 1995, they moved one town over to Edmond, where she attended Edmond Public Schools, graduating from Santa Fe High in 2006. At that time, having had enough of Oklahoma's insane weather, Sophie traveled across the country to Michigan State University where she pursued a degree in chemical engineering. During her first two years at MSU, she worked in the lab of Dr. Pat Walton. In the summer of 2008, she did research at UMass Amherst in the lab of Dr. Neil Forbes. In 2009, she achieved her lifelong dream of living in England (albeit for five weeks as a study abroad in Oxford). After completing her bachelor's, she moved to Raleigh, where she began pursuing her PhD in chemical engineering under the direction of Dr. Greg Reeves. During that time, she achieved another lifelong dream of meeting Alex Trebek as a contestant on Jeopardy! She currently resides in Raleigh with her two cats and mysteriously charming boyfriend.

ACKNOWLEDGMENTS

I must first thank my parents for inspiring my career. They were pursuing doctorates in English when I was born, and apparently this fact rubbed off on me. At about two or three years old, I would occasionally sit quietly and still, imitating what it appeared my parents were doing all the time. When asked “Sophie, what are you doing?” I would respond “Working on my disser-*tay*-tion!” Twenty-some years later, I am proud to present this document as proof that toddler me had no idea what she was signing up for.

My sisters Maddie and Sylvia have also been instrumental in shaping who I am and I must thank them for their support and willingness to house and entertain me in Albuquerque and Stillwater when I needed an escape from grad school.

I have been extremely lucky to have found excellent mentors in Dr. Pat Walton at MSU and Dr. Greg Reeves at NC State. To Dr. Walton I owe my decision to attend graduate school (both in general and specifically at NC State). To Greg I owe my entire graduate career. Choosing his lab is easily the best (professional) decision I’ve made since starting grad school.

It’s amazing how big a difference having friendly, cooperative labmates makes, and I’m grateful to these members of my lab for making it a great work environment. Thanks to my fellow PhD students Ashley Jermusyk and Mike O’Connell for keeping me entertained and sending me pictures of kittens when I’m down. I’ve also had a veritable army of undergraduates working for me, at the head of which was Alex Thomas. Not only did he produce a lot of work towards the BMP project, but he trained and supervised his fellows, including Amy Allen, Josh Chappell, Jeramey Friedman, and Stephanie Smith. Other undergraduates include Spencer McCloud and Ross Garner. These students taught me how to teach and manage others and did a vast amount of lab work, for which I am eternally grateful. Finally, I must thank Christy Carcillo, Daniel Needs, Mick Doriani, Jing Gong, Nick Murphy, and Sarah Garavi for making the lab a really enjoyable place to work. Thanks also to Tom Jacobson, Aydin Beseli, and Hadel Al Asafen for picking up my research where it left off and for making that transition much easier on me.

Many thanks are owed to the students of Dr. Rao, Dr. Haugh, and Dr. Kelly, particularly Nimish Gera, Prasenjit Sarkar, Kyle Grant, Carlos Cruz, and Kevin Carlin, for helpful discussions, provision of lab supplies, and use of lab equipment.

A huge thank you goes out to Dr. Eva Johannes who taught me all I know about confocal microscopy and gave also mentored me as a TA for the BIT microscopy course.

For constant support on the business side of things, I thank Sandra Bailey, Diane Harper, Saundra Doby, Sheila Hayes, and Bona Jones. Without our most excellent support staff, I'd be lost.

I'm lucky to have had excellent roommates in Stephanie Lam and Ezinne Achinivu. Thank you ladies for keeping our home(s) low-stress and for gracefully handling our travails (including that mouse infestation!). I should also thank my fur babies who are kind of like

roommates except that they don’t pay rent. Rusty and Fonzie have added delight and whimsy to my life and have been a welcome distraction from the stress of grad school.

Friends are the family you choose. I have never felt those words to be more true than during these last six(…ish) years. My MSU crew: Lauren Blair, Sara Kramer, and Abby Estock- your support has meant so much to me. I love our Skype (Hangout) dates and wish we could see each other in person more often than once a year. Cathy Semones- you’ve been a lifesaver chica! Pat Fahey, Laura Weiser, Carlos Cruz, and Lauren Ridge- you’ve all helped me grow as a person in so many ways. Thanks for always being there for me, especially when things looked exceedingly grim. Andrew and Lizzie Loder- thanks for hosting all the hangouts at Lake Johnson! You made me feel really at home, no matter the occasion. I will be ever grateful to Daniel, George, Angel, Aleah, Rose, Sean, Gregory, and Elizabeth for lending friendly ears whenever I needed them. Kat, Will, Cat, Ashley, Ashleigh, Shannon, Seth, Jon, Ryan, Tian, Claire, Sam, and Johanna, thank you so much for your support through the tough times. I must thank Mike Noel for his continued support, motivation, and distractions as needed. Finally, to my entire group of friends from all stages of my life, even if you are not named, you have shaped me in some way to help me achieve this monstrous goal. Thank you for your continued support and love.

TABLE OF CONTENTS

LIST OF TABLES

LIST OF FIGURES

1 Introduction: Signaling and Patterning in *Drosophila*

Cell signaling, which is highly conserved between species, is essential to the survival of multicellular and unicellular organisms alike. Many signaling pathways are built upon motifs that are used reiteratively throughout nature, including feedforward loops, positive and negative feedback loops, repression, and cross-repression (*1*). Since we know that cells have a limited range of tools when it comes to communicating with one another, we can apply what we learn in one system, such as tissue patterning, to others like apoptosis misregulation, which can lead to cancer.

1.1 Development

Researchers who study development are driven by the question of how a single cell, which, through processes such as proliferation, differentiation, and migration, can give rise to a fully differentiated adult. This question becomes vastly more complicated when environmental variance is taken into account; therefore, development is a highly regulated process, similar to process control engineering (*2*). During development, unlike in a process such as cruise control, there is no operator to step in should something go awry; therefore, development utilizes several layers of regulation to ensure the desired outcome: a fully differentiated adult. In fact, this process is so tightly controlled that, despite *Drosophila* development being temperature sensitive, an embryo submitted to two different temperatures (one each on the anterior and posterior halves) will still develop properly (*3*).

It is through complex interactions between multiple signaling pathways that embryos are able to consistently develop and reach adulthood.

Tissue patterning often originates with morphogens, which are proteins that influence cell fate in a concentration-dependent fashion (*4*,*5*). In the 1960s, Lewis Wolpert used the pattern of the French flag to describe morphogen gradients; based on the local concentration of morphogen, a cell would differentiate into the color of a stripe on the French flag (*6*,*7*). In order from highest concentration to lowest, the cells would turn blue, white, or red. Morphogens remained a theory until 1988 when Wolfgang Driever and Christiane Nüsslein-Volhard discovered that the protein Bicoid (Bcd) influenced cell fate in a concentration-dependent manner along the anteroposterior axis in the *Drosophila* embryo (*8*,*9*). *bcd* mRNA is deposited at the anterior of the egg during oogenesis; after egg lay, this mRNA is translated into Bcd protein, which diffuses away from its source at the anterior pole (*8*) (**Figure 1.1A,B**). This concentration gradient of Bcd sets the gene expression borders for many crucial AP patterning genes, such as *orthodenticle* (*otd*), *hunchback* (*hb*), and *Krüppel* (*Kr*) (**Figure 1.1C-E**), as well as others like *giant* (*gt*) and *knirps* (*kni*) (*8*,*10*,*11*).

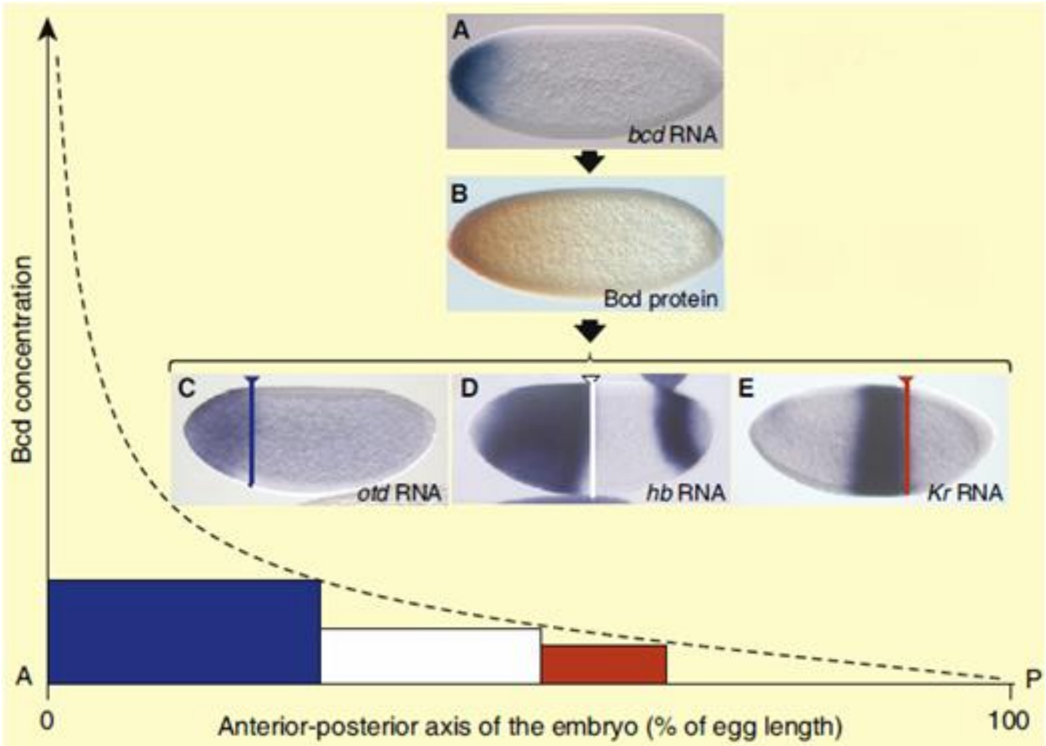

Figure 1.1: The French flag model of morphogens as related to the Bicoid gradient along the anterior-posterior axis of the *Drosophila* embryo. (A) Maternally loaded *bcd* RNA is anchored at the anterior pole. (B) As the RNA is translated into Bcd protein, a gradient forms with its peak at the anterior pole. (C-E) Target genes are expressed above certain thresholds of Bcd concentration, as denoted by the colored boxes under the dotted curve and predicted by Wolpert's French flag model. Highest concentrations of Bcd turn on *orthodenticle* (*otd*) (blue), moderate concentrations turn on *hunchback* (*hb*) (white), and low levels turn on *Krüppel* (*Kr*) (red). Adapted from (*9*).

1.1.1 Methods of gradient formation

While the actions of morphogens are well studied and understood, it is less clear how their gradients are formed. Typical morphogen gradients, such as the anteroposterior Bcd gradient, are formed via diffusion of the morphogen from a localized source (*12*) (**Figure 1.1**). Other morphogen gradients, such as BMP in the pre-gastrulation embryo (discussed in greater detail in **Section 1.2.4**, below), are formed via a shuttling mechanism, in which a carrier protein binds to the morphogen, enabling it to seemingly diffuse against its own concentration gradient (*13*). In the case of BMP, the protein Sog acts as the shuttling molecule, allowing BMP to concentrate at the dorsal midline (*13*). Researchers also speculate that dorsoventral polarity in the *Drosophila* embryo is established via shuttling of the ligand Spätzle (Spz) (*14*). They propose that Spz is cleaved into activating (C-Spz) and inhibiting (N-Spz) forms. C-Spz is responsible for activating Toll signaling at the ventral midline of the embryo; N-Spz can re-associate with C-Spz, forming an inert complex that is no longer capable of activating Toll. Our research suggests a separate shuttling mechanism for establishing dorsoventral polarity, which may act in addition to or instead of the Spz shuttling mechanism, and relies on the results of Toll signaling: release of the inhibitory protein Cactus from the morphogen Dorsal. See **Chapter 5** for more detail. Another proposed mechanism of gradient formation is signal transduction through specialized filopodia known as cytonemes, which can be thought of as trains transporting proteins quickly across a (relatively) long distance (*15*–*17*).Researchers have found that BMP and Hedgehog (Hh) signaling in the *Drosophila* wing disc and maintenance of the female germline stem cells via Hh are transduced via this mechanism (*18*–*20*). Although these mechanisms of morphogen gradient formation may seem vastly different from one another, their final outcome is the same: proper patterning of developing tissue.

1.2 Dorsoventral patterning of the Drosophila melanogaster embryo

From its humble position as a kitchen pest, the fruit fly (*Drosophila melanogaster*) has risen as a model organism for studying disease, behavior, and, importantly for our work, development. Its quick maturation period (10 days at 25°C) enables genetic manipulation in a much shorter time frame than available with vertebrate animals (*21*). Though the fly's life cycle is significantly longer than the several hours required for a bacterial culture, we are interested in studying processes that can only be observed in multicellular organisms, such as intercellular signaling and tissue patterning.

1.2.1 Drosophila genetics

Due to its long history of study, many tools are available for genetic and transgenic manipulation of *Drosophila*. First, the *Drosophila* genome has been fully characterized, allowing scientists to map genetic mutations to phenotypic differences, determine putative actions of unstudied proteins via comparison to other organisms, and further examine the complicated processes involved in gene regulation outside of simple translation (*22*,*23*). A sequenced genome also enables researchers to apply what they learn in *Drosophila* to human health, since approximately 75% of all human disease genes have related sequences in *Drosophila* (*24*). Once genetic manipulation takes place, it is essential for scientists to be able to verify which animals carry the genotype of interest. Therefore, a variety of visible markers have been developed that enable researchers to quickly sort wild type flies from altered ones. Furthermore, the genome can be edited via DNA plasmid injection into the future gametes of developing embryos (*25*–*27*). ϕ31-integrase and specialized fly lines allow researchers to precisely control the genomic location of the transgene (*27*). Additionally, scientists have engineered an elegant system of Gal4-linked drivers and UAS-linked genes (*28*). The yeast protein Gal4 recognizes and binds to UAS sites in the promoter region of genes, turning on expression. This system allows researchers to express genes in specific tissues or at a specific time in development, essentially providing a system with much greater variety than could be generated through single injections. Since UAS-linked genes are not expressed except when Gal4 is present, researchers can maintain stocks containing deleterious mutations that would otherwise render flies non-viable. However, the Gal4/UAS system has its drawbacks. Some drivers are weaker than others, preventing full penetration of the desired phenotype. Furthermore, due to the limited number of chromosomes (four), it is difficult to manipulate multiple genes at the same time. Finally, these methods only allow researchers to *add* genes to the fly. In order to disrupt a gene, the DNA insertion must occur within that gene's locus, a process that is difficult both to control and screen. Mutated versions of genes can be added to the genome, but they must then be crossed for several generations to enable study. Recently, researchers have expanded the Gal4/UAS system to include UAS-linked RNAi constructs (*29*,*30*). This system allows researchers to knock down gene expression of target genes; however, due to the variability of constructs and strength of expression, it may be difficult to create functional RNAi lines for every gene of interest in the fly. Furthermore, RNAi constructs must undergo significant testing to ensure that they are functional *in vitro* before being used in flies, and this testing does not guarantee functionality *in vivo* since RNAi can be affected by off-target, weak, and/or variable effects. New technology allows researchers to use the CRISPR/Cas9 system to edit genes within the fly itself, lending capability to knock out a gene, create a point mutation within a gene, or even simultaneously create double and triple mutants without the added time of testing constructs for functionality (*31–33*). These mutations are heritable, with up to 33% of progeny expressing the altered gene (*31*). Use of CRISPR/Cas9 can save weeks of a researcher's time, enabling him or her to perform experiments (and get results) more quickly.

Our main area of focus is the early *Drosophila* embryo. Several characteristics make this system uniquely simple to study. To begin with, it is a syncytium; that is, there are no cellular membranes separating the nuclei, allowing for nucleus-to-nucleus diffusion of proteins and other molecules (*34*). Furthermore, after nine nuclear divisions (called nuclear cycles (NCs)), lasting about seventy minutes in total, the nuclei migrate to the periphery of the embryo, where they remain, dividing another five times, until cellularization (formation of cellular membranes) and gastrulation (loss of embryonic symmetry) occur, approximately 3-4 hours after egg lay (*34*) (**Figure 1.2**). Since the nuclei are present in a roughly two-dimensional layer, rather than a three-dimensional stack, researchers can effectively "see" development on the surface of the embryo. These traits lend *Drosophila* advantages over other leading model organisms like zebrafish and mice and are why we have chosen it as our system of interest.

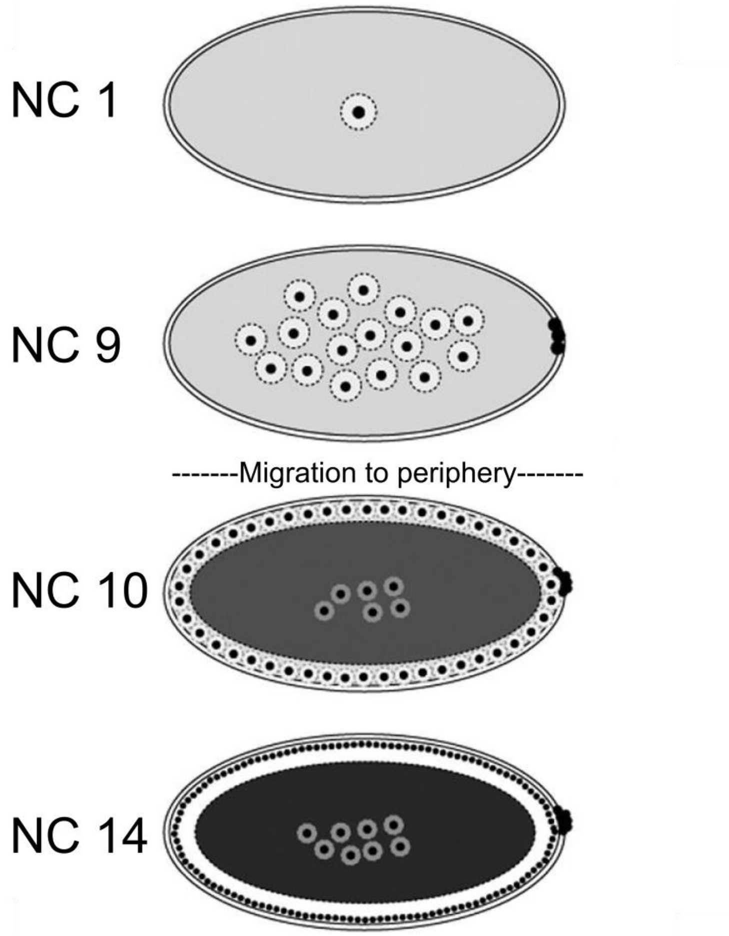

Figure 1.2: Development and nuclear distribution within the *Drosophila* embryo. Anterior is to the left. The cluster of cells at the posterior of the embryo is the pole cells, which will form the adult fly's germ line. Near the end of nuclear cycle (NC) 14, cell membranes begin to envelop the nuclei. After cellularization is complete, the embryo gastrulates. Adapted from (*35*).

1.2.2 Gurken and Pipe signaling determine dorsoventral polarity in the oocyte

The *Drosophila* egg begins as a cyst comprising sixteen cells, one of which will become the oocyte (*36*,*37*). The other fifteen cells become nurse cells, providing the oocyte with essential nutrients. This cluster of oocyte and nurse cells is then enveloped by somatic follicle cells, which are essential to determining the embryonic axes (*36*). The single nucleus within the oocyte translocates to the anterior-dorsal quadrant, thereby determining both AP and DV polarity of the egg. Here, the nucleus establishes local translation of Gurken protein, a homolog of TGFα and the ligand for *Drosophila* Epidermal Growth Factor Receptor (EGFR) (*38*,*39*). Gurken signaling represses *pipe* expression, which sets the ventral extent of Toll signaling (*40*). See **Figure 1.3** and **Section 1.2.3**.

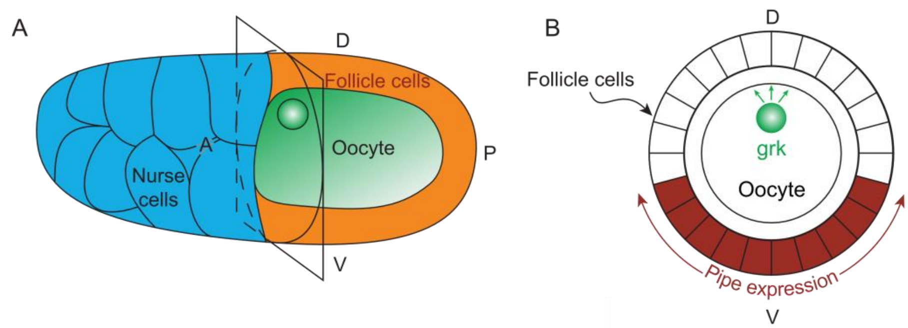

Figure 1.3: Pipe sets the domain of active Toll signaling. (A) In the developing oocyte, the single nucleus migrates to the dorsal-anterior quadrant, where it causes local translation of Gurken (B) A cross section of the oocyte. Gurken signaling through EGFR represses Pipe, limiting it to the ventral side. Adapted from (*41*).

1.2.3 Dorsal establishes the pattern of the DV axis in Drosophila embryos

In the 1970s, researchers at the Max Planck Institute in West Germany discovered that the pattern of the dorsoventral axis is under the control of twelve maternal-effect genes, eleven of which are known as the dorsal group because a loss of any one causes the embryo to develop according to a dorsal fate (*42*). In contrast, absence of the twelfth gene, *cactus*, causes ventralization of the embryo (*43*). About ten years later, the same group discovered that, of these genes, the protein Dorsal acts as the morphogen (*41*,*44*). Dorsal protein is present throughout the embryo and forms a nuclear gradient that peaks at the ventral midline and decays to about 40% of the embryo's circumference (See **Figure 1.4A**). This gradient relays spatial information to the developing embryo; target genes, expressed or repressed as a function of Dorsal concentration, specify the future locations of the mesoderm, neurogenic ectoderm, and dorsal ectoderm (*41*,*45*,*46*) (**Figure 1.4B**,**C**). Dorsal's target genes can be split into four categories: Type I genes (like *snail* (*sna*)) are expressed where nuclear Dorsal levels are highest; Type II genes (such as *ventral nervous system defective* (*vnd*)) appear in ventrolateral domains; Type III^{+} genes (like *short-gastrulation* (*sog*)) have boundaries beyond ~45% DV position and are activated by Dorsal; and Type III^{-} genes (such as *decapentaplegic* (*dpp*)) are also bounded beyond ~45% DV position, but are repressed by Dorsal (See **Figure 1.4B,C**) (*47*).

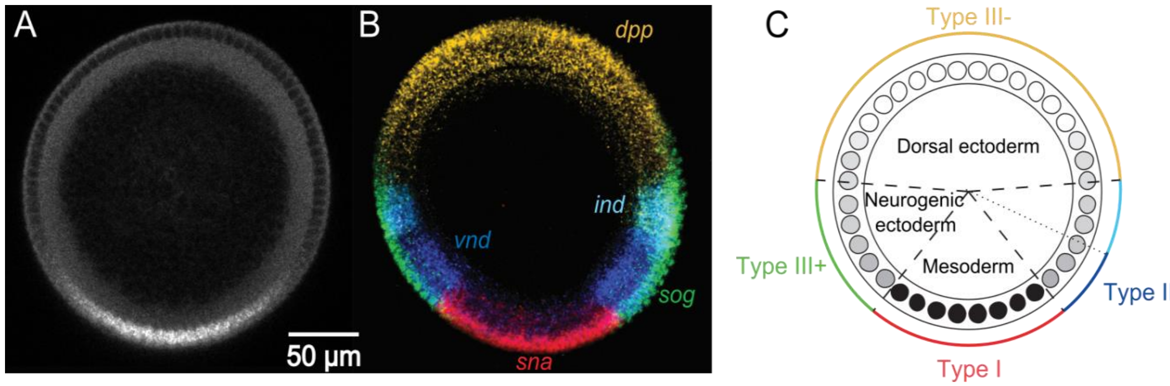

Figure 1.4: The protein Dorsal patterns the DV axis of the *Drosophila* embryo. (A) An antibody staining against Dorsal in an NC 14 embryo. (B) mRNA expression of a variety of Dorsal target genes. (C) The pattern of target genes sets the border for the muscular layers in the adult fly, as delineated by the expression domains of the Dorsal target genes. Type I, II, and III domains are colored in correspondence to the genes in (B). Embryo cross-sections are oriented so that ventral is down. Adapted from (*41*).

Dorsal is regulated by the inhibitory factor Cactus (Cact), which blocks the nuclear localization sequence; it is the spatially regulated degradation of Cact that establishes the nuclear concentration gradient of Dorsal (*48*). Cactus is preferentially degraded on the ventral side of the embryo through a mechanism beginning with Pipe which, through an unknown mechanism, sets off a protease cascade through Nudel (Ndl), Gastrulation-defective (Gd), Snake (Snk), and Easter (Ea), that culminates in cleavage and activation of the Toll receptor ligand Spätzle (Spz) (*40*,*41*). Toll signaling phosphorylates the Dorsal/Cactus complex, causing Cactus to be degraded and allowing Dorsal to enter the nucleus as shown in **Figure 1.5**. See also **Section 1.2.2**.

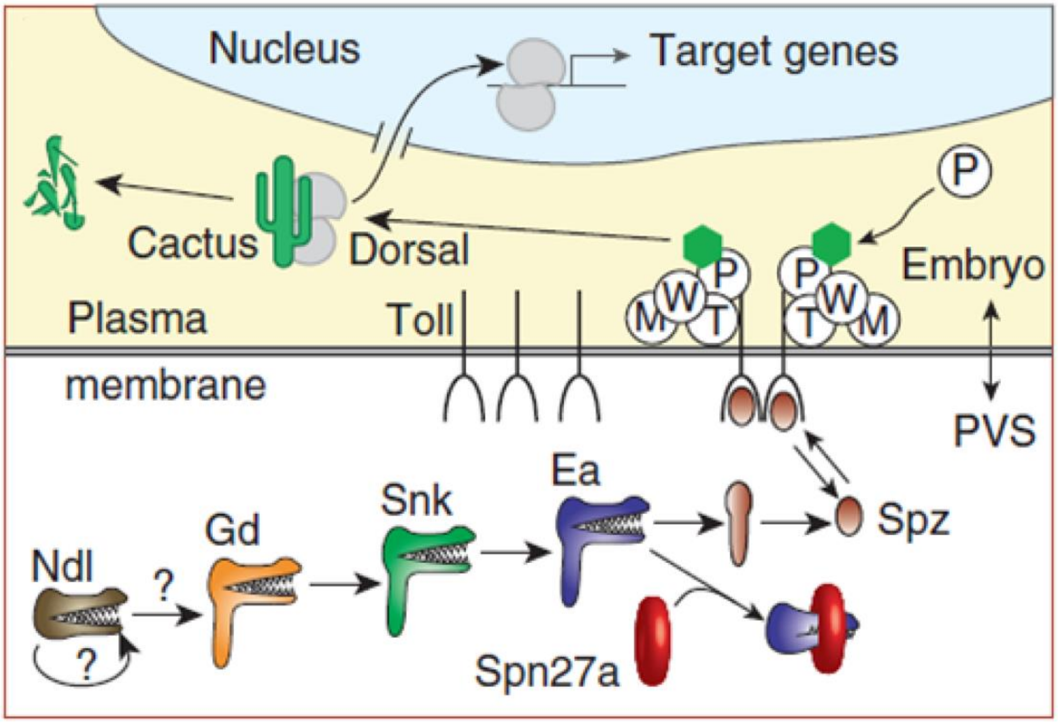

Figure 1.5: The mechanism for Dorsal's release from Cactus and subsequent entry into nuclei on the ventral side of the embryo. In brief, a protease cascade involving Nudel (Ndl), Gastrulation defective (Gd), Snake (Snk), and Easter (Ea) activates the Toll ligand Spätzle (Spz). Tube (T), Pelle (P), Weckle (W), and Myd88 (M) participate in a signaling complex in the cytoplasm associated with Toll. Toll signaling phosphorylates the Dorsal/Cactus complex, causing Cactus to be degraded and allowing Dorsal to enter the nucleus. Adapted from (*41*).

1.2.3.1 NF-κB and IκB

Once their role in development has been completed, Dorsal and Cactus function in the immune response of the larva and adult fly via activation of Spz through a different protease cascade (*49*,*50*). This immune function is similar to the role played by their mammalian homologs, NF-κB and IκB (*50*,*51*). Misregulation of these proteins can lead to a variety of diseases, including cancer, since NF-κB blocks apoptosis (*52*,*53*). Curiously, some of the same immune challenges that activate NF-κB actually induce apoptosis, indicating that NF-κB might have a protective role (*53*). Signaling pathways to activate NF-κB are highly conserved between insects and mammals (*54*); however, the IκB kinase (IKK) homolog in *Drosophila* does not function to activate Dorsal through Toll signaling (*55*). Recently, researchers have confirmed that Pelle, homologous to an IKK regulator in mammals, functions as a Cactus kinase, effectively filling the role of IKK in the system (*56*). See **Figure 1.5**.

Since NF-κB is regulated in much the same way as Dorsal, researchers speculate that it may function in a yet-undiscovered way in the overall development of mammals (*53*). To further support this hypothesis, scientists have recently discovered that NF-κB is crucial to proper embryonic liver development in mice (*57*).

1.2.3.2 Fitting the Dorsal gradient to a Gaussian

In order to analyze the Dorsal gradient and compare differences between genotypes, it would be useful to extract summary parameters from fluorescence data. Based purely on inspection, the Dorsal gradient empirically resembles a Gaussian curve. Using existing MATLAB code, we can precisely trace the perimeter of the embryo, find the nuclei within it, and determine the fluorescence intensity of each nucleus within a 21 μm z-region of the embryo (*58*). This data is then fit to a Gaussian curve of the equation:

$$C(x) = Ae^{-x^2/2\sigma^2} + B + M|x| \tag{1.1}$$

where A is the amplitude, σ the width, and B the basal levels of Dorsal. M is a minor adjustment factor to account for any slight slope of the nuclear Dorsal gradient after the Gaussian portion has decayed to zero. A can be thought of as the amount of Dorsal in the ventral-most nucleus and B as the amount of Dorsal in the dorsal-most nucleus (ignoring the small value of M). σ is a measure of how far into the lateral regions of the embryo the gradient extends. See **Figure 1.6** for a visual depiction of the Gaussian fit. One calculated value that is not present in the Gaussian equation is μ, which denotes the location of the ventral midline relative to the pre-set value. μ can therefore be positive or negative, depending on which direction the estimated ventral midline had to be rotated to match the actual ventral midline.

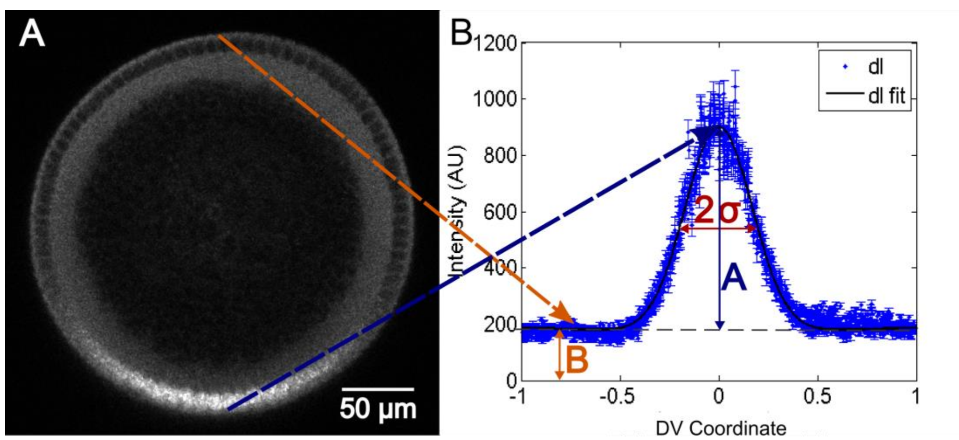

Figure 1.6: Fitting Dorsal fluorescence to a Gaussian. (A) A cross section of a wild type embryo fluorescently stained for Dorsal. (B) The fluorescent data extracted from (A), with labels showing what the Gaussian parameters of A, B, and σ represent. This is the same embryo that appears in **Figure 1.4**.

1.2.3.3 The Dorsal gradient fluctuates in space and time

Several factors seem to complicate Dorsal's ability to consistently pattern the dorsoventral axis. As the tissue develops, nuclei divide, breaking down the Dorsal nuclear gradient during mitosis (*59*). Also, detracting from the idea of a simple concentration-based response, the Dorsal gradient increases in amplitude with respect to time (See **Figure 1.7**).

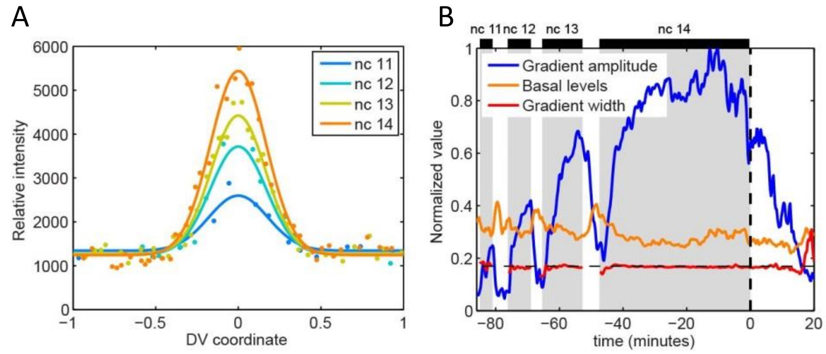

Figure 1.7: The Dorsal gradient increases in amplitude over time but has a constant width. (A) Quantification of the Dorsal gradient in an embryo bearing a Dorsal-Venus (yellow fluorescent protein) construct, imaged live. DV coordinate is a normalized measure of embryo length, with 0 representing the ventral midline, and 1 and -1 representing the dorsal midline. (B) The gradient amplitude (blue) and basal levels of Dorsal-Venus (orange) fluctuate with time, while the width of the gradient (red) remains generally constant. Time = 0 corresponds to gastrulation. Adapted from (*47*).

If concentration of Dorsal were the only factor influencing gene expression, we might expect the domains of target genes to vary greatly with respect to time; however, researchers have found that these domains are fairly well conserved, although they do refine over time (*47*). How then are stable patterns formed? Part of the observed robustness is due to the fact that some proteins expressed by Dorsal target genes, such as Snail, regulate their neighbors (Sog), establishing more precise boundaries than possible with a simple on/off concentration switch (*1*,*11*). Furthermore, expression of Dorsal target genes does not stabilize until NC 14, indicating that perhaps the gene expression during NCs 10-13 functions as a stepping stone to NC 14, potentially allowing enough time for feedback to regulate the gene expression boundaries that will be set at the time of gastrulation (*47*).

Additionally, Liberman et al. found that the width of the Dorsal gradient appears too narrow to pattern some of the Type III genes it is known to influence (See **Figure 1.8**) (*60*). Since differences in cell fate are supposedly determined solely by neighboring cells responding to differing concentrations of a morphogen, how is *ind* expression turned both on and off in a region of the Dorsal gradient where there is no apparent change between neighboring nuclei?

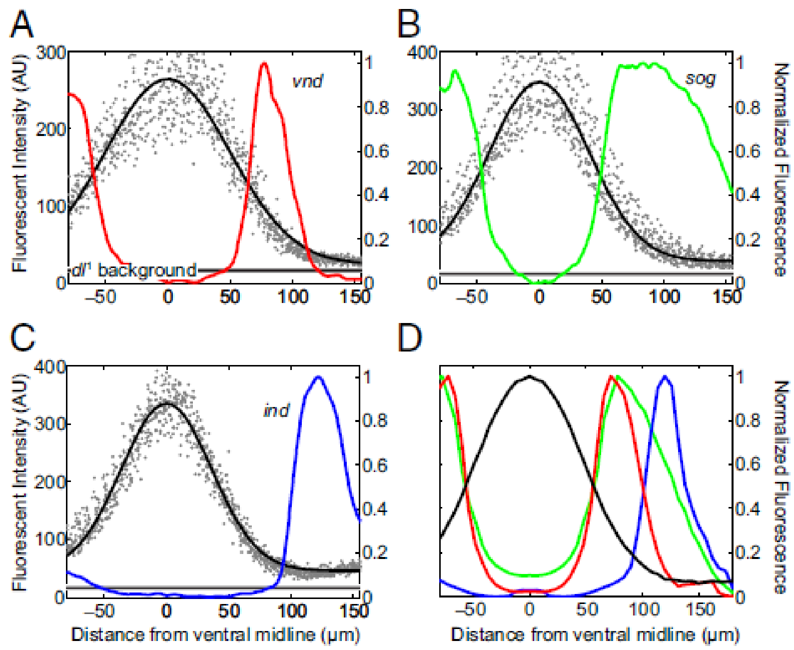

Figure 1.8: Domains of the Dorsal nuclear gradient and select target genes, determined by fluorescent *in situ* hybridization and antibody staining (*60*). (A) *vnd* is a Type II gene that seems to fit the typical idea of a morphogen-influenced fate. (B) *sog* expression extends far beyond where the Dorsal gradient is changing in space. (C) *ind* is expressed completely in a part of the embryo where the Dorsal gradient is flat. (D) The three genes occupy a similar area of the embryo.

Some researchers have explained this phenomenon by arguing that the Dorsal gradient is actually wider than Liberman et al. measured; however, they have not taken into account the fact that the Dorsal gradient is widest at the anterior and posterior ends of the embryo, where their measurements were taken (*47,60–62*). Intuitively, it seems that transcription initiated by Dorsal is not the only factor influencing the expression of these genes. Furthermore, when a Dorsal gradient is artificially expressed along the anteroposterior axis of the embryo, typical domains of gene expression are seen for *sna*, *ind*, and *vnd*; however, *sog* expression appears in a much broader domain than anticipated (*63*). This result suggests that Dorsal target genes are able to respond to more than a single nuclear concentration input. Additionally, recent computational research suggests that the apparently too narrow gradient is due to a misunderstanding of data collected from antibody-stained images; both free dl and dl/Cact complex are contained in the nuclei, and the fluorescence from dl/Cact complex masks the levels of free dl in the dorsolateral regions of the embryo (*64*). Since the anti-dl antibody does not preferentially bind to free dl over dl/Cact complex as evidenced by bright puncta surrounding the nuclei on the dorsal side of the embryo (See **Figure 1.4**), there is no way to distinguish one species from the other. However, researchers have long believed that dl/Cact complex would be unable to enter the nuclei since Cact blocks the nuclear localization sequence on dl. A model created by O'Connell and Reeves supports the hypothesis that, while dl/Cact complex does not necessarily *enter* the nuclei, some complexes may be encapsulated when the nuclear membrane reforms following a mitotic division (*64*). It is the expulsion of this complex from the nuclei that leads to a decrease in basal levels of nuclear dl on the dorsal side of the embryo, a previously unexplained phenomenon (See **Figure 1.7B**).

1.2.3.4 Nucleocytoplasmic Exchange

Through photobleaching experiments, researchers have found that Dorsal rapidly diffuses into and out of the nuclei (*59*). By conducting fluorescence loss in photobleaching

(FLIP) and fluorescence recovery after photobleaching (FRAP) experiments, they could see the nuclei fill (FRAP) or empty (FLIP) depending on what area was bleached, the nucleus or the surrounding cytoplasm, respectively. After about three minutes, the fluorescence levels returned to pre-bleaching levels, establishing that this nucleocytoplasmic exchange happens quickly and readily. Furthermore, this group showed that there are cytoplasmic compartments unique to each nucleus. Diffusion is rapid both within these compartments and between a compartment and its associated nucleus; however, diffusion between compartments is significantly slower. The researchers propose that there is a cytoplasmic pool of Dorsal that enables more global diffusion; however, they hypothesize that this mechanism is significantly more time consuming. Our research suggests that the time scale of global Dorsal diffusion is shorter than previously thought; see **Chapter 5** for more details.

1.2.4 BMP signaling patterns the dorsal side of the embryo

Another commonly studied signaling system in the developing fly is the bone morphogenetic protein (BMP) pathway, which is a part of the TGFβ superfamily (*65*,*66*). The signaling protein Decapentaplegic (Dpp) is a BMP ligand that forms a gradient opposing Dorsal's, with its peak at the dorsal midline (See **Figure 1.4B** for the mRNA pattern) (*45*). Dpp's signaling mechanism is shown in **Figure 1.9**. Dpp and Screw (Scw), another BMP receptor ligand, complex together in a heterodimer, stabilized by the proteins Sog and Twisted gastrulation (Tsg). This complex diffuses through the cytoplasm, and when it reaches the dorsal midline, Tolloid (Tld) cleaves Sog to free the Dpp:Scw complex from Sog and Tsg. Dpp and Scw then bind to their respective receptors, Thickveins (Tkv) and Saxophone (Sax), causing a stronger synergistic signal than is possible via either individually. Dpp signaling causes phosphorylation of the protein Mothers Against Dpp (MAD), which can then be used as a read-out for the signal (*46*). Phosphorylated MAD (pMAD) binds with Medea (Med) in a heterotrimer that acts as a transcription factor to regulate BMP target genes (*67*). Because Dpp is produced only on the dorsal half of the embryo (due to its repression by Dorsal), this mechanism of diffusion is known as facilitated diffusion, or shuttling, described previously in **Section 1.1.1**. In this case, the proteins Sog and Tsg, produced in the ventrolateral regions of the embryo, act as the carrier molecules to cause Dpp to seemingly diffuse against its own concentration gradient (*13*,*46*).

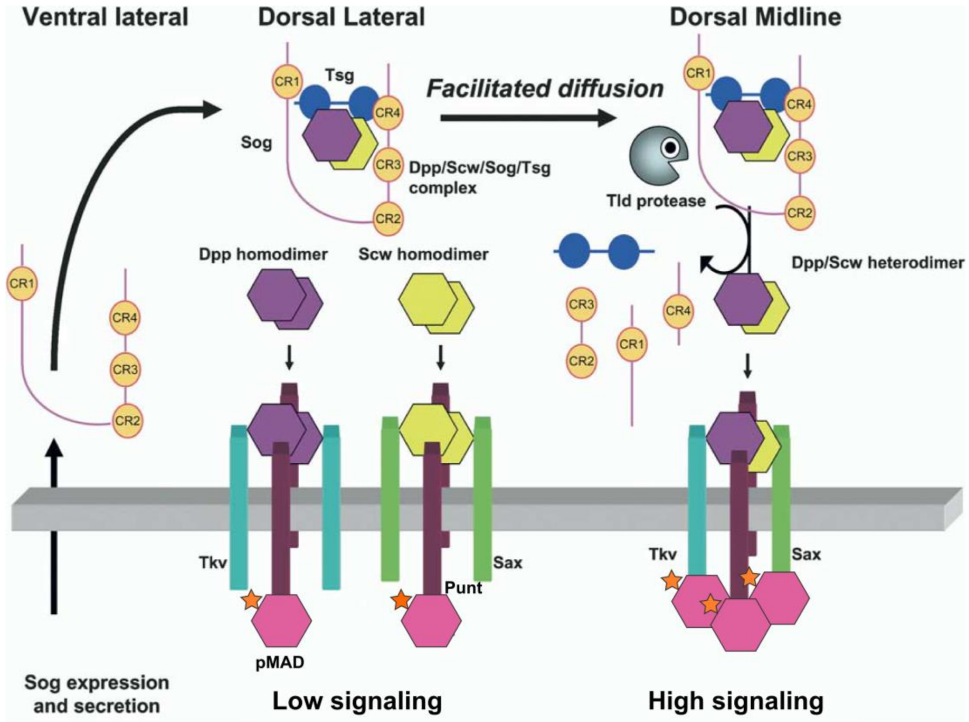

Figure 1.9: The mechanism of BMP signaling in the *Drosophila* embryo. Dpp signals through Tkv, and Scw signals through Sax. It is proposed that signaling via Dpp:Scw heterodimers is more effective than signaling through individual homodimers. Signaling results in phosphorylation of MAD. Adapted from (*13*)**.**

During NC 14, pMAD signaling refines from a broad domain to a narrow stripe (*68*,*69*). Based on careful examination, researchers proposed that this refinement is due to a positive feedback mechanism (*70*,*71*). Other scientists generated a kinetic model to show that positive feedback via a surface-bound BMP-binding protein such as Cv-2 enables the bistable BMP signaling response to act essentially as an on/off switch (*72*). Another group found that, due to multiple levels of regulation via Cv-2, Eiger, a BMP target gene, and Zen, a homeobox transcription factor, BMP signaling in the early *Drosophila* embryo is robust to variations from a 20% decrease to a 250% increase (*71*).

In 2000, several researchers found that embryos derived from mothers who had lowered levels of both *dpp* and *dorsal* presented narrower Dorsal nuclear gradients than observed in wild type embryos (*73*–*76*). Is it possible that genes specified in the lateral areas of the embryo are influenced by both morphogen gradients (*77*)? Since it appears that BMP signaling influences the Dorsal gradient, perhaps other proteins also function to regulate Dorsal's spatial distribution. See **Chapter 4** for more detail.

1.3 Conclusion

This dissertation addresses gaps in the current understanding of how dorsoventral embryonic polarity in *Drosophila melanogaster* is established through the Dorsal and BMP signaling pathways. To facilitate study of the dorsoventral axis, we developed a method for imaging DV cross sections of both fixed and live *Drosophila* embryos using a confocal microscope, presented in **Chapter 2**. In **Chapter 3**, we researched the effect of manipulating the maternal dosage of Dorsal or Cactus on the embryonic Dorsal nuclear gradient. Next, in **Chapter 4**, we studied the interactions between Dorsal signaling on the ventral half of the embryo and BMP signaling on the dorsal half. Finally, in **Chapter 5**, we investigated the formation of the global Dorsal nuclear gradient.

1.4 References

(1) Jermusyk, A. A.; Reeves, G. T. *Transcription Factor Networks*; Elsevier Ltd., 2016; Vol. 4.

(2) Reeves, G. T.; Fraser, S. E. Biological Systems from an Engineer's Point of View. *PLoS Biol.* **2009**, *7* (1), e21.

(3) Lucchetta, E. M.; Lee, J. H.; Fu, L. A.; Patel, N. H.; Ismagilov, R. F. Dynamics of Drosophila Embryonic Patterning Network Perturbed in Space and Time Using Microfluidics. *Nature* **2005**, *434*, 1134–1138.

(4) Turing, A. M. The Chemical Basis of Morphogenesis. *Philos. Trans. R. Soc. Lond. B. Biol. Sci.* **1952**, *237* (641), 37–72.

(5) Gurdon, J. B.; Bourillot, P. Y. Morphogen Gradient Interpretation. *Nature* **2001**, *413* (6858), 797–803.

(6) Wolpert, L. Positional Information and the Spatial Pattern of Cellular Differentiation. *J. Theor. Biol.* **1969**, *25* (1), 1–47.

(7) Wolpert, L. *Principles of Development*, 2nd ed.; Oxford University Press, 2002.

(8) Driever, W.; Nüsslein-Volhard, C. The Bicoid Protein Determines Position in the Drosophila Embryo in a Concentration-Dependent Manner. *Cell* **1988**, *54* (1), 95–104.

(9) Porcher, A.; Dostatni, N. The Bicoid Morphogen System. *Curr. Biol.* **2010**, *20*, 249–254.

(10) Struhl, G.; Struhl, K.; Macdonald, P. M. The Gradient Morphogen Bicoid Is a Concentration-Dependent Transcriptional Activator. *Cell* **1989**, *57* (7), 1259–1273.

(11) Jaeger, J. The Gap Gene Network. *Cell. Mol. Life Sci.* **2011**, *68* (2), 243–274.

(12) Lander, A. D.; Nie, Q.; Wan, F. Y. M. Do Morphogen Gradients Arise by Diffusion? *Dev. Cell* **2002**, *2* (6), 785–796.

(13) Shimmi, O.; Umulis, D.; Othmer, H.; O'Connor, M. B. Facilitated Transport of a Dpp/Scw Heterodimer by Sog/Tsg Leads to Robust Patterning of the Drosophila Blastoderm Embryo. *Cell* **2005**, *120* (3), 873–886.

(14) Haskel-Ittah, M.; Ben-Zvi, D.; Branski-Arieli, M.; Schejter, E. D.; Shilo, B. Z.; Barkai, N. Self-Organized Shuttling: Generating Sharp Dorsoventral Polarity in the Early Drosophila Embryo. *Cell* **2012**, *150* (5), 1016–1028.

(15) Ramírez-Weber, F. A.; Kornberg, T. B. Cytonemes: Cellular Processes That Project to the Principal Signaling Center in Drosophila Imaginal Discs. *Cell* **1999**, *97* (5), 599–607.

(16) Müller, P.; Rogers, K. W.; Yu, S. R.; Brand, M.; Schier, A. F. Morphogen Transport. *Development* **2013**, *140*, 1621–1638.

(17) Lander, A. D. Morpheus Unbound: Reimagining the Morphogen Gradient. *Cell* **2007**, *128* (2), 245–256.

(18) Roy, S.; Huang, H.; Liu, S.; Kornberg, T. B. Cytoneme-Mediated Contact-Dependent Transport of the Drosophila Decapentaplegic Signaling Protein. *Science* **2014**, *343* (6173), 1244624.

(19) Bischoff, M.; Gradilla, A.-C.; Seijo, I.; Andrés, G.; Rodríguez-Navas, C.; González-Méndez, L.; Guerrero, I. Cytonemes Are Required for the Establishment of a Normal Hedgehog Morphogen Gradient in Drosophila Epithelia. *Nat. Cell Biol.* **2013**, *15* (11), 1269–1281.

(20) Rojas-Ríos, P.; Guerrero, I.; González-Reyes, A. Cytoneme-Mediated Delivery of Hedgehog Regulates the Expression of Bone Morphogenetic Proteins to Maintain Germline Stem Cells in Drosophila. *PLoS Biol.* **2012**, *10* (4).

(21) Greenspan, R. J. *Fly Pushing: The Theory and Practice of Drosophila Genetics*, 2nd ed.; Cold Spring Harbor Laboratory Press: Cold Spring Harbor, NY, 2004.

(22) Adams, M. D.; Celniker, S. E.; Holt, R. A.; Evans, C. A.; Goscayne, J. D.; Amanatides, P. G.; Scherer, S. E.; Li, P. W.; Hoskins, R. A.; Galle, R. F.; et al. The Genome Sequence of Drosophila Melanogaster. *Science* **2000**, *287* (5461), 2185–2195.

(23) Myers, E. W.; Sutton, G. G.; Delcher, a L.; Dew, I. M.; Fasulo, D. P.; Flanigan, M. J.; Kravitz, S. a; Mobarry, C. M.; Reinert, K. H.; Remington, K. a; et al. A Whole-Genome Assembly of Drosophila. *Science* **2000**, *287* (2000), 2196–2204.

(24) Bier, E. Drosophila, the Golden Bug, Emerges as a Tool for Human Genetics. *Nat. Rev. Genet.* **2005**, *6* (1), 9–23.

(25) Spradling, A. C.; Rubin, G. M. Transposition of Cloned P Elements into Drosophila Germ Line Chromosomes. *Science* **1982**, *218* (4570), 341–347.

(26) Rubin, G. M.; Spradling, A. C. Genetic Transformation of Drosophila with Transposable Element Vectors. *Science* **1982**, *218* (4570), 348–353.

(27) Bateman, J. R.; Lee, A. M.; Wu, C. T. Site-Specific Transformation of Drosophila via ϕC31 Integrase-Mediated Cassette Exchange. *Genetics* **2006**, *173* (2), 769–777.

(28) Brand, a H.; Perrimon, N. Targeted Gene Expression as a Means of Altering Cell Fates and Generating Dominant Phenotypes. *Development* **1993**, *118* (2), 401–415.

(29) Dietzl, G.; Chen, D.; Schnorrer, F.; Su, K.-C.; Barinova, Y.; Fellner, M.; Gasser, B.; Kinsey, K.; Oppel, S.; Scheiblauer, S.; et al. A Genome-Wide Transgenic RNAi Library for Conditional Gene Inactivation in Drosophila. *Nature* **2007**, *448* (7150), 151–156.

(30) Ni, J.-Q.; Markstein, M.; Binari, R.; Pfeiffer, B.; Liu, L.-P.; Villalta, C.; Booker, M.; Perkins, L.; Perrimon, N. Vector and Parameters for Targeted Transgenic RNA Interference in Drosophila Melanogaster. *Nat. Methods* **2008**, *5* (1), 49–51.

(31) Bassett, A. R.; Tibbit, C.; Ponting, C. P.; Liu, J. L. Highly Efficient Targeted Mutagenesis of Drosophila with the CRISPR/Cas9 System. *Cell Rep.* **2013**, *4*, 220–228.

(32) Cong, L.; Ran, F. A.; Cox, D.; Lin, S.; Barretto, R.; Habib, N.; Hsu, P. D.; Wu, X.; Jiang, W.; Marraffini, L. A.; et al. Multiplex Genome Engineering Using CRISPR/Cas Systems. *Science* **2013**, *339* (6121), 819–823.

(33) Gratz, S. J.; Cummings, A. M.; Nguyen, J. N.; Hamm, D. C.; Donohue, L. K.; Harrison, M. M.; Wildonger, J.; O’connor-Giles, K. M. Genome Engineering of Drosophila with the CRISPR RNA-Guided Cas9 Nuclease. *Genetics* **2013**, *194* (August), 1029–1035.

(34) Foe, V. E.; Alberts, B. M. Studies of Nuclear and Cytoplasmic Behaviour during the Five Mitotic Cycles That Precede Gastrulation in Drosophila Embryogenesis. *J. Cell Sci.* **1983**, *61*, 31–70.

(35) Coppey, M.; Berezhkovskii, A. M.; Kim, Y.; Boettiger, A. N.; Shvartsman, S. Y. Modeling the Bicoid Gradient: Diffusion and Reversible Nuclear Trapping of a Stable Protein. *Dev. Biol.* **2007**, *312* (2), 623–630.

(36) Roth, S.; Lynch, J. A. Symmetry Breaking during Drosophila Oogenesis. *Cold Spring Harb Perspect Biol* **2009**, *1* (2), a001891.

(37) Bastock, R.; St Johnston, D. Drosophila Oogenesis. *Curr. Biol.* **2008**, *18* (23), 1082–1087.

(38) Neuman-Silberberg, F. S.; Schüpbach, T. The Drosophila Dorsoventral Patterning Gene Gurken Produces a Dorsally Localized RNA and Encodes a TGFα-like Protein. *Cell* **1993**, *75* (1), 165–174.

(39) Roth, S.; Schüpbach, T. The Relationship between Ovarian and Embryonic Dorsoventral Patterning in Drosophila. *Development* **1994**, *120*, 2245–2257.

(40) Sen, J.; Goltz, J. S.; Stevens, L.; Stein, D. Spatially Restricted Expression of Pipe in the Drosophila Egg Chamber Defines Embryonic Dorsal–Ventral Polarity. *Cell* **1998**, *95* (4), 471–481.

(41) Reeves, G. T.; Stathopoulos, A. Graded Dorsal and Differential Gene Regulation in the Drosophila Embryo. *Cold Spring Harb. Perspect. Biol.* **2009**, *1* (4), a000836.

(42) Anderson, K. V; Nüsslein-Volhard, C. Information for the Dorsal-Ventral Pattern of the Drosophila Embryo Is Stored as Maternal mRNA. *Nature* **1984**, *311* (5983), 223–227.

(43) Roth, S.; Hiromi, Y.; Godt, D.; Nüsslein-Volhard, C. Cactus, a Maternal Gene Required for Proper Formation of the Dorsoventral Morphogen Gradient in Drosophila Embryos. *Development* **1991**, *112* (2), 371–388.

(44) Roth, S.; Stein, D.; Nüsslein-Volhard, C. A Gradient of Nuclear Localization of the Dorsal Protein Determines Dorsoventral Pattern in the Drosophila Embryo. *Cell* **1989**, *59* (6), 1189–1202.

(45) Podos, S. D.; Ferguson, E. L. Morphogen Gradients: New Insights from DPP. *Trends Genet.* **1999**, *15* (10), 396–402.

(46) Eldar, A.; Dorfman, R.; Weiss, D.; Ashe, H.; Shilo, B.; Barkai, N. Robustness of the BMP Morphogen Gradient in Drosophila Embryonic Patterning. *Nature* **2002**, *419* (19 September 2002), 304–308.

(47) Reeves, G. T.; Trisnadi, N.; Truong, T. V; Nahmad, M.; Katz, S.; Stathopoulos, A. Dorsal-Ventral Gene Expression in the Drosophila Embryo Reflects the Dynamics and Precision of the Dorsal Nuclear Gradient. *Dev. Cell* **2012**, *22* (3), 544–557.

(48) Bergmann, A.; Stein, D.; Geisler, R.; Hagenmaier, S.; Schmid, B.; Fernandez, N.; Schnell, B.; Nüsslein-Volhard, C. A Gradient of Cytoplasmic Cactus Degradation Establishes the Nuclear Localization Gradient of the Dorsal Morphogen in Drosophila. *Mech. Dev.* **1996**, *60* (1), 109–123.

(49) Lindsay, S. A.; Wasserman, S. A. Conventional and Non-Conventional Drosophila Toll Signaling. *Dev. Comp. Immunol.* **2014**, *42* (1), 16–24.

(50) Lemaitre, B.; Meister, M.; Govind, S.; Georgel, P.; Steward, R.; Reichhart, J. M.; Hoffmann, J. A. Functional Analysis and Regulation of Nuclear Import of Dorsal during the Immune Response in Drosophila. *EMBO J.* **1995**, *14* (3), 536–545.

(51) Steward, R. Dorsal, an Embryonic Polarity Gene in Drosophila, Is Homologous to the Vertebrate Proto-Oncogene, c-Rel. *Science* **1987**, *238* (4827), 692–694.

(52) Perkins, N. D. Integrating Cell-Signalling Pathways with NF-κB and IKK Function. *Nat. Rev. Mol. Cell Biol.* **2007**, *8* (1), 49–62.

(53) Li, X.; Stark, G. R. NF-κB-Dependent Signaling Pathways. *Exp. Hematol.* **2002**, *30* (4), 285–296.

(54) Silverman, N.; Maniatis, T. NF-κB Signaling Pathways in Mammalian and Insect Innate Immunity. *Genes Dev.* **2001**, *15*, 2321–2342.

(55) Silverman, N.; Zhou, R.; Stoven, S.; Pandey, N.; Hultmark, D.; Maniatis, T. A Drosophila IκB Kinase Complex Required for Relish Cleavage and Antibacterial Immunity. *Genes Dev.* **2000**, *14* (19), 2461–2471.

(56) Daigneault, J.; Klemetsaune, L.; Wasserman, S. a. The IRAK Homolog Pelle Is the Functional Counterpart of IκB Kinase in the Drosophila Toll Pathway. *PLoS One* **2013**, *8* (9).

(57) Hou, Y.; Li, F.; Karin, Michael; Ostrowski, M. C. Analysis of the IKKβ/NF-κB Signaling Pathway during Embryonic Angiogenesis. *Dev. Dyn.* **2008**, *237* (10), 2926–2935.

(58) Trisnadi, N.; Altinok, A.; Stathopoulos, A.; Reeves, G. T. Image Analysis and Empirical Modeling of Gene and Protein Expression. *Methods* **2013**, *62* (1), 68–78.

(59) DeLotto, R.; DeLotto, Y.; Steward, R.; Lippincott-Schwartz, J. Nucleocytoplasmic Shuttling Mediates the Dynamic Maintenance of Nuclear Dorsal Levels during Drosophila Embryogenesis. *Development* **2007**, *134* (23), 4233–4241.

(60) Liberman, L. M.; Reeves, G. T.; Stathopoulos, A. Quantitative Imaging of the Dorsal Nuclear Gradient Reveals Limitations to Threshold-Dependent Patterning in Drosophila. *Proc. Natl. Acad. Sci. U. S. A.* **2009**, *106* (52), 22317–22322.

(61) Kanodia, J. S.; Rikhy, R.; Kim, Y.; Lund, V. K.; DeLotto, R.; Lippincott-Schwartz, J.; Shvartsman, S. Y. Dynamics of the Dorsal Morphogen Gradient. *Proc. Natl. Acad. Sci. U. S. A.* **2009**, *106* (51), 21707–21712.

(62) Chung, K.; Kim, Y.; Kanodia, J. S.; Gong, E.; Shvartsman, S. Y.; Lu, H. A Microfluidic Array for Large-Scale Ordering and Orientation of Embryos. *Nat. Methods* **2011**, *8* (2), 171–176.

(63) Stathopoulos, A.; Levine, M. Dorsal Gradient Networks in the Drosophila Embryo. *Dev. Biol.* **2002**, *246* (1), 57–67.

(64) O'Connell, M. D.; Reeves, G. T. The Presence of Nuclear Cactus in the Early Drosophila Embryo May Extend the Dynamic Range of the Dorsal Gradient. *PLOS Comput. Biol.* **2015**, *11* (4), e1004159.

(65) Freeman, M. Feedback Control of Intercellular Signalling in Development. *Nature* **2000**, *408* (November), 313–319.

(66) Christian, J. L.; Nakayama, T. Can't Get No SMADisfaction: Smad Proteins as Positive and Negative Regulators of TGF-β Family Signals. *BioEssays* **1999**, *21* (5), 382–390.

(67) Gao, S.; Laughon, A. Decapentaplegic-Responsive Silencers Contain Overlapping Mad-Binding Sites. *J. Biol. Chem.* **2006**, *281* (35), 25781–25790.

(68) Dorfman, R.; Shilo, B. Z. Biphasic Activation of the BMP Pathway Patterns the Drosophila Embryonic Dorsal Region. *Development* **2001**, *128* (6), 965–972.

(69) O'Connor, M. B.; Umulis, D.; Othmer, H. G.; Blair, S. S. Shaping BMP Morphogen Gradients in the Drosophila Embryo and Pupal Wing. *Development* **2006**, *133* (2), 183–193.

(70) Wang, Y.; Ferguson, E. L. Spatial Bistability of Dpp – Receptor Interactions during Drosophila Dorsal – Ventral Patterning. **2005**, *702* (December 2004), 601–604.

(71) Gavin-Smyth, J.; Wang, Y. C.; Butler, I.; Ferguson, E. L. A Genetic Network Conferring Canalization to a Bistable Patterning System in Drosophila. *Curr. Biol.* **2013**, *23* (22), 2296–2302.

(72) Umulis, D. M.; Serpe, M.; O'Connor, M. B.; Othmer, H. G. Robust, Bistable Patterning of the Dorsal Surface of the Drosophila Embryo. *Proc. Natl. Acad. Sci. U. S. A.* **2006**, *103* (31), 11613–11618.

(73) Araujo, H.; Bier, E. Sog and Dpp Exert Opposing Maternal Functions to Modify Toll Signaling and Pattern the Dorsoventral Axis of the Drosophila Embryo. *Development* **2000**, *127* (16), 3631–3644.

(74) Carneiro, K.; Fontenele, M.; Negreiros, E.; Lopes, E.; Bier, E.; Araujo, H. Graded Maternal Short Gastrulation Protein Contributes to Embryonic Dorsal-Ventral Patterning by Delayed Induction. *Dev. Biol.* **2006**, *296* (1), 203–218.

(75) Fontenele, M.; Carneiro, K.; Agrellos, R.; Oliveira, D.; Oliveira-Silva, A.; Vieira, V.; Negreiros, E.; Machado, E.; Araujo, H. The Ca2+-Dependent Protease Calpain A Regulates Cactus/IκB Levels during Drosophila Development in Response to Maternal Dpp Signals. *Mech. Dev.* **2009**, *126* (8-9), 737–751.

(76) Fontenele, M.; Lim, B.; Oliveira, D.; Buffolo, M.; Perlman, D. H.; Schupbach, T.; Araujo, H. Calpain A Modulates Toll Responses by Limited Cactus/IκB Proteolysis. *Mol. Biol. Cell* **2013**, *24*, 2966–2980.

(77) Mizutani, C. M.; Meyer, N.; Roelink, H.; Bier, E. Threshold-Dependent BMP-Mediated Repression: A Model for a Conserved Mechanism That Patterns the Neuroectoderm. *PLoS Biol.* **2006**, *4* (10), e313.

2 Imaging the Dorsal-Ventral Axis of Live and Fixed *Drosophila melanogaster* Embryos*

* Adapted from Carrell, S. N.; Reeves, G. T. Imaging the Dorsal-Ventral Axis of Live and Fixed Drosophila Melanogaster Embryos. In *Tissue Morphogenesis*; Nelson, C. M., Ed.; Methods in Molecular Biology; Springer New York: New York, NY, 2015; Vol. 1189, pp 63–78.

2.1 Abstract

Optimal imaging conditions are of critical importance in developmental biology, as much of the data in the discipline is acquired through microscopy. However, imaging deep sections of tissue, especially live tissue, can be a technical challenge due to light scattering and difficulties in mounting the sample. In particular, capturing high-quality images of dorsal-ventral cross sections requires “end-on” mounting to orient the anterior-posterior axis vertically. Here we present methods to mount and image dorsal-ventral cross sections of both live and fixed *Drosophila melanogaster* embryos. Our methods have the advantages of being rapid, allowing deep optical sections, and not requiring expensive, specialized equipment.

2.2 Introduction

Confocal microscopy has become the gold standard in high-quality imaging, as researchers have begun to rely on fluorescent detection methods for quantitative imaging of molecular species *in situ*. However, confocal microscopy is light-limited, making it difficult to image deep into tissues with a sufficiently high signal-to-noise ratio due to scattering of light through the tissue. This problem is particularly challenging when studying phenomena with spatial variations along the dorsal-ventral (DV) axis, such as the Dorsal (dl) nuclear gradient or mesoderm spreading in the *Drosophila* embryo (*1*–*3*).

To capture the entire DV axis in a single image, a form of "end-on" mounting is required, in which the anterior-posterior axis is aligned with the z-axis of the microscope (*4*–*8*). However, this orientation can prove difficult to achieve due to geometry constraints (fruit fly embryos are egg-shaped). Previous work has circumvented this problem by imaging z-stacks of laterally-mounted embryos and computationally reconstructing the DV axis view (*9*–*12*). However, this technique was time intensive (approximately 45 minutes of imaging time per embryo (*9*)); light scattering problems beyond approximately 100 µm deep into the embryo degraded fluorescent signal; and image quality along the DV was lost at the mid-sagittal plane of the embryo due to poor *z*-axis resolution.

While many methods already exist for mounting *Drosophila* embryos to capture the full DV axis, they tend to be disadvantageous for several reasons (e.g., requiring lengthy time commitments and/or specialized equipment). For fixed embryos, microtome sections of plastic-embedded embryos provide precise cross sections but require more than a day's worth of preparation (for example, see (*13*,*14*)) and a good deal of manual carving with a razor blade. Recently, a microfluidic device has been developed to orient embryos end-on in a high-throughput fashion (*6*). This method is advantageous in that it allows users to quickly generate a large data set (>100 embryos in one experiment) (*15*) and to automate the imaging with a programmable xy-stage. However, this method is not available to most fly biologists, as highly-customized microfluidic equipment is required. Another potential drawback is the depth of tissue penetration; imaging deeper than 75 µm (~15%) into the embryo has not been demonstrated with this device (*6*,*15*–*18*), yet DV patterns have been reported to change significantly up to 150 µm from either pole (*8*,*15*). Fixed embryos have also been embedded in a gel that solidifies near room temperature, allowing for upright orientation of the embryos (*19*). This technique allows for approximately 10 embryos to be mounted simultaneously, and has the advantage of not requiring specialized equipment. While a minimum of 20 minutes is needed to solidify the jelly layer, an overnight incubation leads to better results. The maximum allowed depth of optical section with this technique is not clear.

There are also several techniques available for end-on mounting of embryos for live imaging. Witzberger and colleagues devised a polyacrylimide gel device to hold embryos upright (and also coined the term "end-on imaging") (*4*). This technique produced high-quality images of live embryos at a temporal resolution of 30 seconds. This technique had a further advantage in that approximately 20 embryos could be mounted simultaneously; however, device fabrication may prove a barrier to widespread use. Furthermore, the authors reported a loss in image quality past ~75 µm in tissue depth. Alternatively, embryos have been mounted upright on silicone-coated glass (*5*,*20*–*22*); however, this technique is fragile, in that small perturbations cause the embryo to tip over resulting in the consequence that only one embryo can be realistically mounted at once. The microfluidic array, and possibly the gel-embedding technique, may also be used to image live embryos, but are subject to the same drawbacks described above (*6*,*19*).

Here we present two methods to mount *Drosophila* embryos for direct DV axis imaging. For fixed embryos, we describe in detail a manual cross section technique, which has been used previously (*7*,*8*,*23*). This method has several advantages as compared to those described above. First, the manual cross-sectioning method is less time intensive than previous fixed-embryo methods. Once a researcher is familiar with the technique, up to 75 embryos may be prepared in an hour. Second, the method requires no equipment or special reagents beyond those which most *Drosophila* labs already have on hand. For live embryos, we describe a technique to adhere embryos to an upright, solid surface, similar to the mounting strategy used previously for imaging the DV axis using selective plane illumination microscopy (*8*). This method allows for imaging up to 200 µm into the embryo without prohibitive loss of fluorescent signal. The method has further advantages in that it requires very little manual skill, is rapid (taking less than 30 minutes), and allows for mounting several embryos in the same dish.

2.3 Materials

2.3.1 Manual Cross-sectioning

1. 70% glycerol: Combine 7 mL glycerol with 3 mL DI water in a 15 mL conical tube. Rock on a nutator for 10 minutes to ensure proper mixing. Alternately: vortex for 1 minute or until the viscosity appears consistent throughout the whole tube.

2. Hair loop: Attach a human hair in a small (2 mm diameter) loop to a 1000 µL pipette tip with tape (**Figure 2.1**).

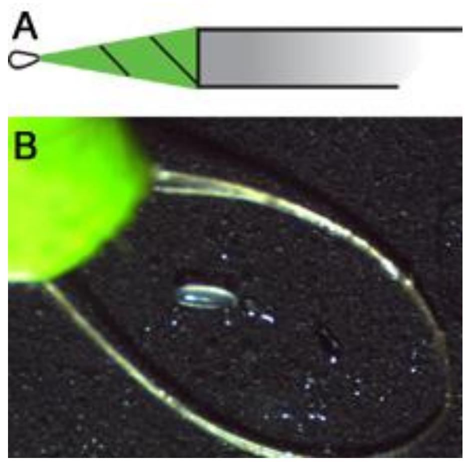

Figure 2.1: Hair loop. (A) Schematic of the hair loop. Tape is green for contrast. (B) Image of a loop around a Drosophila embryo for scale.

3. Razor blade: Single edge industrial no. 9
4. 22 mm coverslips
5. Dissecting microscope with black plate
6. 9-well glass dish
7. Double-sided tape

2.3.2 Mounting Living Embryos

The methods presented here are for use with an inverted confocal microscope. The mounting block has been optimized for use with a Zeiss LD C-Apochromat 40x NA 1.1 water immersion objective, with a working distance of 620 µm. However, the general technique of adhering embryos to a coverslip can also be applied to an upright microscope, or a light sheet microscope (*8*) *(see* **Note 1**).

1. Mesh basket
2. Bleach
3. Hair loop
4. Double-sided tape
5. Glass bottom petri dish: 35 mm diameter, 20 mm glass diameter, coverslip thickness #1.5 (or as recommended by objective manufacturer)
6. Mounting block: Have a machinist create a mounting block that fits the following parameters (**Figure 2.2**):

    Constraints:

    - The height must be highly precise: short enough to bring the embryos within the working distance of the objective but not so short that the embryos are smashed against the coverslip. For a 22 mm coverslip, a mounting block height of 21.5 mm is recommended (*see* **Note 2**).
    - One surface must be perfectly flat to allow a coverslip to be taped to it.
    - Material must be dense enough to not tip over when partially immersed in water.
    - Size must be small enough to sit inside petri dish.

- Once inside the petri dish, the geometry must be such that at least part of the flat side is above the well formed by the glass coverslip on the bottom of the petri dish, so that the coverslip can hang down into the well (**Figure 2.2**).
- Must be able to easily attach and remove double-sided tape.

7. Heptane glue: Cut several short pieces (5-10 cm) of double-sided tape and add them to a 200 mL bottle. Cover with heptane (approximately 1 mL per cm of tape) and shake the bottle gently overnight at room temperature to dissolve the adhesive from the tape (*24*).
8. Diamond scribe for glass etching
9. Sticky coverslip: using a diamond scribe, cut a 22 mm square coverslip roughly in half (*see* **Note 3**). Cover the bottom half of each half with about 10 μL of heptane glue and allow to dry for a minimum of 10 minutes.

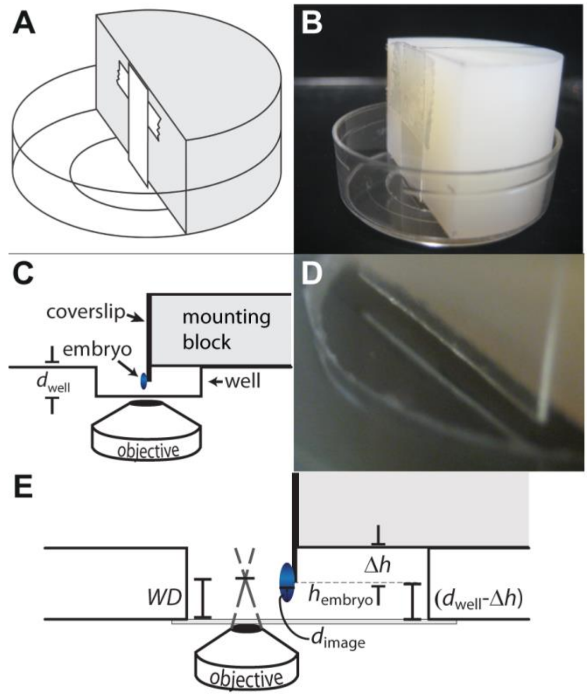

Figure 2.2: Live imaging mounting block. (A) Schematic of the mounting block. The coverslip is attached with a piece of double-sided tape. (B) Image of the mounting block/coverslip in a glass-bottom petri dish. (C) Imaging schematic. The coverslip should be precisely aligned with the top of the mounting block, suspending the embryos in the well. (D) Close-up of the coverslip in the well. Note that the coverslip should not touch the bottom of the well. (E) Close-up schematic of the well, with each of the heights required for calculating the height of the mounting block labeled.

2.4 Methods

2.4.1 Manual Cross-sectioning

Carry out all steps at room temperature (*see* **Note 4**). This procedure is written for a right-handed user. Left-handed users should use mirror-image orientations.

1. Prepare fixed embryos via immunostaining (*see* **Note 5**).
2. Transfer about 70 µL of embryos to one well of a glass dish (*see* **Notes 6 and 7**).

3. Under the microscope (using the black plate), select embryos that are appropriately aged for your application (approximately 100 embryos), and transfer them to the top left of a 22 mm coverslip (*see* **Note 8**).
4. Using an unmodified pipette tip, remove as much of the glycerol as possible, and return it to the glass well (*see* **Note 9**).
5. Use a rolled-up corner of a Kim wipe to remove as much of the remaining glycerol as possible (*see* **Note 10**).
6. Use a hair loop to manipulate an embryo away from the group (*see* **Note 11**) and orient it at a 20° angle (*see* **Note 12**) (**Figure 2.3**).

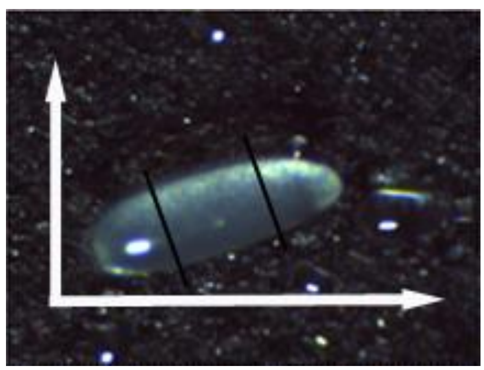

Figure 2.3: Angle for orienting the embryo for cross-sectioning. Black lines indicate where cuts should be made.

7. Use a razor blade to remove approximately 150 μm of tissue from the right end of the embryo (**Figure 2.4**). Be careful to ensure that the razor blade cuts straight down and entirely separates the two sections of tissue (*see* **Note 13**).

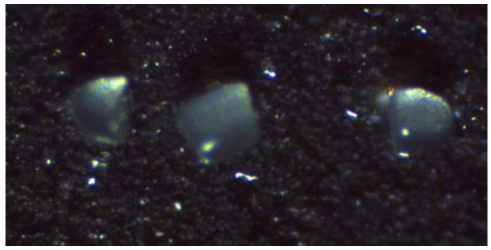

Figure 2.4: Properly cross-sectioned embryo. Each end is ~150 µm long, leaving 200 µm in the middle. Notice how the middle section is roughly square. Although one side of the cross-section is not perfectly perpendicular, this is an acceptable section. Simply orient the section so that the perpendicular side is down on the coverslip (see **Note 13**).

8. Re-orient the embryo if it moved during Step 7 and remove about 150 µm of tissue from the left end (*see* **Note 14**).
9. Carefully manipulate the cross-section away from the cut off sections and to the bottom right corner of the coverslip, at least 2 mm from the bottom and right edges (*see* **Note 15**).
10. Using a hair loop, manipulate the cross-section so that it is standing straight up.
11. Repeat until all embryos are cross-sectioned, aligning them in three columns, approximately 0.5 mm apart from one another (**Figure 2.5**) (*see* **Note 16**).
12. Put two layers of double-sided tape down on a microscope slide. Put another two layers of double-sided tape down about 2 cm from the first set (*see* **Note 17**).
13. Carefully pick up the coverslip with the cross sectioned embryos on it. Place it embryo-side down on the double-sided tape so that both edges are adhered to the

tape but none of the cross-sections are in the tape (**Figure 2.5**). Press down on the sides to ensure proper adhesion (*see* **Note 18**).

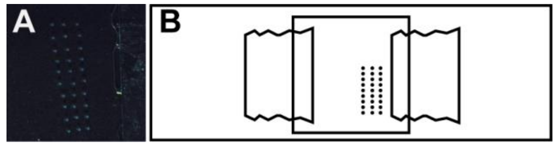

Figure 2.5: Mounted cross-sections . (A) Properly mounted cross-sections. (B) Schematic of the whole slide.

14. Pipette 50-70 µL of 70% glycerol under the coverslip, adding it slowly and all from one edge. Add enough to fill the space between the slide and the coverslip but no more (*see* **Note 19**).
15. While imaging cross-sections, be sure to focus below the level of tissue that has been damaged by the razor blade (**Figure 2.6**). Typical images obtained from this technique are shown in **Figure 2.7**.

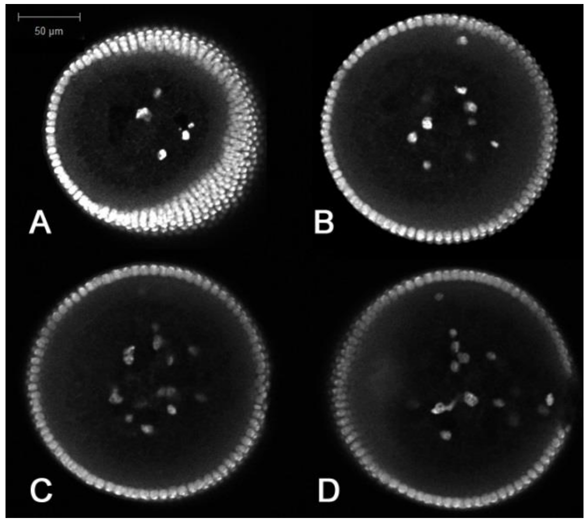

Figure 2.6: Manual cross-sectioning damages the tissue. Images should be taken at a z-depth in between the damaged portions of tissue. (A) The portion closest to the coverslip shows evidence of crushing by the razor blade, as evidenced by the visibility of more than one row of nuclei. (B) Tissue further from the coverslip still shows some signs of damage, particularly in the double row of nuclei visible on the right side. (C) When at an appropriate z-depth, the tissue will appear circular and have no visible marring. (D) The portions furthest from the coverslip also show signs of damage from the razor blade. Nuclei stained with DAPI.

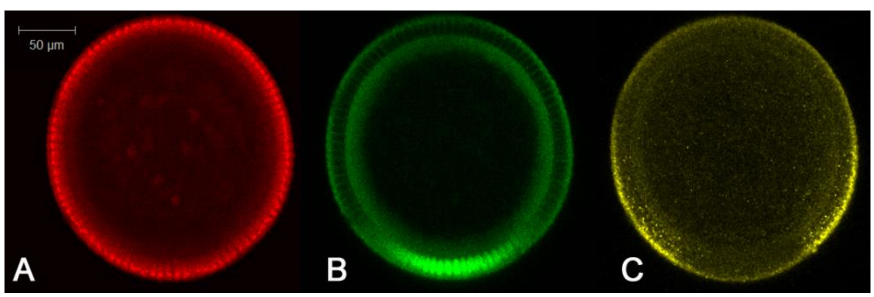

Figure 2.7: Typical images of a cross-sectioned embryo. (A) Nuclei are marked with anti-histone. (B) The protein Dorsal appears in a nuclear gradient that peaks at the ventral midline. (C) sog mRNA appears in the ventro-lateral portion of the embryo. Images are oriented so that ventral is down.

2.4.2 Mounting Live Embryos

This method has been optimized for a 40x N.A. 1.1 water immersion objective mounted on a Zeiss LSM 710 inverted confocal microscope.

1. Anesthetize an appropriate number of flies and transfer them to a collection cage several days before imaging will take place (*see* **Note 20**). Streak a small amount of yeast paste onto a grape juice agar plate, and change the plate daily until ready for imaging.
2. Anesthetize the flies in the cage and allow them to lay embryos for 1-2 hours (*see* **Note 21**).
3. Introduce a new plate streaked with yeast paste to the cage, and allow the flies to lay embryos for 30-45 minutes (*see* **Note 22**). Age the embryos to 30 minutes shy of the desired developmental stage (*see* **Note 23**).
4. Brush embryos from grape juice agar plate into a mesh basket using a paint brush and DI water (*see* **Note 24**).
5. Dechorionate embryos using either option A (dechorionation in bleach) or option B (manual dechorionation) (*24*).

    A. Dechorionation with bleach and embryo selection

    1. Submerge the basket of embryos in 100% bleach for 30 seconds (*see* **Note 25**).
    2. Rinse well with DI water.

3. Remove mesh from basket. Place the mesh onto the now-clean grape juice agar plate (*see* **Note 26**).
4. Select embryos of the desired stage for mounting (*see* **Note 27**).

B. Manual dechorionation and embryo selection

1. Using a brush, transfer embryos from mesh onto a plate with transparent agar or agarose. Cover embryos with a small amount of halocarbon oil (*see* **Note 28**).
2. Using transmitted illumination, select approximately 10-15 embryos of the appropriate stage.
3. Using a brush, transfer the selected embryos to a clean agar gel plate, transferring as little oil as possible.
4. With a hair loop, roll embryos on the clean agar gel to remove as much oil as possible.
5. Place a strip of double-sided tape on a microscope slide.
6. Using a brush, transfer embryos one-by-one to the double-sided tape.
7. With the hair loop, gently roll each embryo until the chorion is removed by the tape.
8. After the chorion is removed from an embryo, transfer it back to a clean agar gel plate to keep it in a moist environment (*see* **Note 29**).

6. Using a hair loop, transfer embryos from agar plate to sticky coverslip (*see* **Note 30**). Embryos will naturally cling to the hair loop, although it may take several tries to pick one up. Orient each embryo perpendicular to the bottom of the coverslip. Place each embryo so that approximately half of embryo is on the coverslip and half is hanging off (*see* **Note 31**). Repeat until the desired number of embryos has been mounted (*see* **Note 32**).
7. Carefully adhere a piece of double-sided tape to the back of the coverslip (the side without the embryos).
8. Adhere the coverslip to the mounting block so that the top of the coverslip is exactly in line with the top of the mounting block (*see* **Note 33**). The embryos will be hanging off the bottom. See **Section 2.3.2** for a description of how to design the mounting block.
9. Put a small amount of DI water into a glass-bottom petri dish (*see* **Note 34**). Gently place the mounting block into the water so that the embryos are submerged.
10. Carefully transfer the glass-bottom dish/mounting block to the microscope and begin collecting images. See **Figure 2.8** and **Figure 2.9** for example images obtained using this method.

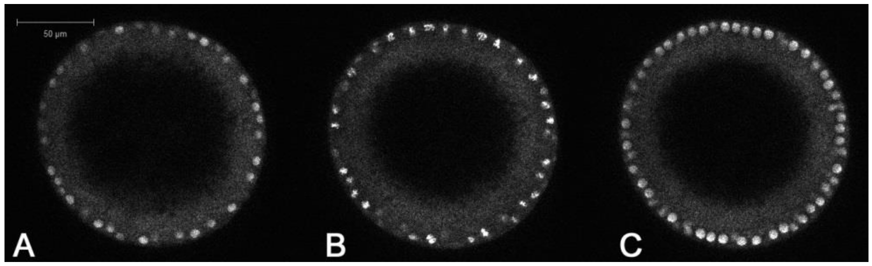

Figure 2.8: Sample images obtained from a live embryo expressing a histone::RFP fusion protein at different development times. (A) Nuclear cycle 11. (B) Mitosis between nuclear cycles 11 and 12. (C) Nuclear cycle 12. Images are taken 10 minutes apart and ~100 µm from the tip of the embryo.

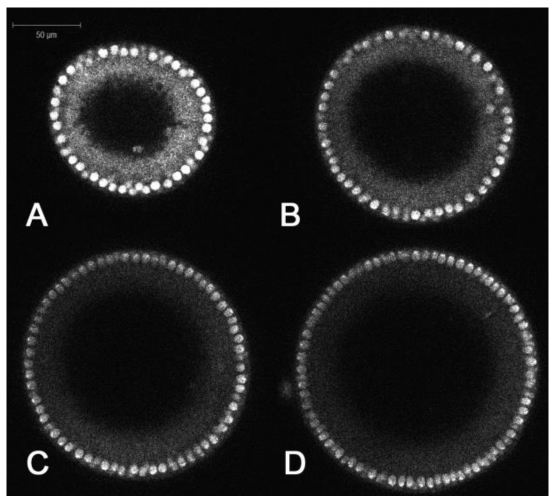

Figure 2.9: Sample images obtained from a live embryo expressing a histone::RFP fusion protein at different depths (A) 50 µm, (B) 100 µm, (C) 150 µm, and (D) 200 µm from the tip of the embryo.

2.5 Notes

1. For other microscope geometries, using heptane glue to adhere embryos to a coverslip is still a useful technique. For upright microscopes, the coverslip must be shorter than the depth of the petri dish used (so that the embryos are covered with

water), and it must be adhered to a short mounting block (so that the coverslip is vertical). The design of the mounting block has very little constraint: it just must be small enough to fit in the dish, it must be dense enough not to tip over when fully submerged in water, and it must have a flat surface for the coverslip to be adhered to. Also, the embryos must be oriented facing up off of the coverslip, and a water-dipping objective is necessary. For light sheet microscopes, the coverslip can be adhered to a block attached to the mounting rod, and embryos should face horizontally off of the coverslip with their AP axis aligned with the z-axis of the imaging objective.

2. The two tightest constraints are (1) that one side must be perfectly flat, and (2) that its height must be a precise amount shorter than the height of the coverslip so that, aligning one end of the coverslip with the top of the mounting block causes the embryos to hang down into the well far enough to be imaged (**Figure 2.2**). The bounds on the height of the mounting block (h_{block}) are determined by a combination of the height of the coverslip ($h_{\mathrm{coverslip}}$), the depth of the well (d_{well}), the portion of the embryo that hangs off the coverslip (h_{embryo}), the desired depth of imaging (d_{image}), and the working distance of the objective lens (WD). If $\Delta h \equiv h_{\mathrm{coverslip}} - h_{\mathrm{block}}$, then:

$$d_{\mathrm{well}} - \Delta h > h_{\mathrm{embryo}}, \text{ and}$$

$$d_{\mathrm{well}} - \Delta h - h_{\mathrm{embryo}} + d_{\mathrm{image}} < WD$$

For our purposes, we had d_{well} = 1 mm, h_{embryo} ~ 250 µm, d_{image} ~ 200 µm, and *WD* = 620 µm. For those numbers, Δ*h* = 0.5 mm worked well, and since $h_{coverslip}$ = 22 mm, we had the mounting block machined to a height of $h_{coverslip}$ = 21.5 mm.

3. A half coverslip is used so that it will fit into the 20 mm diameter well. If the imaging dish has a larger well, or smaller coverslips are available, a whole coverslip may be used.
4. Some researchers find the embryos easier to see in a darkened room.
5. Immunostaining performed according to an established procedure, omitting the Proteinase K step (*25*). Embryos not being prepared should be stored at -20°C and in the dark to prevent loss of fluorescence.
6. To prevent damaging embryos while transferring them, it may be helpful to clip a pipette tip (using scissors) to make a wider opening.
7. This step is optional. Some researchers find this step limits the amount of glycerol that gets placed on the coverslip. It also enables researchers to more accurately select embryos that are the desired age.
8. Embryos are cross-sectioned on the coverslip so that the tissue is as close to the objective as possible due to variability in the height of the cross-sections produced.
9. Some embryos may be removed with the glycerol. This is not an issue. Simply return them to the glass plate with the glycerol. Cover the glass plate with something (an

empty pipette tip box works well) to protect the leftover embryos from light while you cross-section the others.

10. Depending on how much glycerol remains on the coverslip, all four corners of a Kim wipe may be necessary. Excess glycerol allows the embryo to slide on the glass, which can cause the razor blade to slide off the embryo, so it helps to remove as much as possible before attempting to cross-section. However, Kim wipes can leave fibers on the coverslip that can lead to errors in image analysis. If any fibers appear, ensure that they are removed from the area closest to the cross-sectioned embryos.
11. Two or even three similarly-sized embryos may be cross-sectioned at the same time.
12. The angle at which the embryo is oriented is up to the user, so long as it is comfortable to hold the blade perpendicular to the embryo. Embryos are not aligned horizontally because the razor blade blocks the view of the embryo during the cross-sectioning process. If it is difficult to manipulate the embryo, the coverslip may also be rotated, taking care to prevent any previously cross-sectioned embryos from being in line with where the cuts will be made.
13. Straight edges are important for proper imaging. If the tissue sticks to the razor blade, gently set the blade down on the coverslip and use a hair loop to slide it off. It may be easier to cut a straight edge by resting the far edge of the razor blade on the coverslip, then pressing forward towards the embryo. If a cross-section has one side that is perfectly perpendicular to the axis of the embryo and one that is not (as seen

in **Figure 2.4**), orient the embryo so that the perpendicular side is down on the coverslip so that images taken are from a proper DV cross-section.

14. Due to the variance in some gradients, particularly the nuclear gradient of Dorsal, that occurs at the anterior and posterior ends, the desired size of a cross-section is 200 µm, a little bigger than the middle third. The cross-section should look similar to a square at this point, since the diameter of the embryo is also ~200 µm. Sections that are "too tall" will be smashed by the coverslip. Sections that are too short may not have a sufficient amount of undamaged tissue for imaging.
15. The unwanted sections of embryo tissue can be moved to the lower left corner of the coverslip (the "graveyard"), along with any embryos that are not suitable for cross-sectioning due to age or other defect.
16. Any configuration will do, but it is easier to image the embryos when they are neatly arranged.
17. Each layer of double-sided tape is approximately 100 µm thick, so two layers of tape will prevent the coverslip from crushing the 200 µm tall cross-sections.
18. Ensure that the double-sided tape layers lay flat on the microscope slide; any unevenness in the tape layers can cause irregular adherence of the coverslip and subsequent loss of the cross-sections during the next step. The blunt end of a paintbrush works particularly well to adhere the coverslip to the tape. The "graveyard" can be put on the tape.

19. Be careful not to add too much glycerol. If cross-sections "float away" during this step, they may be too short. If many of the cross-sections have been knocked over or appear compressed in the z-direction, they may be too tall.
20. Allowing the flies time to acclimate to the cage seems to lead to better laying.
21. Anesthetizing the flies and allowing them to lay embryos for a short period of time clears the females of any embryos they have not yet laid, ensuring the collection will consist of more precisely aged embryos.
22. The length of the embryo collection period can vary depending on how many flies are present in the cage and the window of desired initial developmental stage of the embryos to be imaged.
23. The remaining steps require about 30 minutes to complete by a researcher who is comfortable with the technique. For new users, it is recommended to allow 45 minutes to 1 hour, since it is better to have to wait some time for the desired developmental stage than to miss it completely.
24. Flies often lay embryos in the yeast paste, so it is important to rinse the yeast paste into the basket as well.
25. The amount of time can vary from 10-40 seconds. Start with the shortest time possible; if the chorion is still present on most embryos, increase this time by 10 second intervals until most embryos appear fully dechorionated. Bleaching the

embryos for too long can lead to decreased viability. We find that 30 seconds is the optimal time.

26. The embryos need to be kept moist to ensure survival; however, embryos will be difficult to manipulate if the surface of the plate is too damp. If DI water remains after the previous step, remove it with a paper towel.
27. After dechorionation, some embryo morphology can be seen, allowing for selection of the proper stage.
28. The halocarbon oil clarifies the chorion. With transmitted light, some embryo morphology can be seen, allowing for selection of the proper stage.
29. As an alternative to using several agar gel plates, one can cut out several sections (one for the halocarbon oil, one for removing the oil, and one for keeping embryos moist after dechorionation) of one plate.
30. This step is critical to the success of the live imaging experiment, so pay careful attention while carrying it out. It will likely take several tries before one is fully comfortable with the method of transferring and orienting embryos. It may be helpful in moving embryos to coat the hair loop in a small amount of heptane glue by rolling it over the surface of the coated coverslip. We find it easier to pick up an embryo with the hair loop so that part of the embryo extends outside the hair loop to allow for proper positioning on the coverslip.

31. It is possible to reorient the embryos once they have been placed on the coverslip, but due to the sticky nature of the heptane glue, they may burst if moved too much. Up to 2/3 of the embryo length may be suspended off the end of the coverslip.
32. The number of embryos mounted is dependent on the user, keeping in mind that it is only possible to image one embryo at a time. It is recommended to mount an excess of embryos to ensure that at least one is the appropriate age and in the appropriate (precisely upright) position.
33. Because the tape is more strongly adhered to the coverslip, it is possible to re-orient the coverslip on the device if it is not perfectly straight. Also, depending on the size of the well, it may be necessary to ensure that the coverslip is attached precisely in the middle of the device.
34. Be careful not to over-fill the petri dish, as the mounting block will take up a lot of volume.

2.6 References

(1) Moussian, B.; Roth, S. Dorsoventral Axis Formation in the Drosophila Embryo--Shaping and Transducing a Morphogen Gradient. *Curr. Biol.* **2005**, *15* (21), R887–R899.

(2) Reeves, G. T.; Stathopoulos, A. Graded Dorsal and Differential Gene Regulation in the Drosophila Embryo. *Cold Spring Harb. Perspect. Biol.* **2009**, *1* (4), a000836.

(3) Leptin, M. Gastrulation Movements: The Logic and the Nuts and Bolts. *Dev. Cell* **2005**, *8* (3), 305–320.

(4) Witzberger, M. M.; Fitzpatrick, J. A. J.; Crowley, J. C.; Minden, J. S. End-on Imaging: A New Perspective on Dorsoventral Development in Drosophila Embryos. *Dev. Dyn.* **2008**, *237* (11), 3252–3259.

(5) DeLotto, R.; DeLotto, Y.; Steward, R.; Lippincott-Schwartz, J. Nucleocytoplasmic Shuttling Mediates the Dynamic Maintenance of Nuclear Dorsal Levels during Drosophila Embryogenesis. *Development* **2007**, *134* (23), 4233–4241.

(6) Chung, K.; Kim, Y.; Kanodia, J. S.; Gong, E.; Shvartsman, S. Y.; Lu, H. A Microfluidic Array for Large-Scale Ordering and Orientation of Embryos. *Nat. Methods* **2011**, *8* (2), 171–176.

(7) Trisnadi, N.; Altinok, A.; Stathopoulos, A.; Reeves, G. T. Image Analysis and Empirical Modeling of Gene and Protein Expression. *Methods* **2012**.

(8) Reeves, G. T.; Trisnadi, N.; Truong, T. V; Nahmad, M.; Katz, S.; Stathopoulos, A. Dorsal-Ventral Gene Expression in the Drosophila Embryo Reflects the Dynamics and Precision of the Dorsal Nuclear Gradient. *Dev. Cell* **2012**, *22* (3), 544–557.

(9) Liberman, L. M.; Reeves, G. T.; Stathopoulos, A.; Liberman, Louisa M, Gregory T Reeves, A. S. Quantitative Imaging of the Dorsal Nuclear Gradient Reveals Limitations to Threshold-Dependent Patterning in Drosophila. *PNAS* **2009**, *106* (52), 22317–22322.

(10) Luengo Hendriks, C. L.; Keränen, S. V. E.; Fowlkes, C. C.; Simirenko, L.; Weber, G. H.; DePace, A. H.; Henriquez, C.; Kaszuba, D. W.; Hamann, B.; Eisen, M. B.; et al. Three-Dimensional Morphology and Gene Expression in the Drosophila Blastoderm at Cellular Resolution I: Data Acquisition Pipeline. *Genome Biol.* **2006**, *7* (12), R123.

(11) Keränen, S. V. E.; Fowlkes, C. C.; Luengo Hendriks, C. L.; Sudar, D.; Knowles, D. W.; Malik, J.; Biggin, M. D. Three-Dimensional Morphology and Gene Expression in the Drosophila Blastoderm at Cellular Resolution II: Dynamics. *Genome Biol.* **2006**, *7* (12), R124.

(12) Fowlkes, C. C.; Hendriks, C. L. L.; Keränen, S. V. E.; Weber, G. H.; Rübel, O.; Huang, M.; Chatoor, S.; DePace, A. H.; Simirenko, L.; Henriquez, C.; et al. A Quantitative Spatiotemporal Atlas of Gene Expression in the Drosophila Blastoderm. *Cell* **2008**, *133* (2), 364–374.

(13) Hemavathy, K.; Meng, X.; Ip, Y. T. Differential Regulation of Gastrulation and Neuroectodermal Gene Expression by Snail in the Drosophila Embryo. *Development* **1997**, *124* (19), 3683–3691.

(14) McMahon, A.; Supatto, W.; Fraser, S. E.; Stathopoulos, A. Dynamic Analyses of Drosophila Gastrulation Provide Insights into Collective Cell Migration. *Science (80-.).* **2008**, *322* (5907), 1546–1550.

(15) Kanodia, J. S.; Kim, Y.; Tomer, R.; Khan, Z.; Chung, K.; Storey, J. D.; Lu, H.; Keller, P. J.; Shvartsman, S. Y. A Computational Statistics Approach for Estimating the Spatial Range of Morphogen Gradients. *Development* **2011**, *138* (22), 4867–4874.

(16) Kim, Y.; Andreu, M. J.; Lim, B.; Chung, K.; Terayama, M.; Jiménez, G.; Berg, C. a; Lu, H.; Shvartsman, S. Y. Gene Regulation by MAPK Substrate Competition. *Dev. Cell* **2011**, *20* (6), 880–887.

(17) Kanodia, J. S.; Liang, H.-L.; Kim, Y.; Lim, B.; Zhan, M.; Lu, H.; Rushlow, C. a; Shvartsman, S. Y. Pattern Formation by Graded and Uniform Signals in the Early Drosophila Embryo. *Biophys. J.* **2012**, *102* (3), 427–433.

(18) Helman, A.; Lim, B.; Andreu, M. J.; Kim, Y.; Shestkin, T.; Lu, H.; Jiménez, G.; Shvartsman, S. Y.; Paroush, Z. RTK Signaling Modulates the Dorsal Gradient. *Development* **2012**, *139* (16), 3032–3039.

(19) Belu, M.; Javier, M.; Ayasoufi, K.; Frischmann, S.; Jin, C.; Wang, K.-C.; Sousa-Neves, R.; Mizutani, C. M. Upright Imaging of Drosophila Embryos. *J. Vis. Exp.* **2010**, No. 43, 1–5.

(20) Kanodia, J. S.; Rikhy, R.; Kim, Y.; Lund, V. K.; DeLotto, R.; Lippincott-Schwartz, J.; Shvartsman, S. Y. Dynamics of the Dorsal Morphogen Gradient. *Proc. Natl. Acad. Sci. U. S. A.* **2009**, *106* (51), 21707–21712.

(21) Mavrakis, M.; Rikhy, R.; Lilly, M.; Lippincott-Schwartz, J. Fluorescence Imaging Techniques for Studying Drosophila Embryo Development. *Curr. Protoc. Cell Biol.* **2008**, *Chapter 4*, Unit 4.18.

(22) Daniels, B. R.; Rikhy, R.; Renz, M.; Dobrowsky, T. M.; Lippincott-schwartz, J. Multiscale Diffusion in the Mitotic Drosophila Melanogaster Syncytial Blastoderm. *Proc. Natl. Acad. Sci. U. S. A.* **2012**, *109* (22), 8588–8593.

(23) Grosshans, J.; Wieschaus, E. A Genetic Link between Morphogenesis and Cell Division during Formation of the Ventral Furrow in Drosophila. *Cell* **2000**, *101* (5), 523–531.

(24) Supatto, W.; McMahon, A.; Fraser, S. E.; Stathopoulos, A. Quantitative Imaging of Collective Cell Migration during Drosophila Gastrulation: Multiphoton Microscopy and Computational Analysis. *Nat. Protoc.* **2009**, *4* (10), 1397–1412.

(25) Kosman, D.; Mizutani, C. M.; Lemons, D.; Cox, W. G.; McGinnis, W.; Bier, E. Multiplex Detection of RNA Expression in Drosophila Embryos. *Science (80-.).* **2004**, *305* (5685), 846.

3 Effects of Dorsal and Cactus Dosage on the Dorsal Nuclear Gradient

3.1 Introduction

The maternal transcription factor Dorsal (dl), homologous to mammalian NF-κB, patterns the DV axis of the developing *Drosophila melanogaster* embryo (*1*,*2*). The IκB homolog Cactus (Cact) binds to Dorsal, retaining it outside the nuclei (*3*). On the ventral side of the embryo, Toll signaling phosphorylates the Dorsal/Cactus complex, causing Cactus to be degraded and allowing Dorsal to enter the nuclei, where it regulates gene expression (*4*–*6*). This regulation results in a nuclear gradient of Dorsal that peaks at the ventral midline and decays to approximately 40% of the embryo's circumference (See **Figure 3.1A**). As shown in **Figure 3.1B**, different genes are turned on at different concentrations of Dorsal. The domains of these genes can be quantified using values for dorsal border (s_D) and ventral border (s_V) (**Figure 3.1C**). For a more detailed description of Dorsal and its regulation, see **Chapter 1**.

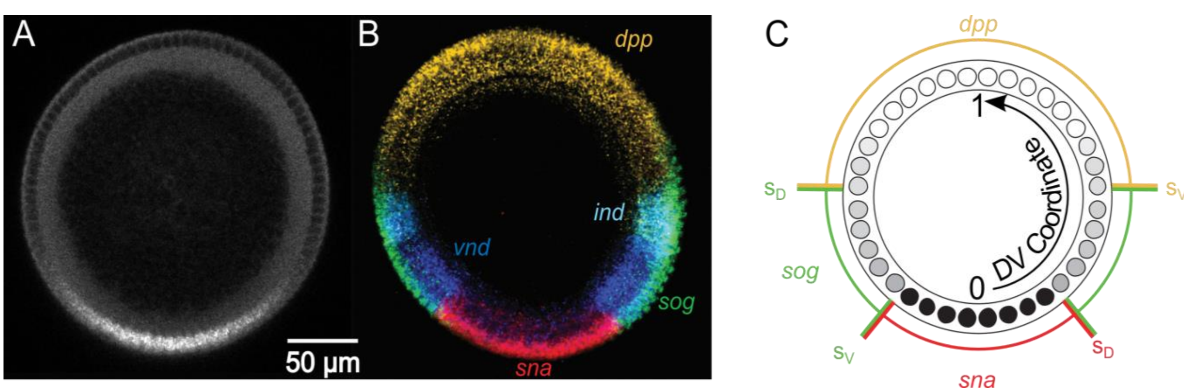

Figure 3.1: The protein Dorsal patterns the DV axis of the *Drosophila* embryo. (A) An antibody staining against Dorsal. (B) mRNA expression of a variety of Dorsal target genes. (C) We use the parameters s_D (dorsal border) and s_V (ventral border) to quantify and compare the extent of domain of dl target genes. Because *sna* represses *sog*, s_D *sna* ~= s_V *sog*. Embryo cross-sections are oriented so that ventral is down. Adapted from (*4*).

Researchers have observed an interesting, previously unexplained phenomenon when studying Dorsal heterozygotes (embryos with a half wild type dose). These embryos have gradients which are shorter than normal (as expected); however, they are also wider and flatter at the peak (*7*). Despite these differences, and the fact that Dorsal concentration sets the borders of genes crucial to proper development, female flies with a half dose of Dorsal produce viable progeny. We studied embryos from mothers with *dorsal* dosages of 1x, 2x, 3x, and 4x. Canonical mutations dl^{1} and dl^{4} were used to reduce the *dorsal* dosage. Increased *dorsal* dosage was achieved by using BAC-recombineered rescue constructs dl^{RC} and $dl^{RC\text{-}2}Dr$ (*8*). With these fly lines, we were able to study the effect of Dorsal dose in embryos with combinations of endogenous and exogenous Dorsal.

Since the protein Cactus regulates Dorsal’s entry into the nucleus, we also investigated the effect of *cactus* dose on the nuclear Dorsal gradient. We analyzed embryos from mothers with 1x, 2x, and 4x doses of *cactus*. Canonical mutations $cact^{1}$ and $cact^{4}$ were used to reduce the dosage. A BAC-recombineered *cactus-cherry* fusion, kindly provided by the Stathopoulos lab, was used to increase the dosage.

Our investigation furthered the work of previous researchers who calculated the ratio of *dorsal* to *cactus* that enabled proper development (*9*). They found that embryos with a double wild type dose of *dorsal* (4x) developed properly, while any increase in dose led to phenotypes similar to those observed when *cactus* dose is reduced. Furthermore, embryos with one copy of *cactus* and three of *dorsal* were viable, while any increase in the

1:3 ratio led to ventralization. These results informed our decisions of which fly lines could be studied.

3.2 Results and Discussion

3.2.1 **dorsal *dosage***

As previously reported, a half maternal dose of *dorsal* significantly shortens and widens the embryonic nuclear gradient (*7*,*10*,*11*). Furthermore, this gradient is not as sharply peaked as the wild type, having a flat top. We have repeated this experiment, with the results presented in **Figure 3.2A** and **D**. In this study, we used the canonical mutation dl^{4} and a "cleaned up" version of the dl^{1} mutation, $dl^{1.2.5}$, which was generated by crossing flies with the mutated chromosome with flies with a wild type chromosome, then sorting their progeny for homozygous female sterility. In this way, we hoped to eliminate any other deleterious mutations present on the dl^{1} chromosome, which was generated via random mutation with ethyl methanesulfonate. To increase the maternal *dorsal* dose, we used previously-generated rescue constructs (*8*). See **Table 3.1** for a detailed description of the lines used, the abbreviated name used throughout this document, and the copy number of endogenous, exogenous, and total Dorsal. The chromosome $dl^{RC\text{-}2}Dr$ was generated so that we could ensure that all embryos from this line came from mothers with three copies of *dorsal* (as the gene *Dr* is homozygous lethal) without having to separate the adults into two populations.

Table 3.1: List of fly lines used in dl dosage experiments. All information is presented as [genotype second chromosome]; [genotype third chromosome]. dl- on the second chromosome indicates a loss-of-function allele; dl+ on the third chromosome indicates a gain-of-function allele; and a single + indicates a wild type chromosome. When only one label is present, the genotype is homozygous. $dl^{RC\text{-}2}Dr$ is a chromosome carrying the dorsal rescue construct that has been recombined with the allele Drop (Dr).

Abbrev.	End. dl	Ex. dl	Total dl	Line
dl-/+	1	0	1	$dl^{1.2.5}$/CyO; PrDr/TM3
wt	2	0	2	yw
dl-/+; dl+/+	1	1	2	dl^{4}/CyO; $dl^{RC\text{-}2}$Dr/TM3
dl-; dl+	0	2	2	$dl^{1.2.5}$; dl^{RC}
+; dl+/+	2	1	3	sp/CyO; $dl^{RC\text{-}2}$Dr/TM3
+; dl+	2	2	4	sp/CyO; dl^{RC}

Because the dl gradient varies in amplitude (A) and basal levels (B) over time while the width parameter σ is conserved, we use width as our measure for comparing different genotypes (*8*,*12*,*13*). Furthermore, A and B can vary from experiment to experiment due to slight variations in protocol and microscope settings, including laser drift. Since we have combined data from several experiments, we opted to analyze only parameters which are not so dependent on exactness of protocol.

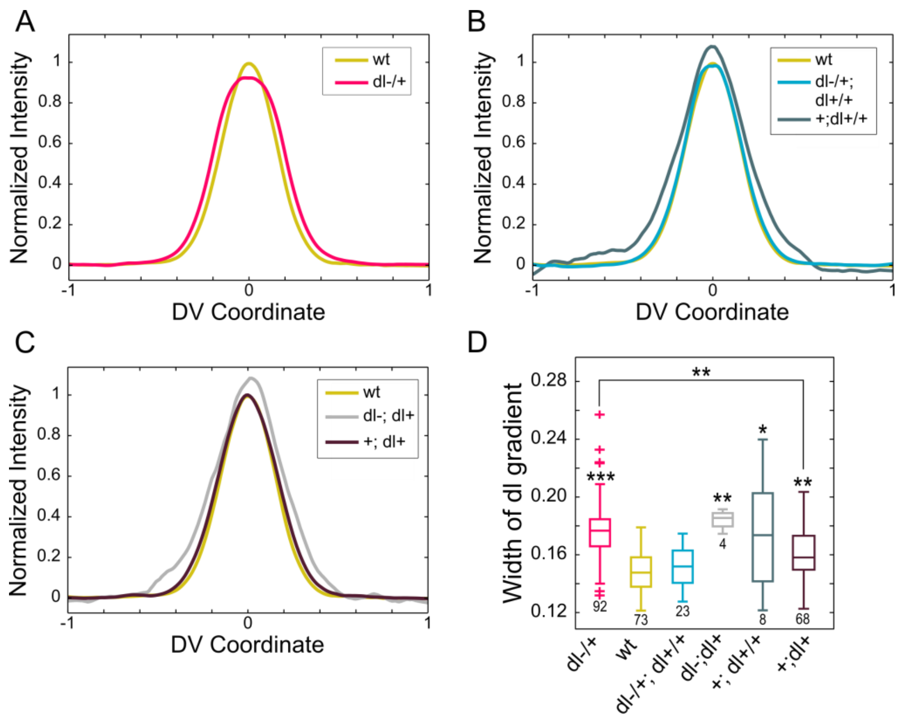

Figure 3.2: Varying the maternal Dorsal dose influences the embryonic nuclear gradient. (A) Normalized Dorsal gradient in embryos from mothers with 2 (wt) and 1 (dl-/+) copies of Dorsal. (B) Normalized Dorsal gradient in embryos from mothers with 2 (wt, dl-/+; dl+/+) and 3 (+; dl+/+) copies of Dorsal. Note that the gradients from mothers with 2 copies of Dorsal are indistinguishable from one another. (C) Normalized Dorsal gradient in embryos from mothers with 2 (wt, dl-; dl+) and 4 (+; dl+) copies of Dorsal. (D) Boxplot of the width of the Dorsal gradient in the genotypes shown in (A-C). Asterisks indicate statistical significance (* $p<0.05$, ** $p<10^{-5}$, ***$p<10^{-10}$) from wt unless otherwise noted. Plus signs indicate statistical outliers. Values below the boxes indicate sample size.

As expected, embryos from mothers with 1 copy each of endogenous and exogenous *dorsal* had gradients that were indistinguishable from wild type (See **Figure 3.2B,D**). This result lends support to our assumption that the dl^{RC} locus is regulated similarly to the native locus. Curiously, embryos from mothers with two copies of exogenous *dorsal* but no endogenous copies had gradients that were statistically wider than wild type, despite having the proper copy number. Due to the small number of samples, this experiment should be repeated to determine whether this finding is accurate.

Since lowering the *dl* dose widened the resulting nuclear gradient, it may be expected that increasing the dose would narrow it. However, our research showed the opposite: that increasing *dl* dose to 3 or 4 copies significantly widened the gradient (**Figure 3.2B-D**). This result indicates that there could be feedback or saturation mechanisms in place during development to regulate the *Drosophila* Dorsal gradient. For a more detailed discussion on this subject, see **Chapter 5**.

While we analyzed the effect of *dl* dosage on three dl target genes (*sna*, *sog*, and *dpp*, see **Figure 3.1**), we found that the only gene with statistically different border placement, as quantified by s_D and s_V, is *sog*, which is the only gene we will be discussing. Curiously, *sna* sets the ventral border of *sog*, so we would expect to see similar variance for s_V *sog* and s_D *sna*. We expect that this minor discrepancy is due to the low number of embryos stained for *sna* (~40 total) versus *sog* (~150 total). In fact, the p-value obtained from the t-test between s_D *sna* in wt *and dl-/+* embryos is 0.09, which indicates a 91% probability that the two samples are different. We have found that a sample size of 15 embryos per genotype is suitable for accurate statistical analysis, so with only about 10 embryos per genotype, it is not unreasonable to expect that increasing N would decrease the p-value below 0.05, the standard threshold for statistical significance. Furthermore, the *sog* border refines over time as *sna* expression increases (*8*). When this information is taken into account, we do not find the slight statistical discrepancy between the borders of *sog* and *sna* to be problematic.

In our experiments, we found that the *sog* domain varied from wild type in only two genotypes: *dl-/+* (1x *dl*) and *+; dl+* (4x *dl*). Since both genotypes widened the dl gradient, it might be expected that the ventral border of the *sog* domain would move dorsally (increased s_V) in both cases. We found this analysis to hold true only for the 4x *dl* embryos, as s_V shrank in the 1x *dl* embryos (**Figure 3.3A,B**). We expect that this shrinking effect could be due to differences in the absolute level of dl since the width parameter only accounts for the relative level. Because gene expression presumably relies on the absolute concentration of dl, a wider gradient could specify a narrower *sna* domain if the gradient were also shorter in amplitude. However, as mentioned previously, there is wide variation in amplitude from embryo to embryo, which makes it difficult to determine whether differences are due to noise or signal. This apparent discrepancy may also occur because we are modeling a non-Gaussian shape (the flatter dl heterozygote gradient) as a Gaussian.

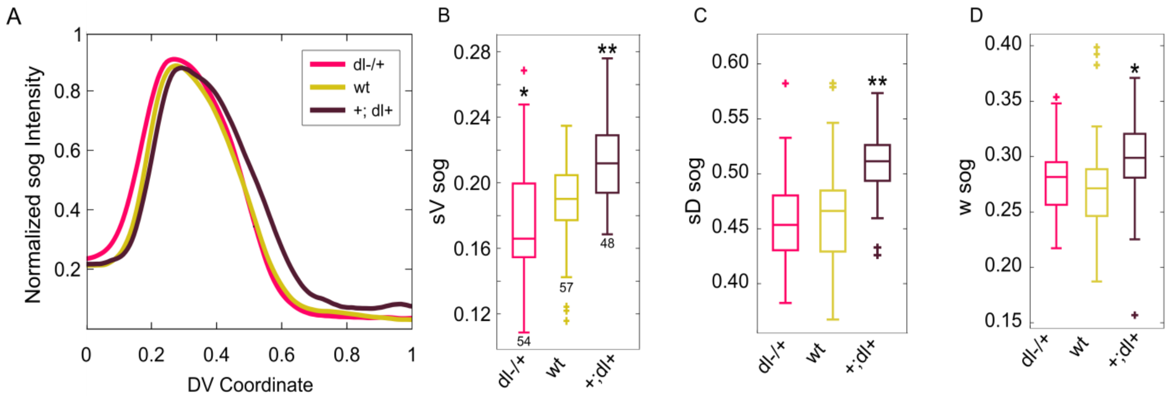

Figure 3.3: The *sog* domain changes with maternal *dorsal* dose. (A) Normalized *sog* expression pattern in embryos from mothers with 1 (*dl-/+*), 2 (wt), and 4 *(+; dl+*) copies of *dorsal*. (B) Boxplot of the ventral border of *sog*. (C) Boxplot of the dorsal border of *sog*. (D) Boxplot of the width of the domain of *sog*, equivalent to s_D - s_V. Note: The same data set was used to generate all four figures. Asterisks indicate statistical significance (* $p<0.05$, ** $p<10^{-5}$) from wt. Plus signs indicate statistical outliers. Values below boxes indicate sample size.

Surprisingly, the decrease in s_V in the dl heterozygotes was not carried through to the dorsal border (s_D) or width (w) of the *sog* domain (**Figure 3.3**). The dorsal border of *sog* is more graded, with a gradual decline, than the ventral border; therefore, small differences may be less apparent. As shown in **Figure 3.3D**, it appears that w is slightly greater in *dl* heterozygotes due to the decrease in s_V; however, with a p-value of 0.48, this difference is not statistically relevant.

In embryos with 4 copies of *dl*, we found the expected result: a wider Dorsal gradient results in an expanded *sog* domain. In fact, the *sog* domain in these embryos is statistically expanded under all three metrics, indicating that the domain has both expanded and shifted dorsally.

3.2.2 cactus *dosage*

Since Cact regulates dl's entry into the nucleus and enables its accumulation at the ventral midline (see **Chapter 5**), we decided to investigate the effect of its dosage on the dl gradient. We used the loss-of-function alleles $cact^1$ and $cact^4$ to reduce the maternal dose and the fluorescently-tagged gain-of-function *cact-cherry*, which was BAC-recombineered to include a 50kb region around the *cact* locus to ensure that it was regulated in a similar fashion to wild type *cact*. See **Table 3.2** for a description of the fly lines used, the abbreviations used throughout this document, and the numbers of exogenous, endogenous, and total *cact*.

Table 3.2: List of fly lines used in *cact* dosage experiments. cact(x) on the second chromosome indicates a loss-of-function allele; cact+ on the third chromosome indicates a gain-of-function allele.

Abbrev.	End. cact	Ex. cact	Total cact	Line
cact1/+	1	0	1	$cact^1$/CyO; PrDr/TM3
cact4/+	1	0	1	$cact^4$/CyO; PrDr/TM3
wt	2	0	2	yw
+; cact+	2	2	4	sp/CyO; cact-cherry

As discussed previously in **Section 3.2.1**, our main metric of comparison is the width of the Dorsal gradient. We found that the Dorsal gradient widened in *cact4/+* embryos and narrowed in *+; cact+* embryos (**Figure 3.4**). Curiously, the allele $cact^1$ did not cause a statistically significant widening of the gradient (as defined by a p-value of <0.05) even though it has the same *cact* dose as *cact4/+*. However, the p-value was 0.07, indicating a 93% probability that it was actually different than wt. Since *cact1/+* had similar properties to *cact4/+* in all other metrics, we propose that this discrepancy is not significant enough to warrant further investigation.

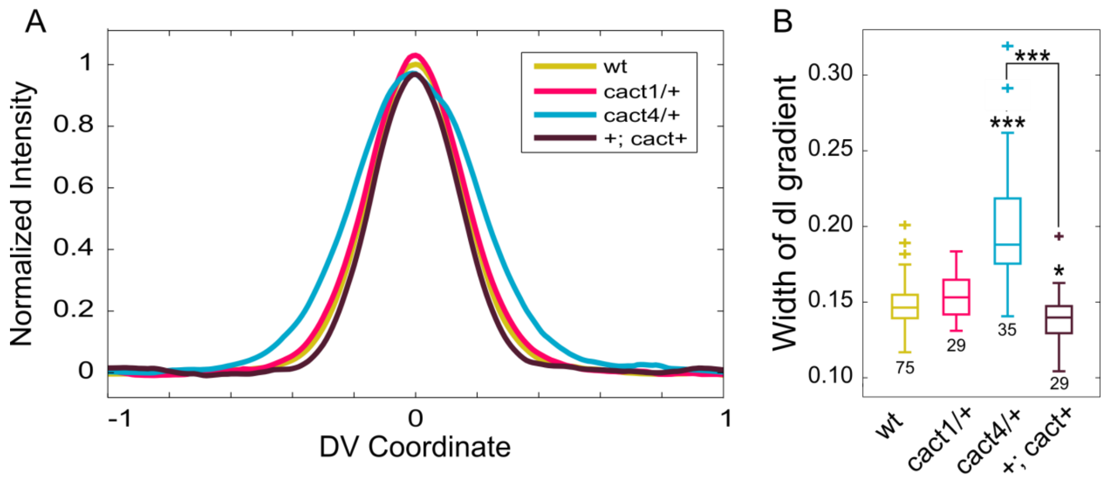

Figure 3.4: Changing the maternal dose of *cact* affects the embryonic Dorsal gradient. (A) Normalized Dorsal gradient in embryos from mothers with 2 (wt), 1 (cact1/+ and cact4/+), and 4 (+; cact+) copies of *cact*. (B) Boxplot of the widths of the gradients shown in (A). Asterisks indicate statistical significance (* $p<0.05$, *** $p<10^{-10}$) from wt unless otherwise noted. Plus signs indicate statistical outliers. Values below the boxes indicate sample size.

In this experiment, our results fall in line with our expectations. Because Cactus inhibits Dorsal, decreasing the maternal dose should decrease the formation of Dorsal/Cactus complex, enabling Dorsal to more readily enter the nuclei and widen the gradient. Conversely, adding extra Cactus should create more Dorsal/Cactus complexes, thereby further inhibiting Dorsal from crossing the nuclear membrane and narrowing the gradient.

Differences in the Dorsal nuclear gradient may not be biologically relevant unless they also affect the border placement of Dorsal target genes. With that in mind, we looked at two genes, *sog* and *dpp*. See **Figure 3.1** for the wild type domains of these genes. As expected from our analysis of the Dorsal gradient, the dorsal border of *sog*, s_D, expands dorsally (essentially widening) in cact heterozygotes and shrinks (essentially narrowing) in 4x *cact* embryos (**Figure 3.5**). Curiously, the ventral border (s_V) expanded in all three fly lines. This effect was expected in the heterozygotes because the ventral border of *sog* is set by the high-concentration threshold target gene *sna*. If the Dorsal gradient widens, the *sna* domain should widen in response, thereby expanding s_V dorsally. We would expect to see the opposite reaction in embryos with 4x *cactus* because the *sna* domain should narrow along with the Dorsal gradient. Without directly investigating the *sna* domain, it is difficult to know whether it is responsible for this discrepancy or if some other factor is at work.

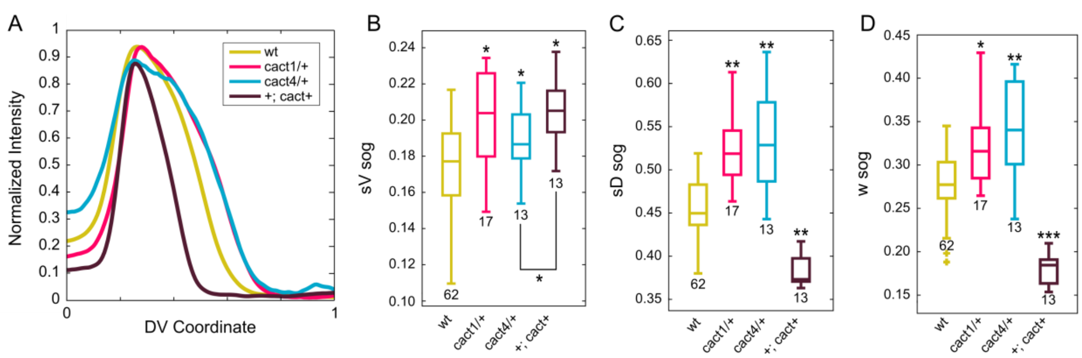

Figure 3.5: The *sog* domain changes with maternal *cactus* dose. (A) Normalized *sog* expression pattern in embryos from mothers with 1x (*cact1/+* and *cact4/+*), 2 (wt), and 4 (*+; cact+*) copies of Cactus. (B) Boxplot of the ventral border of *sog*. (C) Boxplot of the dorsal border of *sog*. (D) Boxplot of the width of the domain of *sog*, equivalent to s_D - s_V. Note: The same data set was used to generate all four figures. Asterisks indicate statistical significance (* $p<0.05$, ** $p<10^{-5}$, ***$p<10^{-10}$) from wt unless otherwise noted. Plus signs indicate statistical outliers. Values below the boxes indicate sample size.

Interestingly, the width of the *sog* domain, as measured by w, widens and narrows as the Dorsal gradient widens and narrows, respectively. We found a similar result in **Section 3.2.1** for embryos with 4 copies of Dorsal. In the 4x *cact* embryos, perhaps the change in w, as opposed to the changes in s_V and s_D is the biologically relevant one. An increased s_V and a decreased s_D would yield a significantly narrower *sog* domain, which is what we found.

The last gene we investigated was *dpp*, which is repressed by Dorsal, limiting it to the dorsal half of the embryo. Again, our results matched what was expected from our gradient analysis; heterozygotes had narrower *dpp* domains (with a larger s_V), and embryos with 4x *cactus* had expanded *dpp* domains (smaller s_V). See **Figure 3.6**.

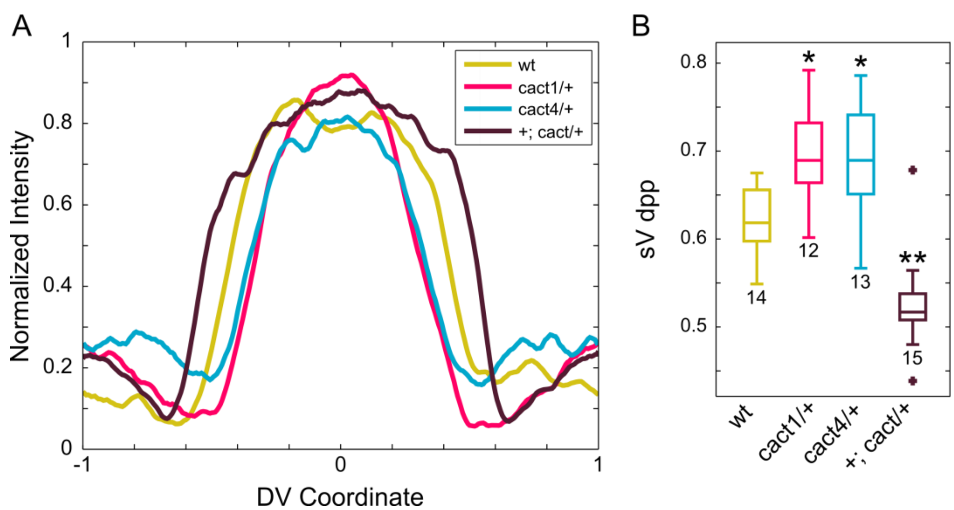

Figure 3.6: The *dpp* domain changes with maternal *cactus* dose. (A) Normalized *dpp* expression pattern in embryos from mothers with 1x (*cact1/+* and *cact4/+*), 2 (wt), and 4 (*+; cact+*) copies of *cactus*. Note: on this plot, the dorsal midline is 0 and the ventral midline is +/- 1. (B) Boxplot of the ventral border of *dpp*. Asterisks indicate statistical significance (* $p<0.05$, ** $p<10^{-5}$) from wt. Plus signs indicate statistical outliers. Numbers below the boxes indicate sample size.

Because *dpp* s_V and *sog* s_D are related, though not exactly the same, our findings from *dpp* match our *sog* results. Since *sog* takes up more of the embryo in *cact* heterozygotes there is less room for *dpp* at the dorsal midline. Similarly, because the *sog* domain contracts in embryos with 4x *cactus*, the *dpp* domain can expand to fill the "empty" embryo domain.

3.3 Conclusion

While the downstream effects of the Dorsal gradient have been well-studied, less is known about how it reliably places gene borders when the maternal dosage is compromised. In this study, we explored the effects of increasing and decreasing the maternal dose of both *dorsal* and its inhibitor *cactus*. Our results for *cactus* fell in line with expectation; decreased dose leads to a wider Dorsal gradient with dorsally expanded gene borders, while increased dose had the opposite effect of a narrower gradient and ventrally expanded gene borders, with one exception: increased dose actually caused the *sog* ventral border to expand dorsally. Further work should be conducted to determine if an expanded *sna* domain is responsible for this effect as anticipated. Our *dorsal* results were less clear, with a widening of the gradient in embryos that had both increased and decreased levels of maternal *dorsal*. Furthermore, the change in gradient did not always affect the border placement of target genes; in fact, only one gene (*sog*) had changes of statistical significance. Our work provides the foundation for future researchers to explore the feedback and regulation that control the Dorsal gradient.

3.4 Methods

3.4.1 Fluorescent in situ Hybridization

All embryos were aged to NC 14 (approx. 2-4 hours after egg lay), then fixed in 37% formaldehyde according to standard protocols (*14*). A combination fluorescent *in situ* hybridization/fluorescent immnuostaining was performed according to standard protocols (*14*). Briefly, fixed embryos were washed in PBS/Tween and hybridized at 55 ^{o}C overnight with anti-sense RNA probes, which were generated according to standard lab protocol. The embryos were then washed and incubated with primary antibodies at 4 ^{o}C overnight. The next day, they were washed and incubated for 1-2 hrs with fluorescent secondary antibodies at room temperature. The embryos were then washed and stored in 70% glycerol at -20 ^{o}C. Embryos were imaged within one month of completing the protocol.

Antibodies used were anti-dorsal 7A4 (deposited to the DSHB by Ruth Steward (DSHB Hybridoma Product anti-dorsal 7A4)) (1:10), donkey anti-mouse- 488 (Invitrogen A21202, Lot 81493) (1:500), rabbit anti-histone (abcam ab1791, Lot 940487) (1:5000), donkey anti-rabbit-546 (Invitrogen A10040, Lot 107388) (1:500), goat anti-biotin (ImmunoReagents, Raleigh, NC, GtxOt-070-D, Lot 19-19-112311) (1:50,000), donkey anti-goat-647 (Invitrogen A21447, Lot 774898) ((1:500), goat anti-fluorescin (Rockland 600-101-

096, Lot 19458) (1:500), rabbit anti-fluorescin (Life Technologies A889, Lot 1458646) (1:500), goat anti-histone (Abcam, ab12079, Lots GR6952-4 and GR129411-1) (1:100), donkey anti-rabbit-350 (ImmunoReagents, DkxRb-003-D350NHSX) (1:500). For some experiments the nuclear stain Draq5 (Cell Signaling #4084S) was used instead of an anti-histone antibody.

3.4.2 Mounting and Imaging of Fixed Embryos

Embryos were cross sectioned and mounted in 70% glycerol as described previously (*15*). Briefly, a razor blade was used to remove the anterior and posterior thirds of the embryo, leaving a cross section roughly 200 µm long by 200 µm in diameter. These sections were then oriented such that the cut sides became the top and bottom. Sections were then imaged at 20x on a Zeiss LSM 710 microscope. 15 z-slices 1.5 µm apart were analyzed, for a total section size of 21 µm.

3.4.3 Image analysis

Images of embryo cross sections were analyzed using a previously derived algorithm (*16*). Briefly, the border of the embryo was found computationally, then the nuclei were segmented using a local thresholding protocol. The intensity of dl in each segmented nucleus was calculated as the ratio between the intensity in the dl channel divided by the intensity in the nuclear channel. The intensity of mRNA expression was calculated as average intensity within an annulus roughly 18 µm wide around the perimeter of the embryo. mRNA profiles were fit to canonical parameters; those with a goodness of fit (gof) less than 0.7 were omitted from study.

All dl gradients were fit to a Gaussian, and these fits were used to determine the width parameter, σ. Gradients with a gof less than 0.8 were eliminated from the results. Normalized intensity plots were generated by fitting each embryo's data to its own Gaussian by subtracting the B value and 70% of the M value, then dividing by the A value. ($X = (x - B - 0.7M)/A$)). The average normalized intensity plot was generated by averaging the plots of all embryos in the specified genotype.

Multiple experiments with statistically similar wild type controls were analyzed simultaneously to generate the data in this report. Statistical significance was calculated using two-tailed homoscedastic t-tests.

3.5 Acknowledgements

I would like to thank undergraduate researchers Josh Chappell and Alex Thomas for conducting the cactus experiments and one Dorsal experiment, respectively. Thanks to ImmunoReagents for provision of antibodies and helpful discussion. I am extremely thankful to Eva Johannes of NCSU CMIF for aiding me in collecting the best images possible. I thank the Stathopoulos lab for kind provision of fly lines and DNA constructs.

3.6 References

(1) Roth, S.; Stein, D.; Nüsslein-Volhard, C. A Gradient of Nuclear Localization of the Dorsal Protein Determines Dorsoventral Pattern in the Drosophila Embryo. *Cell* **1989**, *59* (6), 1189–1202.

(2) Anderson, K. V; Nüsslein-Volhard, C. Information for the Dorsal-Ventral Pattern of the Drosophila Embryo Is Stored as Maternal mRNA. *Nature* **1984**, *311* (5983), 223–227.

(3) Roth, S.; Hiromi, Y.; Godt, D.; Nüsslein-Volhard, C. Cactus, a Maternal Gene Required for Proper Formation of the Dorsoventral Morphogen Gradient in Drosophila Embryos. *Development* **1991**, *112* (2), 371–388.

(4) Reeves, G. T.; Stathopoulos, A. Graded Dorsal and Differential Gene Regulation in the Drosophila Embryo. *Cold Spring Harb. Perspect. Biol.* **2009**, *1* (4), a000836.

(5) Bergmann, A.; Stein, D.; Geisler, R.; Hagenmaier, S.; Schmid, B.; Fernandez, N.; Schnell, B.; Nüsslein-Volhard, C. A Gradient of Cytoplasmic Cactus Degradation Establishes the Nuclear Localization Gradient of the Dorsal Morphogen in Drosophila. *Mech. Dev.* **1996**, *60* (1), 109–123.

(6) Sen, J.; Goltz, J. S.; Stevens, L.; Stein, D. Spatially Restricted Expression of Pipe in the Drosophila Egg Chamber Defines Embryonic Dorsal-Ventral Polarity. *Cell* **1998**, *95* (4), 471–481.

(7) Liberman, L. M.; Reeves, G. T.; Stathopoulos, A. Quantitative Imaging of the Dorsal Nuclear Gradient Reveals Limitations to Threshold-Dependent Patterning in Drosophila. *Proc. Natl. Acad. Sci. U. S. A.* **2009**, *106* (52), 22317–22322.

(8) Reeves, G. T.; Trisnadi, N.; Truong, T. V; Nahmad, M.; Katz, S.; Stathopoulos, A. Dorsal-Ventral Gene Expression in the Drosophila Embryo Reflects the Dynamics and Precision of the Dorsal Nuclear Gradient. *Dev. Cell* **2012**, *22* (3), 544–557.

(9) Govind, S.; Brennan, L.; Steward, R. Homeostatic Balance between Dorsal and Cactus Proteins in the Drosophila Embryo. *Development* **1993**, *117*, 135–148.

(10) Chung, K.; Kim, Y.; Kanodia, J. S.; Gong, E.; Shvartsman, S. Y.; Lu, H. A Microfluidic Array for Large-Scale Ordering and Orientation of Embryos. *Nat. Methods* **2011**, *8* (2), 171–176.

(11) Ambrosi, P.; Chahda, J. S.; Koslen, H. R.; Chiel, H. J.; Mizutani, C. M. Modeling of the Dorsal Gradient across Species Reveals Interaction between Embryo Morphology and Toll Signaling Pathway during Evolution. *PLoS Comput Biol* **2014**, *10* (8), e1003807.

(12) O'Connell, M. D.; Reeves, G. T. The Presence of Nuclear Cactus in the Early Drosophila Embryo May Extend the Dynamic Range of the Dorsal Gradient. *PLOS Comput. Biol.* **2015**, *11* (4), e1004159.

(13) DeLotto, R.; DeLotto, Y.; Steward, R.; Lippincott-Schwartz, J. Nucleocytoplasmic Shuttling Mediates the Dynamic Maintenance of Nuclear Dorsal Levels during Drosophila Embryogenesis. *Development* **2007**, *134* (23), 4233–4241.

(14) Kosman, D.; Mizutani, C. M.; Lemons, D.; Cox, W. G.; McGinnis, W.; Bier, E. Multiplex Detection of RNA Expression in Drosophila Embryos. *Science* **2004**, *305* (5685), 846.

(15) Carrell, S. N.; Reeves, G. T. Imaging the Dorsal-Ventral Axis of Live and Fixed Drosophila Melanogaster Embryos. In *Tissue Morphogenesis*; Nelson, C. M., Ed.; Methods in Molecular Biology; Springer New York: New York, NY, 2015; Vol. 1189, pp 63–78.

(16) Trisnadi, N.; Altinok, A.; Stathopoulos, A.; Reeves, G. T. Image Analysis and Empirical Modeling of Gene and Protein Expression. *Methods* **2013**, *62* (1), 68–78.

4 Novel Interactions Between the NF-κB and BMP Signaling Pathways in the *Drosophila* Embryo

4.1 Abstract

During nuclear cycles 10-14, two conserved signaling pathways act to pattern the DV axis of the *Drosophila* embryo: the Dorsal pathway and the Dpp pathway. On the ventral side of the embryo, the transcription factor Dorsal, homologous to NF-κB, triggers expression of the genes that initiate the DV pattern. Dorsal is present in a nuclear gradient, with the highest concentration at the ventral midline and a steady decay to about 40% of the embryo's circumference. Beyond the expression domain of Dorsal, the dorsal side of the embryo is patterned by BMP signaling via the ligand Dpp, which signals through the receptor Thickveins (Tkv). This active signaling complex phosphorylates the receptor Smad protein MAD. Two phospho-MAD (pMAD) molecules bind to the co-Smad Medea (Med); this heterotrimer then enters the nuclei to facilitate expression of target genes. Together, the nuclear gradient of Dorsal and BMP signaling work to pattern the DV axis of developing Drosophila embryos.

Because robustness of tissue patterning is essential for proper embryonic development, regulatory loops must exist to ensure correct placement of target genes in the face of perturbed conditions. As an example, embryos with a half dose of Dorsal protein survive to adulthood. Feedback through the Dpp signaling network is a prime candidate for enhancing the robustness of Dorsal patterning of DV gene expression. We investigated the effects on the shape of the Dorsal gradient of overexpression of MAD and Medea individually, as well as expression of constitutively active and dominant negative forms of

the receptor Tkv. We found that in each of these cases, the Dorsal gradient was statistically wider than wild-type, indicating interactions between the two signaling pathways. These interactions between the NF-κB and BMP signaling pathways may be necessary to ensure robust gene expression in the developing *Drosophila* embryo.

4.2 Introduction

4.2.1 Dorsoventral patterning of the Drosophila embryo

In the *Drosophila* embryo, dorsoventral patterning is under the control of two signaling pathways: Dorsal (ventral side) and BMP (dorsal side). For a more thorough description of both, see **Chapter 1**. **Figure 4.1** presents a wild type embryo stained for both Dorsal and pMAD (the signal transducer of BMP signaling in *Drosophila* embryogenesis).

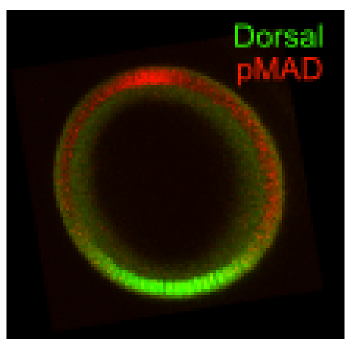

Figure 4.1: Dorsal (green) and pMAD (red) patterns in a wild type *Drosophila* embryo. Cross section is oriented such that ventral is down.

4.2.1.1 Dorsal pathway

The maternal transcription factor Dorsal is present in a nuclear gradient with its peak at the ventral midline (*1*,*2*). This concentration gradient is responsible for placing the domains of target genes that will specify the different tissue layers (*2*,*3*). The protein Cactus binds to Dorsal, preventing it from entering the nuclei (*4*,*5*). Toll signaling, which is highest at the ventral midline, phosphorylates the Dorsal/Cactus complex, freeing Dorsal and causing Cactus to be ubiquitinated and degraded (*2*,*5*).

4.2.1.2 BMP pathway

BMP signaling is used throughout nature for embryonic development in both vertebrates and invertebrates (*6–9*). In *Drosophila*, it is used both in embryogenesis and in development of the wing disc later in *Drosophila* development (*7*). While BMP signaling is complex, involving many proteins and gene interactions, this report focuses on only a few players. See **Chapter 1** for a more thorough discussion of BMP signaling in the context of *Drosophila* embryogenesis. The Dorsal Type III- target gene *decapentaplegic* (*dpp*), expressed only on the dorsal half of the embryo, encodes the BMP ligand Dpp (*10*). When Dpp binds to its receptor Thickveins (Tkv), it causes phosphorylation of the protein Mothers Against Dpp (MAD) (*11*). Phospho-MAD (pMAD) binds with Medea (Med) in a 2:1 heterotrimer that acts as the BMP transcription factor (*12*). See **Figure 4.2**.

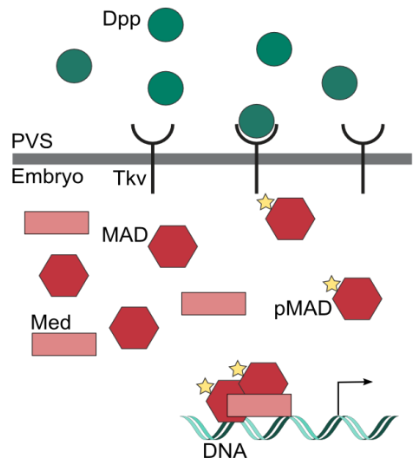

Figure 4.2.: Simplified diagram of BMP signaling. The BMP ligand Dpp (encoded by a Dorsal target gene) binds to its receptor Thickveins (Tkv). The active signaling complex phosphorylates the protein MAD, which combines with Medea (Med) in a heterotrimer to form an active transcription factor.

4.2.2 UAS/Gal4 system

As described previously (**Chapter 1**), *Drosophila* geneticists have developed a mechanism for expressing transgenes in a tissue-specific fashion (*13*). This system involves the yeast Gal4/UAS system, by which a tissue-specific Gal4 driver is used to drive expression of a UAS-linked gene. In the experiments presented in this chapter, we used the maternal driver matα-gal4, which is expressed maternally and then loaded into the eggs. In order to ensure that the phenotypic changes we found were due to the UAS-linked gene and not the altered chromosome containing matα-gal4, we conducted a control experiment that showed no statistical difference between embryos from these mothers and those from wild type mothers. We did not need to conduct similar experiments for the UAS-linked genes as they are not expressed in the absence of Gal4. While there is the potential for these transgenes to disrupt native gene expression, they were designed to integrate into the chromosome at locations in which there will be no known gene disruption (*14*,*15*)

4.3 Results

See **Chapter 1** for an overview of data analysis methods. In brief, we fit both Dorsal and pMAD nuclear gradients to a Gaussian and used the Gaussian parameters to describe the width, amplitude, and basal levels of the gradients.

4.3.1 Over-expression of signaling cofactors

4.3.1.1 MAD

When we overexpressed MAD using the construct UAS-MAD-GFP, we found that the Dorsal gradient widened in response (See **Figure 4.3**). We did not see any statistical difference in the pMAD gradient between wild type embryos and those with added MAD; however, the pMAD gradient varies in width and intensity with respect to time, refining from a broad, low-intensity gradient in early NC 14 to a sharp, high-intensity gradient in late NC 14, making any differences difficult to detect (*7*,*18*). While our other work (see **Chapter 5**) indicates that fluorescently tagging a protein may interfere with its endogenous expression, we expect that a similar effect is not occurring here because the pMAD gradient itself is unaltered. Furthermore, MAD is downstream of the shuttling mechanism that is known to act on the BMP signaling pathway at this stage, and the pMAD pattern itself is established by a positive feedback loop, which might further make boundary formation robust (*16*,*17*).

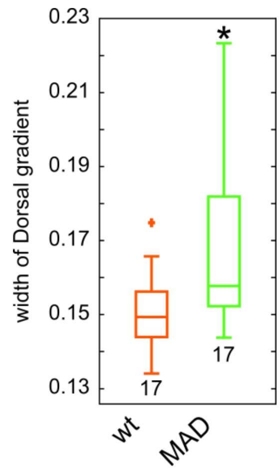

Figure 4.3: Boxplot of width of Dorsal gradient in over-expressed MAD and wt embryos. Plus signs indicate statistical outliers. Asterisk indicates statistical significance p<0.01 from wt. The value below each box indicates sample size.

4.3.1.2 Medea

We used two different UAS-Medea-GFP fly lines to investigate the effect of additional Medea on the Dorsal gradient in order to increase confidence in our results (*14*). Similar to what we saw with the overexpression of MAD, overexpression of Medea widened the Dorsal gradient, as shown in **Figure 4.4**.We did not find a statistically significant difference between the two over-expressed Medea lines, indicating that they function similarly to one another.

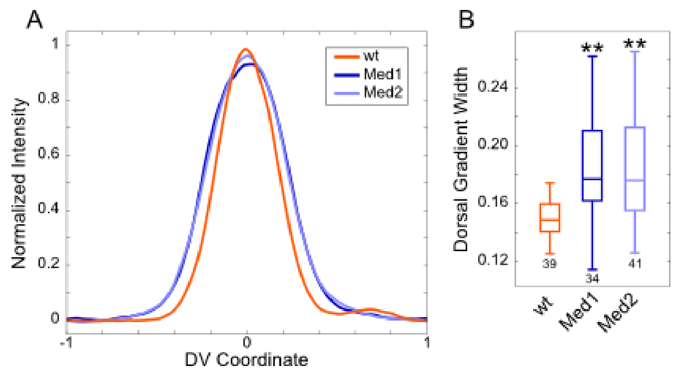

Figure 4.4: Over-expression of Medea widens the Dorsal gradient. (A) Average normalized plot of the Dorsal gradient in embryos from mothers with wild type (wt) or extra (Med1, Med2) Medea. (B) Boxplot of the width of the Dorsal gradient in the same embryos. Asterisks indicates statistical significance $p < 10^{-5}$ from wild type. The value below each box indicates sample size.

We also analyzed the differences in gene borders of Dorsal target genes. See **Figure 4.5** for a graphical description of the gene domains as well as the variables used to describe them. s_D corresponds to the dorsal border of a gene (the border of that gene which is closer to the dorsal midline) and s_V to the ventral border (the border closer to the ventral midline).

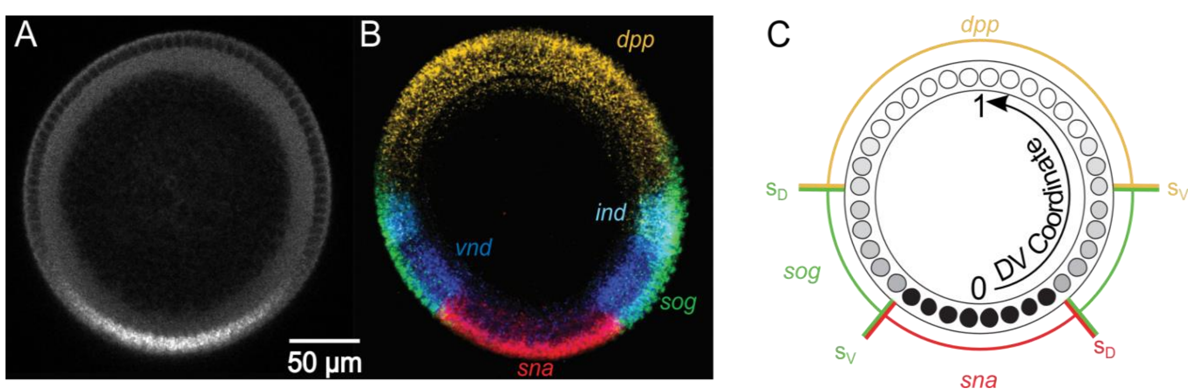

Figure 4.5: The protein Dorsal patterns the DV axis of the *Drosophila* embryo. (A) An antibody staining against Dorsal. (B) mRNA expression of a variety of Dorsal target genes. (C) We use the parameters s_D (dorsal border) and s_V (ventral border) to quantify and compare the extent of domain of dl target genes. Because *sna* represses *sog*, s_D *sna* ~= s_V *sog*. Embryo cross-sections are oriented so that ventral is down. Adapted from (*2*).

We analyzed the expression borders of *snail* (*sna*) and *short gastrulation* (*sog*). We found that increasing Medea increased the domain of *sna*, thereby increasing s_D (See **Figure 4.6A,B**). This result falls in line with expectations as *sna* is turned on at high concentrations of Dorsal; therefore, a wider Dorsal gradient should lead to a wider domain of *sna*. The ventral border of *sog*, s_V, was similarly changed; that is, it increased with increased *sna* s_D (**Figure 4.6C,D**). Since *sog* is repressed by *sna*, we expected to find that s_V *sog* would follow s_D *sna*. Although the difference in s_V *sog* between Med-GFP1 and wt is not statistically significant (as defined by a p-value of less than 0.05), the p-value of 0.06 indicates a 94% probability that the two populations are distinct. With such a small number of samples (5), we expect that increasing n would decrease the p-value, eliminating the apparent discrepancy between the two overexpressed Medea lines. We also analyzed the dorsal border (s_D) and width (w) of *sog*; neither was affected by increased Med. Because the dorsal border of *sog* is graded (**Figure 4.6C**), there is less precision in computationally placing it, leading to a lower likelihood of discovering statistical differences. Because w=s_D-s_V, the lack of precision in s_D is carried over into w; therefore, we do not find the lack of statistical difference in these variables remarkable.

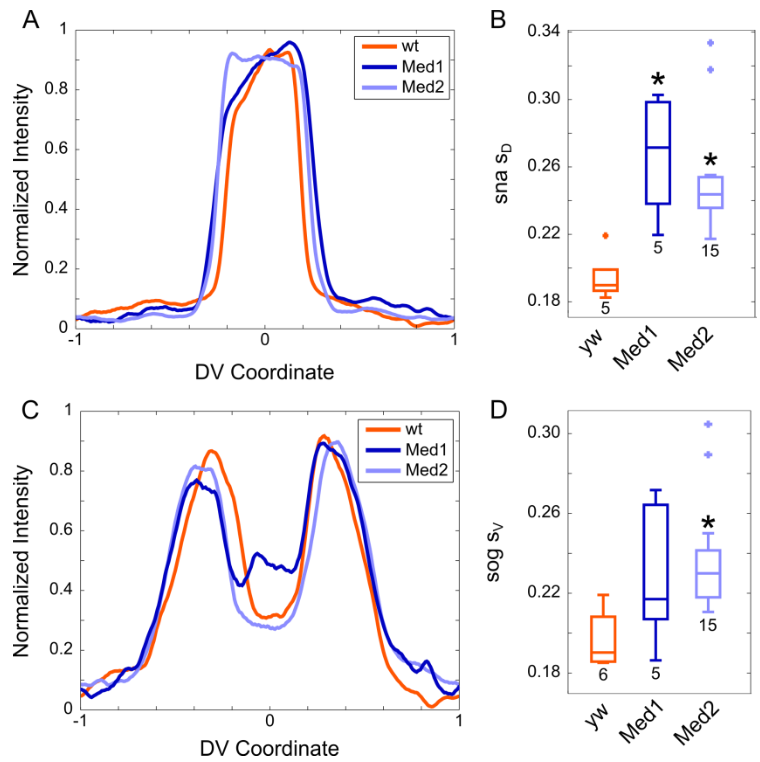

Figure 4.6: RNA profiles in embryos from mothers over-expressing Medea. (A) and (B) *sna* domain. (A) The average normalized *sna* profile in embryos from mothers with wild type (wt) or over-expressed (Med1 and Med2) Medea. (B) Boxplot of the dorsal border (s_D) of *sna*. (C) and (D) *sog* domain. (C) Average normalized *sog* profiles in embryos with the same genotypes as (A). (D) Boxplot of the ventral border (s_V) of *sog*. Plus signs indicate statistical outliers. Asterisk indicates statistical significance $p<0.003$ from wild type. The value below each box indicates sample size.

Overall, our results match what was found in the MAD experiments; that is, increased levels of BMP signaling transducers widen the Dorsal gradient. Our target gene analysis further confirmed our results; a wider Dorsal gradient led to an expansion of the *sna* domain and a corresponding expansion of the ventral border of *sog*.

4.3.2 Manipulating Tkv signaling strength

To further bolster our results, we manipulated the BMP pathway in a different manner. Instead of changing the transducer levels, we changed the activity of the receptor using constitutively active and dominant negative forms of the Thickveins (Tkv) receptor. These constructs were again expressed using the Gal4/UAS system, using the matα-gal4 driver described previously. When analyzing the embryos from these mothers, we found that each genotype could be sorted (by eye) into two populations, based on the presence or absence of a pMAD gradient (See **Figure 4.7**). In the case of the constitutively active (*tkv**) construct, we found a population with regular pMAD gradients (*tkv** r) and one with ubiquitously high expression of pMAD throughout the embryo (*tkv** u). In the dominant negative (tkv^{dn}) construct, we again found a population with regular pMAD gradients (tkv^{dn} r) and ones without detectable gradients, expressing pMAD at a ubiquitously low level throughout the embryo (tkv^{dn} n). To explain the presence of two distinct populations, we hypothesize that the matα-gal4 driver is not strong enough to promote UAS-linked constructs at consistently high levels throughout the whole germline. The embryos with perturbed pMAD gradients (ubiquitous high or low expression) are the expected result of increased (*tkv**) or decreased (tkv^{dn}) BMP signaling.

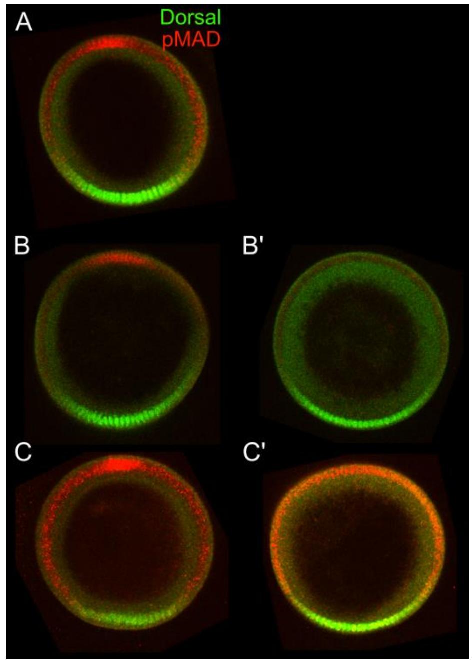

Figure 4.7: Examples of pMAD and Dorsal expression in embryos from mothers expressing tkv* and tkv^{dn}. Dorsal is included to orient the embryos. While some embryos had a wild-type peak, others had abnormal expression. (A) Dorsal and pMAD expression in a wild type embryo. Note: this is the same embryo that appears in **Figure 4.1**. (B) Dorsal and pMAD expression in embryos from mothers expressing *tkv*^{dn}. (B) wild type-like pMAD expression. (B') no pMAD gradient. (C) Dorsal and pMAD expression in embryos from mothers expressing *tkv**. (C) wild type-like pMAD expression. (C') Ubiquitous pMAD expression.

Another surprising discovery was that females carrying both the matα-gal4 driver and a *tkv* construct produced viable progeny. Since BMP signaling is crucial to proper DV patterning, we expected that embryos from these mothers would be unable to develop beyond embryogenesis. Based on the presence of two populations in each case, we propose that the embryos with a "wt-like" pattern of pMAD are the ones that survive to adulthood. We found no statistical difference in the pMAD gradient between wt and the embryos that had a "wt-like" expression pattern of pMAD, further supporting our hypothesis.

4.3.2.1 Constitutively active Tkv

When we analyzed embryos that had a constitutively active form of the Thickveins receptor (*tkv**), we found that the Dorsal gradient widened as expected in the population of embryos with ubiquitous pMAD expression (*tkv** u), since our previous results suggested that increased BMP signaling would lead to a wider gradient (**Figure 4.8**).

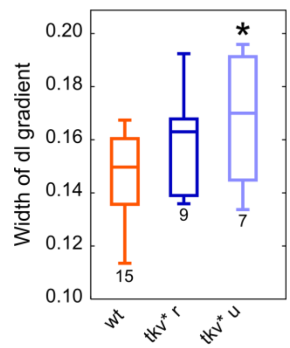

Figure 4.8: The Dorsal gradient widens in embryos that have ubiquitous pMAD expression in a *tkv** background (tkv* u). tkv* r are embryos with regular pMAD expression. Asterisk indicates statistical significance $p<0.05$ from wild type. The value below each box indicates sample size.

Curiously, neither the width (**Figure 4.8**) nor the amplitude of the Dorsal gradient were statistically different from wt in embryos with higher BMP signaling that had a regular pMAD gradient, again supporting our hypothesis that these embryos were the ones that survived to adulthood due to a lower expression of the constitutively active receptor.

We also investigated the basal and maximal levels (amplitude plus basal levels) of pMAD in these embryos. For the embryos that had ubiquitous pMAD, we used the average nuclear intensity of pMAD throughout the embryo instead of the calculated fit to a

Gaussian. We found that the basal level in the embryos expressing wt-like pMAD gradients was nearly identical to that in wild type embryos while the average value in the ubiquitously expressing embryos was higher, though less than the maximum pMAD concentration in wt embryos, as calculated by amplitude (A) + basal level (B) (**Figure 4.9**). This result indicates that the constitutively active thickveins receptor is causing high levels of nuclear pMAD import. Furthermore, the *tkv** regular embryos have pMAD gradients virtually indistinguishable from wt, again indicating that separating the tkv* embryos into two populations is biologically justified.

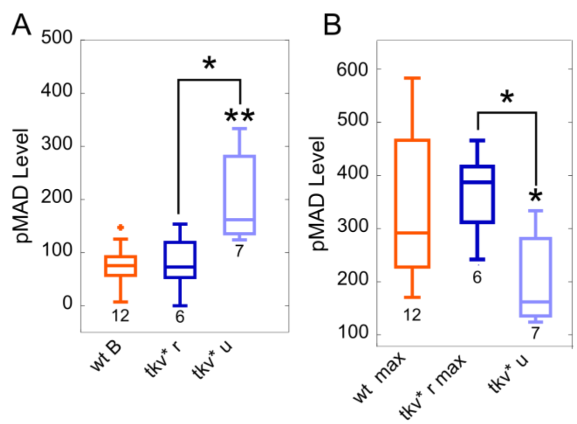

Figure 4.9: The basal and maximum levels of pMAD in *tkv** embryos. (A) The basal level in wt and *tkv** regular embryos compared to the average pMAD level in the *tkv** ubiquitous embryos. (B) The maximum level of pMAD in wt and *tkv** regular embryos compared to the average pMAD level in the ubiquitous population. Asterisks indicates statistical significance (*$p<0.05$, **$p<10^{-3}$) from wt unless otherwise noted. The value below each box indicates sample size.

4.3.2.2 Dominant negative Tkv

As mentioned above, embryos with a dominant negative form of the thickveins receptor (*tkv^dn*) were split into two populations: those expressing a wt-like pMAD gradient and those with low ubiquitous pMAD expression (See **Figure 4.7**). We found that both populations had Dorsal gradients statistically wider than wild type (**Figure 4.10**). This result was surprising since we expected knocking down BMP signaling to have the opposite effect as increasing it; that is, we expected to find narrower Dorsal gradients. However, our results agree with those found previously for *tkv^dn* (*19*). While previous work did not directly investigate the Dorsal gradient, it was found that the *sna* domain increased as would be expected with an increased Dorsal domain and similar to what we found when we over-expressed Medea.

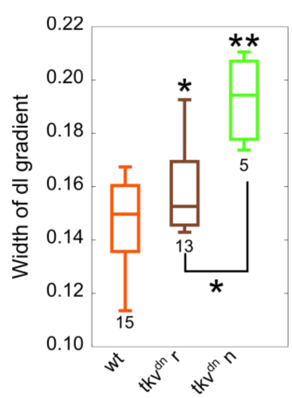

Figure 4.10: The Dorsal gradient widens in embryos from mothers expressing *tkv^dn*. The difference is exacerbated when there is no detectable pMAD gradient. Asterisks indicates statistical significance (*p<0.05, **$p<10^{-5}$) from wt unless otherwise noted. The value below each box indicates sample size.

We found the expected result in *tkv*^{dn} embryos with a wt-like pMAD gradient; both the amplitude and basal level were lower than in wild type embryos, indicating that there was less phosphorylation of MAD occurring due to the knockdown of Tkv activity. Furthermore, the average pMAD level in the embryos with ubiquitously low pMAD expression was the same as the basal level in wt embryos, indicating that, in these embryos, there is little-to-no MAD phosphorylation.

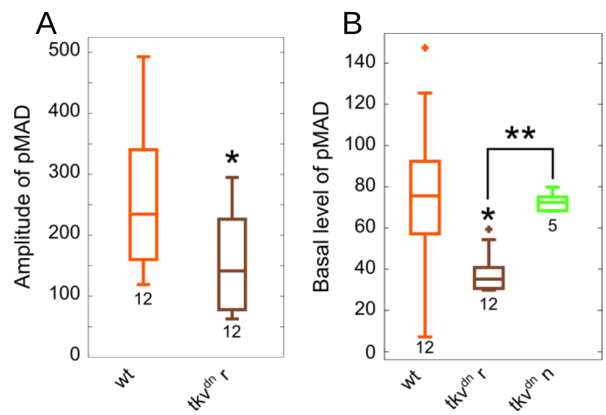

Figure 4.11: The dominant negative receptor *tkv*^{dn} lowers both the amplitude and basal level of the pMAD gradient. (A) The amplitude of the pMAD gradient in embryos that express a wt-like pMAD gradient. (B) The basal level in regular (*tkv*^{dn} r) and the average pMAD level in no gradient (*tkv*^{dn} r) embryos. Asterisks indicates statistical significance (*$p<0.05$, **$p<10^{-5}$) from wt unless otherwise noted. Plus signs indicate statistical outliers. The value below each box indicates sample size.

4.3.2.3 Perturbing tkv signaling in a dl heterozygous background

Previous researchers had found that they needed to perturb both BMP signaling and Dorsal dose to see a strong effect on the Dorsal gradient (*19*,*20*). In fact, they found that increasing the maternal dose of *dpp* resulted in a phenotypic change only when accompanied by a reduction in *dorsal* dose (*19*,*20*). While we were able to find phenotypic differences in embryos carrying only *tkv**, we wanted to replicate these prior results.

We found that the amplitude of the Dorsal gradient embryos carrying mutations in both *dl* and *tkv* is statistically lower than wild type. However, it is difficult to distinguish whether this effect is due only to the *dorsal* half dose, which lowers the amplitude, or if it is also partially due to the perturbation to the BMP pathway.

When we analyzed *tkv** and tkv^{dn} embryos in a *dorsal* heterozygous background, we found that they behaved as expected; that is, a change that makes the Dorsal gradient wider (manipulating *tkv*) added to one that also makes the gradient wider (Dorsal half dose) results in gradients that are also wider than wt (**Figure 4.12**), in some cases, synergistically (see below). When investigating the embryos from *dl/+; tkv** mothers, we found two distinct populations with ubiquitous pMAD, designated “high” and “low”, contrary to the single ubiquitous pMAD population found in our previous experiment.

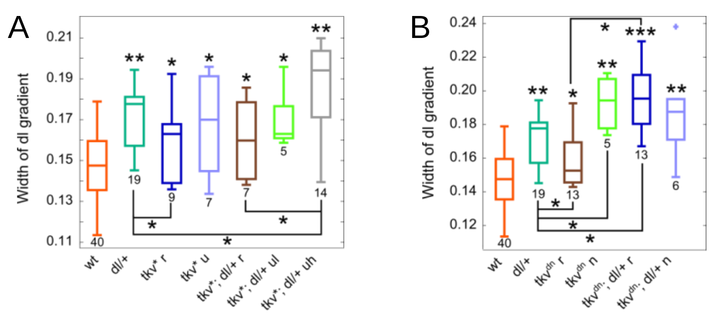

Figure 4.12: Width of dl gradient in (A) embryos with increased BMP signaling due to the *tkv** construct and (B) embryos with decreased BMP signaling due to the tkv^{dn} construct, both in a wild type background and in a *dl* heterozygous background. The data for *tkv* mutants without dl/+ are the same as presented above and reproduced here for comparison. Asterisks indicates statistical significance (*p<0.05, **$p<10^{-5}$, ***$p<10^{-10}$) from wt unless otherwise noted. Plus signs indicate statistical outliers. The value below each box indicates sample size.

When analyzing *tkv** embryos with wt-like pMAD gradients, we found that adding a *dl* null allele did not have a statistical effect on the width of the Dorsal gradient. In fact, the width in these embryos was indistinguishable from *dl/+*, indicating that the null allele had a larger influence on the width than *tkv**. In embryos with high ubiquitous pMAD expression, adding a *dl* null allele did widen the gradient statistically over the *dl* null allele alone. While the difference was not statistically significant between *tkv** ubiquitous and *tkv*; dl/+* ubiquitous high, the p-value was 0.07, which indicates a 93% chance that the populations are distinct. With a low sample number, it is possible that further experiments would find a statistical difference.

In the tkv^{dn} embryos, we found a similar pattern. Alone, tkv^{dn} did not cause the Dorsal gradient in embryos expressing a wt-like pMAD gradient to widen as much as the *dl* null allele alone. Combined, the two acted synergistically to widen the gradient more than either alone. Curiously, we did not see as much of an effect in the embryos with no detectable pMAD gradient. While tkv^{dn} alone widened the Dorsal gradient more in these embryos than the *dl* null allele, the two did not combine to widen the gradient further. In fact, the width of the gradient in tkv^{dn}*; dl/+* embryos is indistinguishable from either individual mutation in the no pMAD gradient population.

We also analyzed the pMAD gradient in these embryos. We found that the maximum pMAD level in *tkv*; dl/+* regular embryos was significantly lower than wt and the average pMAD level in both ubiquitous populations was lower than the maximum level in wt embryos. When we compared these average values to the basal levels in wt embryos, we found that the low ubiquitous population average pMAD levels were comparable to the basal level in wt embryos, while the high ubiquitous population pMAD levels were significantly higher (**Figure 4.13B**). Furthermore, the *tkv*; dl/+* regular embryos had a *lower* basal pMAD level than wild type. Perhaps this difference is due to the absence of one copy of *dl*. Future experiments must be done to control for this possibility.

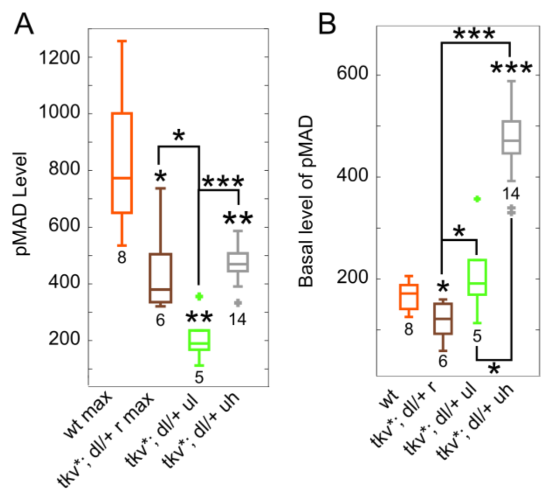

Figure 4.13: Amplitude and basal levels of pMAD in *tkv*; dl/+* embryos. Note: the values for ubiquitous samples are the same in panels A and B (the average nuclear intensity of pMAD). Asterisks indicates statistical significance (*$p<0.05$, **$p<10^{-3}$, ***$p<10^{-5}$) from wt unless otherwise noted. Plus signs indicate statistical outliers. The value below each box indicates sample size.

When we investigated the pMAD gradient in tkv^{dn}*; dl/+* embryos, we found more curious results. While the amplitude and basal levels of tkv^{dn}*; dl/+* regular pMAD gradients decreased from wt as it had previously, the average level of pMAD in the no pMAD gradient population increased over the basal level in wt embryos (**Figure 4.14**). An increased pMAD level indicates that more MAD is being phosphorylated throughout these embryos than what would be expected at the ventral midline of a wt embryo, which is curious in a background where BMP signaling should be universally lowered.

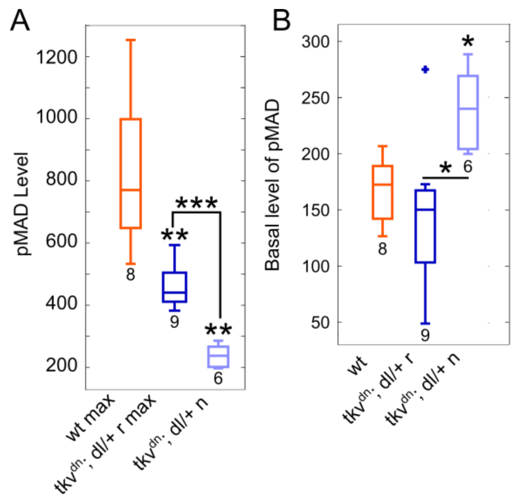

Figure 4.14: Amplitude and basal levels of pMAD in *tkv^{dn}; dl/+* embryos. Note: the values for no pMAD gradient are the same in panels A and B (the average nuclear intensity of pMAD). Asterisks indicates statistical significance (*p<0.05, **p<10^{-3}, ***p<10^{-5}) from wt unless otherwise noted. Plus signs indicate statistical outliers. The value below each box indicates sample size.

4.4 Discussion

Our results clearly suggest feedback between the Dorsal and BMP signaling pathways. While we could not directly identify any players, we propose several possibilities. First, Cactus, the inhibitor of Dorsal, is affected by maternal BMP signaling, indicating cross-talk between the two pathways (*21*,*22*). One explanation is the need for patterning to be scale invariant; that is, embryos of varying sizes need to have gradients that take up proportionally, not absolutely, the same distance along the DV axis. If one embryo had a circumference of 100 µm while another had a circumference of 200 µm, the Dorsal and pMAD gradients should each occupy about 50% of that circumference. If scaling does not occur and the average embryo is 150 µm in circumference, each gradient would need 75 µm. In the small embryo, the gradients would overlap, leading to indistinct and irregular gene borders and to improper placement of muscular layers. In the large embryo, approximately 50 µm of the most lateral tissue would remain unpatterned, leading to extraneous undeveloped tissue that would interfere with proper development. Therefore, we propose that the mechanism by which increased BMP signaling causes the Dorsal gradient to widen is important for proper scaling so that a larger embryo, in which the pMAD gradient takes up a larger absolute proportion of the embryo would have a Dorsal gradient that similarly takes up a larger proportion. In our experiments, we have increased BMP signaling so that the embryo perhaps responds as if it were larger than it actually is, leading to the expansion of the Dorsal gradient into the more lateral regions.

Our results from knocking down BMP signaling indicate that some other mechanism may be at work since the Dorsal gradient in these embryos also widened. In this instance, it is possible that the Dorsal gradient expands to reach the nuclei that would remain unpatterned by a lack of BMP signaling, possibly enabling the embryo to develop properly. Both mechanisms could function in the case of perturbed BMP signaling depending on how much the pMAD gradient was disrupted.

Our results with heterozygous *dorsal* embryos conflict with those of previous researchers, who found that the Dorsal gradient narrowed when *dorsal* dose was decreased and BMP signal increased via over-expression of Dpp (*20*). This group used a different staining technique and did not computationally quantify the gradient; instead, they counted the number of nuclei along the ventral midline that were stained for Dorsal. While this method certainly has merit, it might not be as accurate as fluorescent techniques. Furthermore, they used a microtome to generate 4 µm thick cross-sections of the embryo and do not mention where precisely within the embryo each slice came from. After these results were published, other researchers have determined that the wild type Dorsal gradient narrows at the anterior and posterior ends (*3*). Had the section come from the anterior- or posterior-most 50 µm of tissue, it would be narrower even in a wild type embryo. Finally, the effects of a *dl* heterozygote on the Dorsal gradient may be masking the effect of increased Dpp. As discussed previously (**Chapter 3**), a decreased *dorsal* dose leads to gradients that are wider than wt when fit to Gaussian parameters. However, the target gene thresholds read the *absolute* concentration; these boundaries will shift ventrally due to the decreased amplitude.. Indeed, this group found similar results when they studied *tkv^{dn}; dl-/+* embryos: a narrowing of the *sna* domain, which is what we found when analyzing *dorsal* heterozygotes.

When we analyzed the pMAD gradient in *tkv** mutants in a *dl/+* background, we found that the amplitude was significantly decreased from wt in all cases. Without the *dl/+*

mutation, we found this decrease in only the *tkv*^{dn} embryos. Since constitutively active Tkv should increase phosphorylation of MAD throughout the embryo, this decrease in pMAD levels could be due to the loss of one copy of *dl*. Future work should be undertaken in order to determine if this hypothesis is correct. Furthermore, our results in the *tkv*^{dn}*; dl/+* no pMAD gradient population were different than those from the previous experiment; average pMAD levels *increased* over the basal levels in wt embryos.

Since we did not analyze the pMAD gradient in embryos heterozygous for *dorsal*, we cannot state that a decreased dose of *dorsal* is responsible for these results. Furthermore, we could not compare to our previous data (without the *dorsal* mutation) as the basal pMAD levels for wt were statistically different between experiments. Because the calculations of basal level and amplitude depend significantly on laser power, we do not find this result striking.

Due to the difficulty of obtaining mother flies bearing all three necessary chromosomes (*dl* null, UAS-tkv* or -tkv^{dn}, and matα-gal4) and the limited information we gained from their embryos, we propose that studying manipulated levels of tkv alone, not in addition to a *dl* heterozygote, is sufficient to draw proper conclusions, especially because the effect of a half *dl* dose may be overwhelming the effect of manipulated BMP signaling.

4.5 Conclusion

Our research has shown that manipulating the BMP signaling pathway has an effect on the Dorsal pathway. When we increased BMP signaling by overexpressing MAD, Medea, and the constitutively active thickveins receptor, we found that the Dorsal gradient widened, perhaps due to a mechanism also responsible for scaling. However, we did not see a narrowing of the gradient when we knocked down BMP signaling using a dominant negative form of the thickveins receptor; instead, we found that the gradient also widened, perhaps in response to the shrinking of the pMAD domain. More work should be done on this topic to further understand the mechanisms responsible for relaying information between these two essential patterning pathways.

4.6 Methods

4.6.1 Fluorescent in situ Hybridization

All embryos were aged to NC 14 (approx. 2-4 hours after egg lay), then fixed in 37% formaldehyde according to standard protocols (*23*). A combination fluorescent *in situ* hybridization/fluorescent immnuostaining was performed according to standard protocols (*23*). Briefly, fixed embryos were washed in PBS/Tween and hybridized at 55 ^{o}C overnight with anti-sense RNA probes, which were generated according to standard lab protocol. The embryos were then washed and incubated with primary antibodies at 4 ^{o}C overnight. The next day, they were washed and incubated for 1-2 hrs with fluorescent secondary antibodies at room temperature. The embryos were then washed and stored in 70% glycerol at -20 ^{o}C. Embryos were imaged within one month of completing the protocol.

Antibodies used were anti-dorsal 7A4 (deposited to the DSHB by Ruth Steward (DSHB Hybridoma Product anti-dorsal 7A4)) (1:10), rabbit anti-phospho-SMAD1 (FabGennix PMAD-140AP) (1:500), donkey anti-mouse-488 (Invitrogen A21202, Lot 81493) (1:500), rabbit anti-histone (abcam ab1791, Lot 940487) (1:5000), donkey anti-rabbit-546 (Invitrogen A10040, Lot 107388) (1:500), goat anti-biotin (ImmunoReagents, Raleigh, NC, GtxOt-070-D, Lot 19-19-112311) (1:50,000), donkey anti-goat-647 (Invitrogen A21447, Lot 774898) ((1:500), donkey anti-goat 546 (Invitrogen A11056) (1:500), goat anti-fluorescin (Rockland 600-101-096, Lot 19458) (1:500), rabbit anti-fluorescin (Life Technologies A889, Lot 1458646) (1:500), goat anti-histone (Abcam, ab12079, Lots GR6952-4 and GR129411-1) (1:100), donkey anti-rabbit-350 (ImmunoReagents, DkxRb-003-D350NHSX) (1:500). For some experiments the nuclear stain Draq5 (Cell Signaling #4084S) was used instead of an anti-histone antibody. For the MAD overexpression experiment, the nuclear stain DAPI was used.

Antisense RNA probes were generated according to standard lab protocol.

4.6.2 Mounting and Imaging of Fixed Embryos

Embryos were cross sectioned and mounted in 70% glycerol as described previously (*24*). Briefly, a razor blade was used to remove the anterior and posterior thirds of the embryo, leaving a cross section roughly 200 µm long by 200 µm in diameter. These sections were then oriented such that the cut sides became the top and bottom. Sections were then imaged at 20x on a Zeiss LSM 710 microscope. 15 z-slices 1.5 µm apart were analyzed, for a total section size of 21 µm.

4.6.3 Image analysis

Images of embryo cross sections were analyzed using a previously derived algorithm (*25*). Briefly, the border of the embryo was found computationally, then the nuclei were segmented using a local thresholding protocol. The intensity of dl in each segmented nucleus was calculated as the ratio between the intensity in the dl channel divided by the intensity in the nuclear channel. The intensity of mRNA expression was calculated as average intensity within an annulus roughly 18 µm wide around the perimeter of the embryo. mRNA profiles were fit to canonical parameters; those with a goodness of fit (gof) less than 0.7 were omitted from study.

All dl gradients were fit to a Gaussian, and these fits were used to determine the width parameter, σ. Gradients with a gof less than 0.8 were eliminated from the results. Normalized intensity plots were generated by fitting each embryo's data to its own Gaussian by subtracting the B value and 70% of the M value, then dividing by the A value. ($X = (x - B - 0.7M)/A$)). The average normalized intensity plot was generated by averaging the plots of all embryos in the specified genotype. We conducted the same analysis for pMAD gradients with the exception that we set the gof threshold to 0.7. See **Chapter 1** for a more thorough explanation.

Multiple experiments with statistically similar wild type controls were analyzed simultaneously to generate the data in this report. Statistical significance was calculated using two-tailed homoscedastic t-tests.

4.7 Acknowledgements

Many thanks to Alex Thomas and Jeramey Friedman who did many of the experiments presented here. Thanks to Tom Schwarz for provision of the UAS-MAD-GFP lines. Thanks to Laurel Raftery for provision of the UAS-Medea and UAS-Medea-GFP lines.

4.8 References

(1) Roth, S.; Stein, D.; Nüsslein-Volhard, C. A Gradient of Nuclear Localization of the Dorsal Protein Determines Dorsoventral Pattern in the Drosophila Embryo. *Cell* **1989**, *59* (6), 1189–1202.

(2) Reeves, G. T.; Stathopoulos, A. Graded Dorsal and Differential Gene Regulation in the Drosophila Embryo. *Cold Spring Harb. Perspect. Biol.* **2009**, *1* (4), a000836.

(3) Reeves, G. T.; Trisnadi, N.; Truong, T. V; Nahmad, M.; Katz, S.; Stathopoulos, A. Dorsal-Ventral Gene Expression in the Drosophila Embryo Reflects the Dynamics and Precision of the Dorsal Nuclear Gradient. *Dev. Cell* **2012**, *22* (3), 544–557.

(4) Roth, S.; Hiromi, Y.; Godt, D.; Nüsslein-Volhard, C. Cactus, a Maternal Gene Required for Proper Formation of the Dorsoventral Morphogen Gradient in Drosophila Embryos. *Development* **1991**, *112* (2), 371–388.

(5) Bergmann, A.; Stein, D.; Geisler, R.; Hagenmaier, S.; Schmid, B.; Fernandez, N.; Schnell, B.; Nüsslein-Volhard, C. A Gradient of Cytoplasmic Cactus Degradation Establishes the Nuclear Localization Gradient of the Dorsal Morphogen in Drosophila. *Mech. Dev.* **1996**, *60* (1), 109–123.

(6) De Robertis, E. M.; Kuroda, H. Dorsal-Ventral Patterning and Neural Induction in Xenopus Embryos. *Annu. Rev. Cell Dev. Biol.* **2004**, *20*, 285–308.

(7) O'Connor, M. B.; Umulis, D.; Othmer, H. G.; Blair, S. S. Shaping BMP Morphogen Gradients in the Drosophila Embryo and Pupal Wing. *Development* **2006**, *133* (2), 183–193.

(8) Freeman, M. Feedback Control of Intercellular Signalling in Development. *Nature* **2000**, *408* (November), 313–319.

(9) Christian, J. L.; Nakayama, T. Can't Get No SMADisfaction: Smad Proteins as Positive and Negative Regulators of TGF-β Family Signals. *BioEssays* **1999**, *21* (5), 382–390.

(10) Podos, S. D.; Ferguson, E. L. Morphogen Gradients: New Insights from DPP. *Trends Genet.* **1999**, *15* (10), 396–402.

(11) Eldar, A.; Dorfman, R.; Weiss, D.; Ashe, H.; Shilo, B.; Barkai, N. Robustness of the BMP Morphogen Gradient in Drosophila Embryonic Patterning. *Nature* **2002**, *419* (19 September 2002), 304–308.

(12) Gao, S.; Laughon, A. Decapentaplegic-Responsive Silencers Contain Overlapping Mad-Binding Sites. *J. Biol. Chem.* **2006**, *281* (35), 25781–25790.

(13) Brand, a H.; Perrimon, N. Targeted Gene Expression as a Means of Altering Cell Fates and Generating Dominant Phenotypes. *Development* **1993**, *118* (2), 401–415.

(14) Miles, W. O.; Jaffray, E.; Campbell, S. G.; Takeda, S.; Bayston, L. J.; Basu, S. P.; Li, M.; Raftery, L. A.; Ashe, M. P.; Hay, R. T.; et al. Medea SUMOylation Restricts the Signaling Range of the Dpp Morphogen in the Drosophila Embryo. *Genes Dev.* **2008**, *22* (18), 2578–2590.

(15) Dudu, V.; Bittig, T.; Entchev, E.; Kicheva, A.; Jülicher, F.; González-Gaitán, M. Postsynaptic Mad Signaling at the Drosophila Neuromuscular Junction. *Curr. Biol.* **2006**, *16* (7), 625–635.

(16) Shimmi, O.; Umulis, D.; Othmer, H.; O'Connor, M. B. Facilitated Transport of a Dpp/Scw Heterodimer by Sog/Tsg Leads to Robust Patterning of the Drosophila Blastoderm Embryo. *Cell* **2005**, *120* (3), 873–886.

(17) Umulis, D. M.; Serpe, M.; O'Connor, M. B.; Othmer, H. G. Robust, Bistable Patterning of the Dorsal Surface of the Drosophila Embryo. *Proc. Natl. Acad. Sci. U. S. A.* **2006**, *103* (31), 11613–11618.

(18) Dorfman, R.; Shilo, B. Z. Biphasic Activation of the BMP Pathway Patterns the Drosophila Embryonic Dorsal Region. *Development* **2001**, *128* (6), 965–972.

(19) Carneiro, K.; Fontenele, M.; Negreiros, E.; Lopes, E.; Bier, E.; Araujo, H. Graded Maternal Short Gastrulation Protein Contributes to Embryonic Dorsal-Ventral Patterning by Delayed Induction. *Dev. Biol.* **2006**, *296* (1), 203–218.

(20) Araujo, H.; Bier, E. Sog and Dpp Exert Opposing Maternal Functions to Modify Toll Signaling and Pattern the Dorsoventral Axis of the Drosophila Embryo. *Development* **2000**, *127* (16), 3631–3644.

(21) Fontenele, M.; Carneiro, K.; Agrellos, R.; Oliveira, D.; Oliveira-Silva, A.; Vieira, V.; Negreiros, E.; Machado, E.; Araujo, H. The Ca2+-Dependent Protease Calpain A Regulates Cactus/IκB Levels during Drosophila Development in Response to Maternal Dpp Signals. *Mech. Dev.* **2009**, *126* (8–9), 737–751.

(22) Fontenele, M.; Lim, B.; Oliveira, D.; Buffolo, M.; Perlman, D. H.; Schupbach, T.; Araujo, H. Calpain A Modulates Toll Responses by Limited Cactus/IκB Proteolysis. *Mol. Biol. Cell* **2013**, *24*, 2966–2980.

(23) Kosman, D.; Mizutani, C. M.; Lemons, D.; Cox, W. G.; McGinnis, W.; Bier, E. Multiplex Detection of RNA Expression in Drosophila Embryos. *Science* **2004**, *305* (5685), 846.

(24) Carrell, S. N.; Reeves, G. T. Imaging the Dorsal-Ventral Axis of Live and Fixed Drosophila Melanogaster Embryos. In *Tissue Morphogenesis*; Nelson, C. M., Ed.; Methods in Molecular Biology; Springer New York: New York, NY, 2015; Vol. 1189, pp 63–78.

(25) Trisnadi, N.; Altinok, A.; Stathopoulos, A.; Reeves, G. T. Image Analysis and Empirical Modeling of Gene and Protein Expression. *Methods* **2013**, *62* (1), 68–78.

5 A Facilitated Diffusion Mechanism Establishes the *Drosophila* Dorsal Gradient*

* Adapted from Carrell, S. N.; O'Connell, M. D.; Allen, A. E.; Smith, S. M.; Reeves, G. A Facilitated Diffusion Mechanism Establishes the Drosophila Dorsal Gradient. *bioRxiv* 2016. This chapter reflects my contribution to the article

5.1 Summary

The transcription factor NF-κB plays an important role in the immune system as an apoptotic and inflammatory factor. In the *Drosophila melanogaster* embryo, a homolog of NF-κB called Dorsal (dl) patterns the dorsal-ventral (DV) axis in a concentration-dependent manner. During early development, dl is sequestered outside the nucleus by Cactus (Cact), homologous to IκB. Toll signaling at the ventral midline breaks the dl/Cact complex, allowing dl to enter the nucleus where it transcribes target genes. Here we show that dl accumulates on the ventral side of the embryo over the last 5 cleavage cycles and that this accumulation is the result of facilitated diffusion of dl/Cact complex. We speculate that Cact plays a role supplemental to excluding dl from the nucleus in DV axis specification by shuttling dl towards the ventral midline. Given that this mechanism has been found in other, independent systems, we suggest it may be more prevalent than previously thought.

5.2 Introduction

In a developing organism, tissues are patterned by long-range signaling enacted through morphogen concentration gradients that carry the positional information necessary to control gene expression in a spatially-dependent fashion. In the *Drosophila* blastoderm, the transcription factor Dorsal (dl) acts as a morphogen to regulate the spatial patterning of greater than 50 genes along the dorsal-ventral (DV) axis (*1*,*2*). However, despite its centrality to development, the mechanism that controls the formation of the dl nuclear concentration gradient at the whole-embryo scale is not well understood.

At the single nucleus/cell level, dl is sequestered to the cytoplasm in an inactive complex with the IκB homolog Cactus (Cact). On the ventral side of the embryo, Toll signaling results in the degradation of Cact, freeing dl to enter the nucleus where it regulates transcription. This mechanism, combined with a ventral-to-dorsal gradient of Toll signaling, would seem sufficient to develop a gradient of nuclear dl concentration (*3*). In fact, when dl was first discovered to be the primary morphogen for DV axis specification, it was observed that dl protein is homogenously distributed throughout the embryo and only differs in its nuclear localization. However, the staining technique used Horseradish Peroxidase (HRP) as the detection molecule for a biotin/avidin complex (*3*). This method relies on accumulating large protein complexes to amplify the signal, reducing its sensitivity when the concentration of target protein is low (*4*). In the intervening 25 years, newer, more specific techniques have been developed. Using a fluorescently-labeled secondary antibody, we have found that dl accumulates both in the nuclei and in the cytoplasm on the ventral side of the embryo over time (*5*) (see **Figure 5.1A-D**).

In this study, we investigate the mechanism of dl nuclear concentration gradient formation at the whole-embryo scale. Our experimental data support the hypothesis that a mechanism of facilitated diffusion is responsible for the global formation of the dl nuclear concentration gradient. Under this “shuttling” hypothesis, a dorsal-to-ventral concentration gradient of cytoplasmic dl/Cact complex develops as the result of Toll-mediated degradation of Cact, which drives the overall flux of dl towards the ventral side of the embryo. Besides ventrally-directed dl accumulation, our experimental results verify that the shuttling mechanism can account for several other previously inadequately explained phenotypes, such as duplicated dl gradient peaks, regions of depleted dl, dl heterozygous phenotypes, and widened dl-GFP gradients (*5*–*8*).

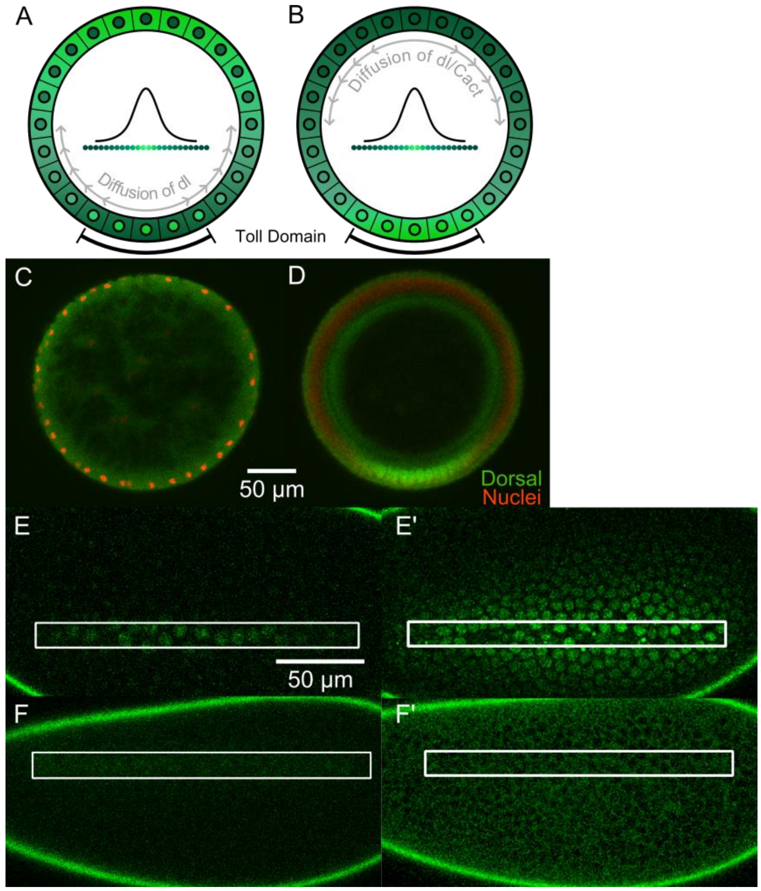

Figure 5.1: Dorsal Accumulates on the Ventral Side of the Embryo. (A) Current research suggests that dl does not rapidly diffuse from nucleus to nucleus and therefore it is locally depleted from the area around each nucleus. (B) We propose that total dl accumulates at the ventral midline due to diffusion. "Toll Domain" indicates that active Toll receptors are being formed on the ventral side of the embryo. (C) and (D) Cross-sections of wild type embryos, stained for dl and nuclei. (C) dl is equally distributed throughout the embryo when it is young. (D) Total dl has accumulated at the ventral midline by late NC 14. Compare to (B). (E) and (F) dl-paGFP results indicate that dl diffuses throughout the embryo. Activation area in the white box. Anterior to the left. (E and E') Activation near the ventral midline approx. (E) 3 minutes and (E') 90 minutes after first activation. (F and F') Activation near the dorsal midline approx. (F) 3 minutes and (F') 90 minutes after first activation.

The mechanism of facilitated diffusion has been previously described and is responsible for gradient formation in other systems, such as the Dpp/BMP signaling pathway (*9–13*); it has also been suggested for the formation of the Spätzle gradient upstream of Toll signaling (*14*). The dl/Cact system has each of the features required for facilitated diffusion (*15*): (1) the primary molecule (dl) binds to a "carrier" molecule (Cact) that protects it from capture, (2) the primary/carrier complex is diffusible (due to the syncytial state of the early embryo), and (3) the complex is broken in a spatially-dependent manner (through Toll signaling on the ventral side of the embryo). If these features are in place, the primary molecule (dl) accumulates over time at the site of complex degradation (the ventral side of the embryo). Therefore, we conclude that Cact performs a role in dl gradient formation additional to regulating dl's entry into the nucleus: shuttling dl to the ventral side to form the mature gradient.

5.3 Results

5.3.1 Dorsal accumulation on the ventral side of the embryo results from movement of the dl/Cact complex

Initially, Dorsal is uniformly distributed along the DV axis of the developing embryo (**Figure 5.1C**); during nuclear cycles 11-14, it accumulates on the ventral side (**Figure 5.1B,D**). This observation is consistent with previously-published fluorescent images of anti-dl immunostainings in fixed embryos and in images of dl-GFP fluorescence in live embryos (*1*,*5*,*6*,*16*). The mechanism for this overall polarization of total dl in the embryo could be asymmetric degradation or production; however, previous modeling work and our experimental results favor an overall flux of dl to the ventral side of the embryo (*17*). Using a photoactivatable GFP (paGFP) tag (*18*), we noticed that dl appears in regions of the embryo over 8-10 nuclei away from the site of paGFP activation in the time span of 90 minutes. Given a cell diameter (i.e., the average distance between the centroids of two neighboring nuclei) of roughly 7 μm, this translates to an effective diffusivity of ~0.5-0.9 $\mu m^2/s$ and a time scale to cross one cell diameter that is on the order of minutes. When activated near the ventral midline, dl-paGFP diffuses from its location of activation and fills adjacent nuclei (**Figure 5.1E**). When activated on the dorsal side of the embryo, dl-paGFP diffuses and shows a typical pattern of exclusion from nuclei in more dorsal regions and moderate uptake into the nuclei in more lateral regions (**Figure 5.1F**). As discussed previously, this flux of dl could be due to diffusion of free dl, dl/Cact complex, or both species (*19*).

Computational results showed that the mechanism of facilitated diffusion can be tested by altering three biophysical parameters to slow the mechanism of facilitated diffusion: (1) decreasing the dl dosage, (2) lowering the diffusivity of dl or Cact, and (3) increasing the width of the active Toll domain (*17*). The model predicts that these perturbations will each result in a hallmark progression of phenotypes (depending on the strength of the perturbation): the dl gradient first widens, then becomes flat at the top, then splits into two peaks (**Figure 5.2**). We conducted experiments to address all three parameters, and found that they supported our hypothesis.

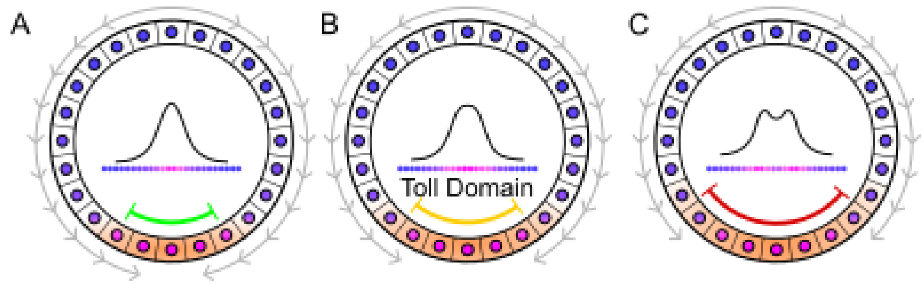

Figure 5.2: Perturbations to Gradient Formation Parameters Result in a Hallmark Progression of Phenotypes. First, the peak expands (A), then flattens (B), then splits in two (C). Arrows indicate diffusion of dl/Cact complex, the Toll domain is highlighted in orange, and the nuclear concentration is indicated by blue-pink gradient.

5.3.2 Decreasing dl dosage widens and flattens the dl gradient

In embryos from mothers heterozygous null for dl (hereafter referred to as *dl*/+ embryos), the shape of the gradient becomes slightly wider, flatter, and lower in amplitude, with the slope maintained in the lateral regions but peak levels of the gradient flattened (*6*) (**Figure 5.3**). From a functionality perspective, this phenotype is striking because the portion of the dl gradient that is lost (the peak concentration) is superfluous as any level above the threshold level for high-concentration target genes will result in expression, while the portion of the gradient that is necessary for patterning gene expression boundaries — the graded portion between 20% and 45% DV position — is maintained.

To explain this effect, one simple hypothesis is that the ventral-most nuclei *would have* reached normal dl levels, but only if there were enough dl present. Since the total amount of dl is compromised, the ventral most nuclei reach a lower-than-normal concentration of dl. However, models of dl gradient formation that lack the shuttling mechanism predict the loss of 50% dl nuclear concentration globally in *dl*/+ embryos, rather than a spatially patterned loss (*17*).

In contrast, the shuttling hypothesis can make sense of the heterozygous phenotype when combined with an additional assumption of active Toll receptor saturation, which is independent of the shuttling model and its predictions. Under this assumption, wild type embryos have enough dl/Cact complex to saturate active Toll receptors in the ventral-lateral regions of the embryo, which allows a significant flux of dl/Cact complex to reach the ventral midline and results in a smoothly-peaked, Gaussian-like curve. In embryos with half the normal dl dosage, active Toll receptors in the tails of the gradient are not saturated; therefore, less dl/Cact complex arrives at the ventral midline, and these embryos never accumulate a smooth peak of the dl gradient (**Figure 5.3B,D**).

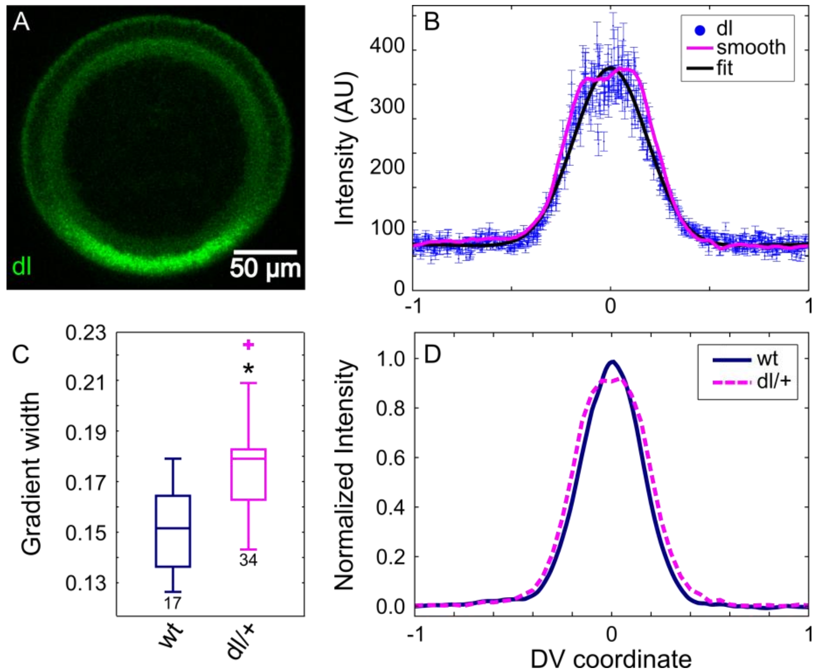

Figure 5.3: Embryos from Mothers Heterozygous for dl Have a Different-Shaped dl Gradient. (A) Cross-section of a NC 14 embryo from a mother heterozygous for dl stained for dl. (B) Plotted nuclear intensity of embryo in (A) as a function of DV coordinate (each blue dot is one nucleus). Error bars indicate SEM of nuclear intensity. Pink curve is the smoothed data; black curve is a fit of the data to a Gaussian. (C) Box plot of gradient widths (σ) for embryos from mothers with 2 (wt) and 1 (dl/+) copies of dl. Here and elsewhere in the paper, boxes indicate interquartile range (IQR): from the 25th to the 75th percentile of the data, whiskers extend a maximum of 1.5 times the width of the IQR from the box, and outliers (plus signs) are defined as points that lie outside the whiskers. Numbers indicate sample size. Asterisk indicates statistical significance of $p<10^{-4}$ from wt. (D) Normalized average plot of dl gradient in embryos from (C).

5.3.3 Decreased diffusion of dl/Cact complex widens the dl gradient

Other researchers have generated several GFP-tagged versions of dl in order to study its dynamics in living embryos (*5*,*20*). In each case, tagging dl with an extra protein moiety caused the dl gradient to expand. If the gradient develops via a diffusion mechanism, this result would seem counterintuitive. One would expect that increasing the size of a molecule would decrease its diffusivity, and thus restrict the spatial range of the gradient. On the other hand, a shuttling mechanism would predict the opposite: lowering the diffusivity of dl/Cact complex should widen the gradient. To test this prediction, we analyzed dl and Cact constructs tagged with proteins that either dimerize or tetramerize in order to form large clusters of dl/Cact complex.

Other studies have shown that tagging dl with a monomeric Venus (dl-mVenus) causes the dl gradient to widen (width parameter $\sigma = 0.16 \pm 0.01$; compare to $\sigma = 0.14 \pm 0.01$ for wild type) ,while a GFP tag causes a much greater widening ($\sigma = 0.20 \pm 0.02$) (*5*,*6*). We surmised that the difference between these scenarios is that Venus is an obligate monomer while the GFP construct weakly dimerizes (*21*). To carefully measure the effect of dimerization of the protein tag on gradient width, we repeated these experiments to control for differences in fluorescent protein tag, protocol, researcher, and equipment. First, we analyzed the gradient in embryos that had one endogenous copy of dl replaced with dl tagged with the weakly-dimerizing GFP (dl-dGFP) (*5*). We found that the dl gradient in these embryos widened significantly ($\sigma = 0.21 \pm 0.03$) as compared to wild type, with σ values that closely match previous work (*5*,*6*) (**Figure 5.4A,B**).

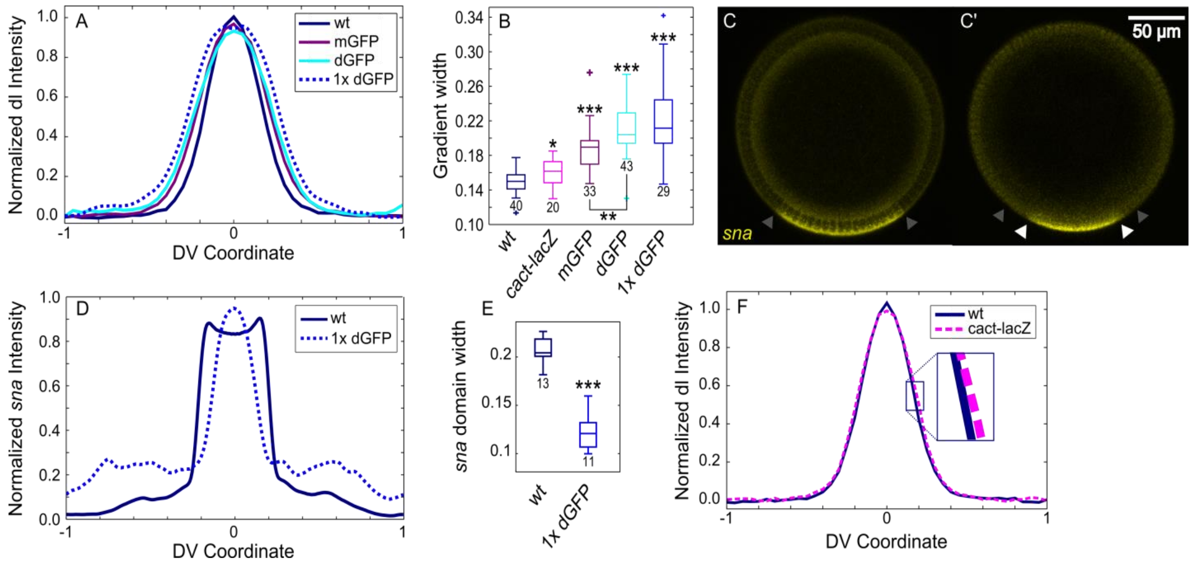

Figure 5.4: Decreasing Diffusion of dl/Cact Increases the Width of the dl Gradient. (A) Normalized average plots of the dl gradient in embryos with 2 copies of wt dl (wt), 1 copy of wt dl and 1 copy of dl-mGFP (mGFP), 1 copy of wt dl and 1 copy of dl-dGFP (dGFP), and 1 copy of dl-dGFP (1x dGFP). (B) Box plot of gradient widths (σ) for embryos shown in (A) and (F). (C) and (C') *sna* domain in wt (C) and 1x dGFP (C') embryos. Gray arrowheads indicate the wt domain of *sna*; white indicate the *sna* domain in 1x dGFP embryo. (D) Normalized average plots of the *sna* intensity in wt and 1x dGFP embryos. (E) Box plot of *sna* domain width for embryos shown in D. (F) Normalized average plots of the dl gradient in embryos from mothers with 2 copies of wt *cact* (wt) and 1 copy of wt *cact* and 1 copy of *cact-lacZ* (cact-lacZ). Inset shows more clearly that cact-lacZ is slightly wider than wt. Asterisks indicate statistical significance (*$p<0.02$; **$p<10^{-3}$; ***$p<10^{-11}$) from wt unless otherwise noted. Numbers indicate sample size. See also **Figure 5.5**.

The weak dimerization of GFP can be abolished by the A206K mutation (*21*); therefore, we designed dl-GFP constructs with the obligate monomer version of GFP (dl-mGFP) to investigate the effect of increasing the mass of dl without causing dimerization. Embryos carrying these constructs have gradients slightly wider than wild type ($\sigma = 0.19 \pm 0.03$), comparable to our measurements in embryos with the monomeric Venus tag ($\sigma = 0.18 \pm 0.03$) (**Figure 5.4B**, see also **Figure 5.5A,B**). We expect that the widening effect in embryos that carry a monomeric tag is likely due to the increased mass of the dl protein and not the dimerization of the tag. We also designed dl-Venus constructs that had weak dimerization restored due to a K206A mutation (dl-dVenus); embryos carrying this dl-dVenus transgene had dl gradients that were significantly wider than those in embryos carrying the dl-mVenus transgene ($\sigma = 0.19 \pm 0.02$), matching the trend seen in dl-mGFP and dl-dGFP embryos (see **Figure 5.5A,B**). Taken together, these data indicate that the weak dimerization of the fluorescent tags, which presumably slows diffusion of dl/Cact complex, is the key factor in widening the gradient.

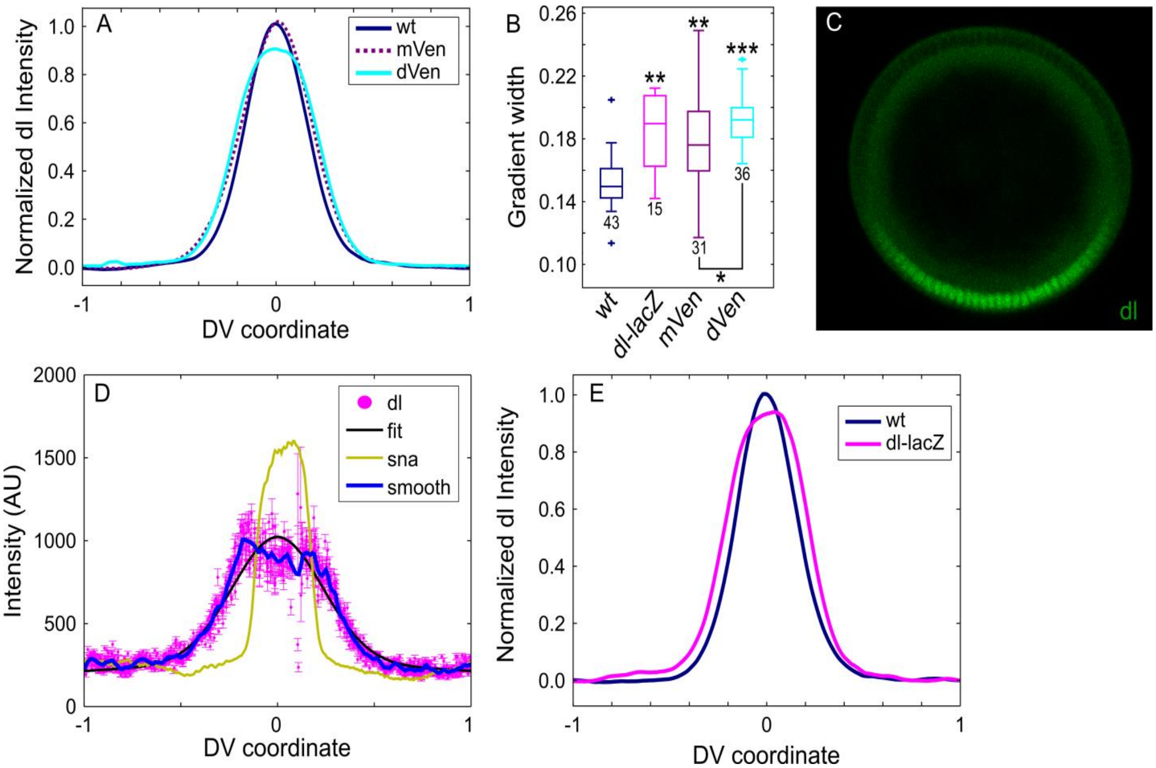

Figure 5.5: Decreasing Diffusion of dl/Cact Widens the dl Gradient. (A) Normalized average plots of the dl gradient in embryos from mothers with 2 copies of wt dl (wt), 1 copy of wt dl and 1 copy of dl-mVenus (mVen), and 1 copy of wt dl and 1 copy of dl-dVenus (dVen). Note that dVen has a flat top. (B) Box plot of gradient widths (σ) for embryos shown in (A) and (E). Asterisks indicate statistical significance (*$p<0.02$; **$p<10^{-5}$; ***$p<10^{-17}$) from wt unless otherwise noted. Numbers indicate sample size. (C) Cross-section of a NC 14 embryo from a mother homozygous null for wt dl with 1 copy of dl-dGFP, stained for dl. This is the same embryo as presented in **Figure 5.4(C')**. (D) Plotted nuclear intensity of dl and *sna* in the embryo shown in (C) and **Figure 5.4(C')**. (E) Normalized average plots of the dl gradient in wt embryos and embryos from mothers with 1 copy of wt dl and 2 copies of dl-lacZ (dl-lacZ).

It was also observed that a single copy of dl-dGFP was unable to complement null mutations in the endogenous dl gene; two copies are necessary to rescue the mutant (*5*,*6*). This result contrasts dl-mVenus, which complements at one copy. Our shuttling hypothesis explains this phenotype, as embryos from *dl* mothers carrying one copy of dl-dGFP have two defects in shuttling: a lower copy number of dl and a reduced diffusivity of the dl/Cact complex. These embryos have highly widened gradients ($\sigma = 0.22 \pm 0.04$) (see **Figure 5.4A,B** and **Figure 5.5C,D**). We surmised that these gradients are perturbed enough to severely disrupt gene expression, perhaps not becoming strongly-peaked enough to turn on high-threshold genes, such as *snail* (*sna*). Therefore, we analyzed *sna* expression in embryos from *dl*; *dl-dGFP*/+ mothers, and found that these embryos either lacked *sna* expression or expressed *sna* in a very narrow domain (**Figure 5.4C-E** and **Figure 5.5D**), confirming our hypothesis that the double perturbation results in a breakdown of the typically robust patterning system.

To investigate the effect of larger complexes on dl/Cact diffusion, we evaluated the effect of a *dl-lacZ* transgene on the dl gradient (*22*). As the protein product of *lacZ*, β-galactosidase (β-gal), tetramerizes, we expect that this fusion will slow the diffusion of dl to a greater extent than dGFP. However, we found that two copies of this transgene in a *dl/+* background were needed in order to see an effect on the width of the dl gradient, which widened as predicted by the shuttling model (**Figure 5.5B,E**). This effect is likely due to the fact that *dl-lacZ* acts as an antimorphic allele (*22*); such dl-βgal fusion proteins are suspected to be expressed at very low levels in surviving fly lines (*23*).

In order to study the effect of decreased Cact diffusion on dl gradient formation, we examined embryos from mothers carrying a single copy of a *cact-lacZ* transgene in a heterozygous *cact* background (*24*). We expect that this fusion will slow diffusion of the dl/Cact complex without affecting the diffusion of free dl. In these embryos, the dl gradient is expanded (**Figure 5.4B,F**), indicating an inability of Cact to properly shuttle dl to the ventral midline. In a naïve model, where Cact does not shuttle dl and there is no flux toward the ventral midline, we do not expect changing the diffusion of Cact to have such an effect on the dl gradient. It is important to note that, under the typical morphogen gradient phenomenon, decreasing the diffusivity of the morphogen would result in a narrower (more concentrated) gradient. Since our results consistently show that the dl gradient widens rather than narrows when the diffusivity of dl or Cact is reduced, we conclude that dl/Cact complex, and not free dl, is the dominant diffusive species.

5.3.4 Increasing the width of the active Toll domain results in a split peak of dl

The shuttling hypothesis predicts that widening the active Toll domain results first in a widened, then flattened, then split dl gradient (**Figure 5.2**). As the extent of the Toll domain is controlled by Gurken/EGFR signaling during oogenesis (*25*,*26*), we analyzed embryos from mothers carrying a hypomorphic EGFR allele ($egfr^{t1}$) (*7*). We found that embryos from mothers heterozygous for this allele have significantly widened dl gradients, and most (10/12) embryos from homozygous mothers have gradients so wide that a split peak forms (see **Figure 5.6**). This result is consistent with previous reports that various *gurken* and *egfr* mutations generate a duplicated dl gradient as measured by dl staining, Twist staining, and sites of ventral furrow formation (*7*), which is not readily explained in the absence of a shuttling phenomenon (*2*,*27*).

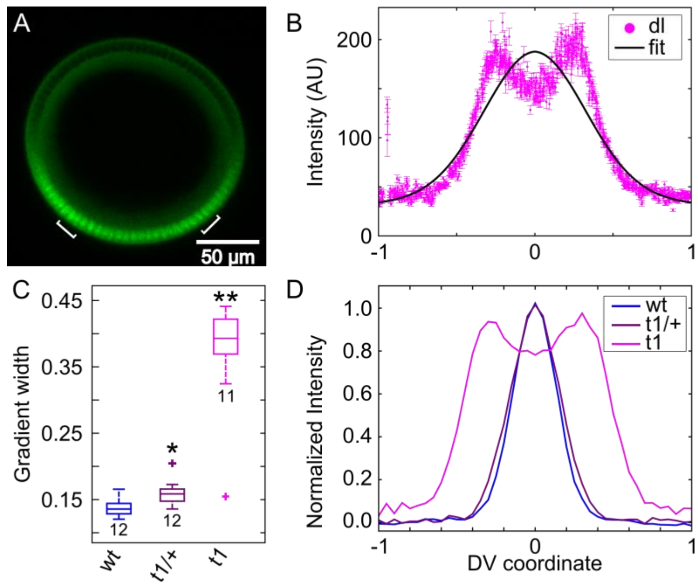

Figure 5.6: The Hypomorphic Allele *egfr*^{t1} Significantly Widens the dl Gradient. (A) Cross-section of an embryo from a mother homozygous for *egfr*^{t1} stained for dl. Brackets indicate peaks of nuclear dl. (B) Plotted nuclear intensity of embryo in (A) as a function of DV coordinate (each pink dot is one nucleus). The shape has changed significantly from wild type, as the Gaussian curve (black) does not represent the gradient well. Error bars indicate SEM of nuclear intensity. (C) Box plot of gradient widths (σ) for embryos from mothers with 0 (wt), 1 (t1/+), and 2 (t1) copies of *egfr*^{t1}. Numbers indicate sample size. Asterisks indicate statistical significance (* $p<0.01$, ** $p<10^{-8}$) from wt. (D) Normalized average plot of dl gradient in embryos from (C).

5.3.5 An anteroposterior gradient of dl supports the shuttling hypothesis

It has been suggested that a shuttling phenomenon also occurs through the processing of Spätzle (Spz), the ligand for Toll signaling (*14*), which may explain some of the phenotypes described here. To determine whether the hallmark phenotypes of shuttling could occur without assistance from the protease cascade or Spz processing, we expressed a constitutively active form of Toll (Toll^{10b}) at the anterior pole of the developing embryo using the *bicoid* 3' UTR and the *bicoid* promoter (*8*). Embryos from mothers carrying this construct (*bcd> toll^{10b}: bcd 3' UTR*) have an anterior-posterior (AP) dl gradient in addition to the native DV gradient. Naïvely, one may expect that the existence of two gradients in active Toll signaling would result in higher concentrations of nuclear dl where these two gradients overlap. In contrast, the shuttling hypothesis predicts that dl nuclear concentration would be *lower* in the region of overlap, as the two competing dl/Cact sinks cause Cact to shuttle dl toward both the anterior pole and the ventral midline (see **Figure 5.7A,B**). This prediction is borne out in experiment, as these embryos show a decreased intensity of the dl gradient in the region of overlap. Furthermore, 64% (9/14) of these embryos show a visible narrowing of the *sna* expression domain at roughly 30% egg length, consistent with previously published numbers (*8*). There is a dip in dl nuclear intensity at this location as well (**Figure 5.7B**).

We also examined embryos from mothers carrying a homozygous mutation in *gastrulation defective* (*gd^{7}*), which eliminates the endogenous ventral-to-dorsal gradient. Swapping the *bicoid* promoter for the stronger *hsp83* promoter (*hsp83> toll^{10b}: bcd 3' UTR*) (*8*), we were able create a wider dl gradient at the anterior pole. Half of these embryos (7/16) show two peaks of dl both by eye and when the nuclear intensity is plotted (**Figure 5.7C,D**). Furthermore, these embryos have a double peak of *sna* (*28*). In order to determine whether or not this double peak phenomenon was a result of the embryo's geometry at the pole, we analyzed embryos with an AP dl gradient initiated by the weaker *bicoid* promoter. These embryos showed no such double peak effect (see **Figure 5.8**). These results further support our shuttling hypothesis as the dl gradient progresses from narrow (weak promoter) to double peak (strong promoter) much as it does in the native DV system when the Toll domain expands.

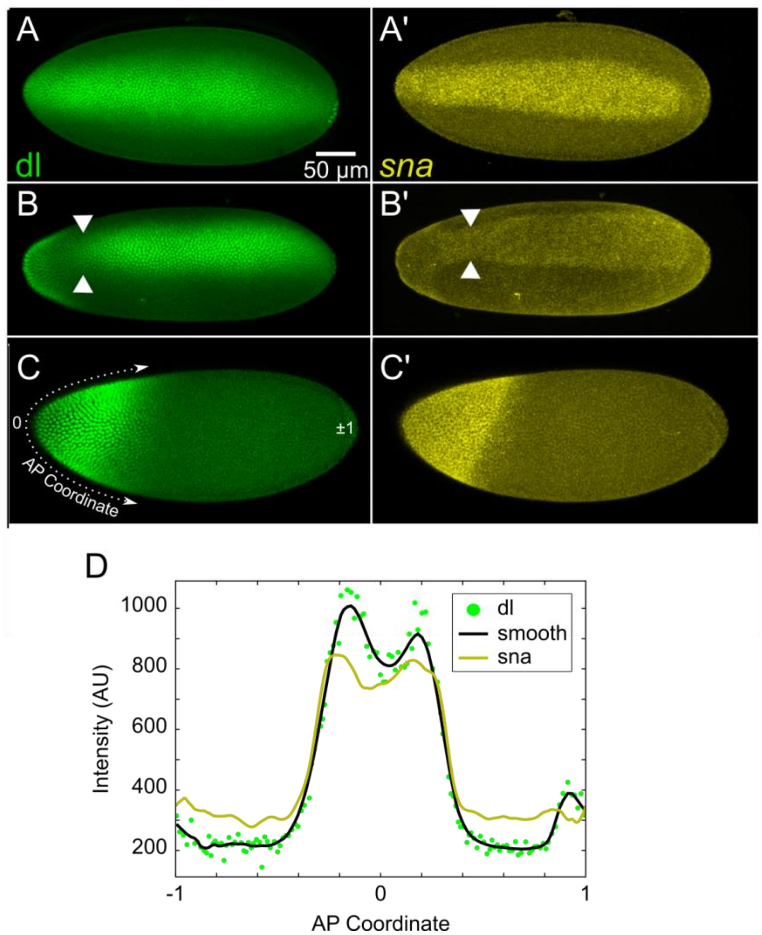

Figure 5.7: An Ectopic, Anterior-Posterior Dorsal Gradient Exhibits Shuttling Phenomena. (A) and (A') dl and *sna* expression in a wild type embryo. (B) and (B') dl and *sna* expression in an embryo with an anteroposterior gradient of dl driven by the *bcd* promoter in addition to the wild type DV gradient. White arrowheads indicate a narrowing of each domain at ~30% EL. (C) and (C') dl and *sna* expression in an embryo with an anteroposterior gradient of dl driven by the *hsp83* promoter and the DV gradient abolished by a homozygous mutation in *gd*. (D) Plot of dl and *sna* domains from the embryo in (C). Each green dots is one nucleus and the black curve is a smoothing of the dl data. Embryo images are maximal intensity projections. See also **Figure 5.8**.

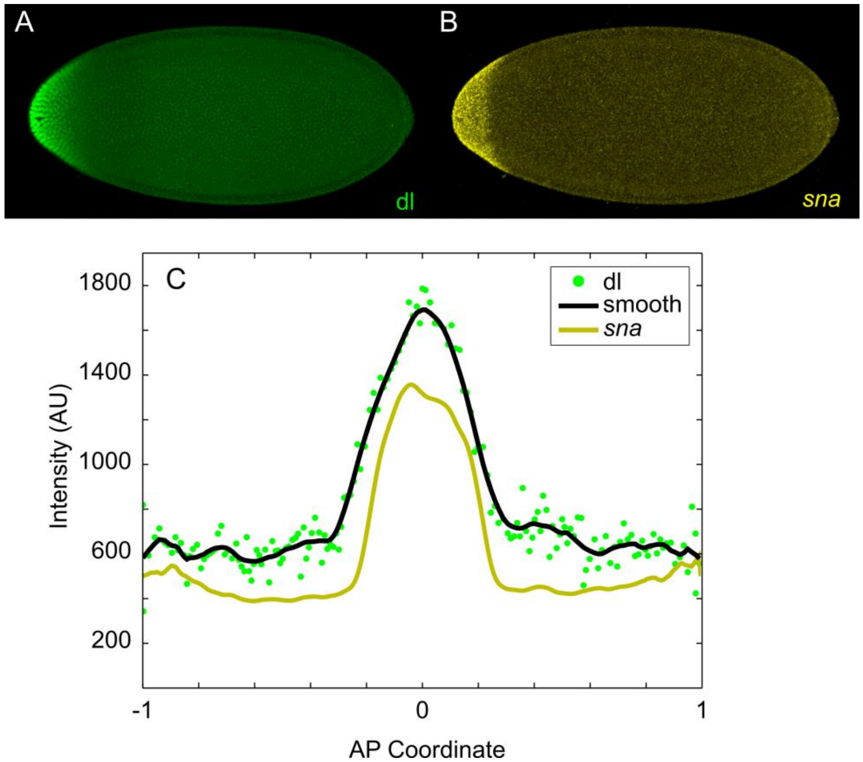

Figure 5.8: Embryos with AP dl Gradients Under the Control of a Weaker (bcd) Promoter Do Not Exhibit the Double-Peak Phenomenon. (A) Embryo stained for dl. (B) Embryo stained for *sna*. (C) Plot of embryo shown in (A) and (B).

5.4 Discussion

In this study, we investigated the formation of the dl morphogen gradient in the early *Drosophila* embryo. Based on our experimental results, we conclude that the dl gradient is established by a facilitated diffusion, or "shuttling" mechanism, in which dl/Cact complex diffuses towards the ventral midline where Cact is degraded. Furthermore, our hypothesized mechanism makes sense of several previously unexplained phenomena in the literature.

Besides dl binding to Cact, the shuttling mechanism requires two phenomena to occur. First, dl/Cact complex must be able to move throughout the embryo. Our experiments with dl-paGFP show that dl does indeed move through the embryo in a manner that appears to be consistent with diffusion. In contrast, a previous report showed that each nucleus has its own well-mixed cytoplasmic pool of dl to draw from, and that dl does not readily diffuse from pool to pool (*20*). This observation was confirmed by a study which showed that barriers to diffusion exist in the early embryo, despite the lack of cell membranes (*29*). However, these results do not contradict our hypothesized mechanism, which relies on movement of dl from one pool to another, because the time scales are different (seconds vs. minutes). Furthermore, observational evidence supports a diffusion-based shuttling mechanism, as lowering the diffusivity of either dl or Cact widens the gradient (**Figure 5.4** and **Figure 5.5**), rather than the narrowing that one might expect from a morphogen gradient established by (non-facilitated) diffusion. The shuttling mechanism explains why dl tagged with a weakly dimerizing GFP widens the gradient more than one tagged with monomeric Venus (*5*), and also explains the related observation that one copy of dl-mVenus complements loss of endogenous dl while one copy of dl-dGFP does not (*5*,*6*). Similarly, this mechanism makes sense of the observation that dl tagged with β-galactosidase, which forms tetramers, is antimorphic (*22*), as the dl moieties in tetramers of dl-βgal dimerize with untagged dl to disrupt the formation of the endogenous dl gradient.

Second, the shuttling mechanism requires the ventral midline to be a sink for the dl/Cact complex. This condition becomes especially clear in embryos that have an ectopic AP dl gradient in addition to the endogenous DV gradient (*8*). In these embryos, a second sink for the dl/Cact complex is established, and the two competing sinks form a local minimum in the dl gradient near to where they overlap, rather than the global maximum one might expect if the two gradients were additive as they would be in a model without facilitated diffusion (**Figure 5.7B**). This result has been previously observed as a "gap" in the *sna* domain where the two gradients overlap (*8*). These results support our hypothesis that the Toll domain acts as a sink, a necessary condition for shuttling.

In this system, it appears that active Toll receptors are somewhat limiting as they are easily saturated with dl/Cact complex. This saturation is not essential to the shuttling mechanism *per se*, but it is necessary for the mechanism to explain several observations of the dl/Cact system. Under wild type conditions, a significant flux of dl/Cact complex can bypass the saturated active Toll receptors in the tails of the gradient, which results in the accumulation of a smooth, intense peak of dl signaling at the ventral midline of the embryo. However, in embryos from *dl*/+ mothers, there is not enough dl/Cact complex to saturate active Toll receptors in the tails of the gradient, and thus there is less accumulation of dl at the ventral midline (*6*) (See **Figure 5.3**). Similarly, when the Toll gradient is greatly expanded, as in embryos from *egfr*^{t1} mothers (*7*), the domains of saturated Toll receptors move further from the ventral midline, resulting in a split peak (**Figure 5.6**). Additionally, the split-peak phenomenon has also been observed in the dl gradient in abnormally large embryos (*30*). This specific phenotype could be explained by shuttling of the Toll ligand Spz (*14*); however, we observed the same phenomenon in embryos with an ectopic AP dl gradient established by constitutively active Toll. In both cases, ventrally- (anteriorly-) diffusing dl/Cact complex does not make it to the ventral midline (anterior pole) before being dissociated, leaving the ventral- (anterior-) most nuclei somewhat devoid of dl. A similar mechanism, in which the removal rate of BMP ligands surpasses the rate of BMP flux to the dorsal midline, has been suggested to explain the computationally-predicted split-peak phenotype for the BMP system in the early embryo (*31*).

A shuttling mechanism has been proposed in several other contexts and in multiple organisms (*9*–*14*). For example, during the same stage of *Drosophila* development, shuttling of the BMP ligands Dpp and Scw through the actions of Sog and Tsg is responsible for the concentration of BMP signaling to a narrow, intense stripe at the dorsal midline of the embryo (*9*,*12*,*13*,*31*–*35*). A similar mechanism is also present in BMP signaling in vertebrate embryos to specify the DV axis (*34*). In light of these examples, we speculate that facilitated diffusion may be a more prevalent mechanism of morphogen gradient formation than previously appreciated.

5.5 Experimental Procedures

5.5.1 Fly lines

yw flies were used as wild type. *dl-paGFP*, *dl-mGFP*, and *dl-dVenus* were created by BAC recombineering. For live imaging, flies carrying *dl-paGFP* were crossed to flies carrying H2A-RFP on the second chromosome (BS# 23651). *dl/+* flies were created by cleaning up dl^{1} via two homologous recombinations with yw to generate $dl^{1.2.5}$. *cact/+*; *cact-full lacZ 25* flies were obtained from David Stein (*24*). *dl-lacZ* flies were obtained from Shubha Govind (*22*). *dl-dGFP* and *dl-mVenus* flies and the original BACs used to create them were obtained from Angela Stathopolous. *dl-mGFP,*$dl^{1.2.5}$ flies were created by homologous recombination. Presence of *dl-mGFP* was confirmed by w^{+}. Presence of $dl^{1.2.5}$ was confirmed via sequencing by GENEWIZ, Research Triangle Park, NC. $egfr^{t1}$*/CyO* flies were obtained from the Bloomington Stock Center (# 2079). Flies carrying the *bcd>*$toll^{10b}$*: bcd 3'UTR* construct were obtained from Angela Stathopolous. The plasmid carrying *FRT-stop-FRT hsp83>* $toll^{10b}$*: bcd 3'UTR* was also obtained from Angela Stathopoulos. To remove the FRT-stop-FRT cassette, we crossed flies carrying this construct into a line carrying hsFLP on the X chromosome (BS# 8862). To remove the native DV dl gradient, flies carrying the $toll^{10b}$*: bcd 3'UTR* construct were crossed into a gd^{7} background. *dl-paGFP* was injected into the fly line yw; VK33 (landing site: third chromosome 65B2) by Duke University Model Systems, Durham, NC. *dl-dGFP* was inserted on the second chromosome at landing site attP40 by Genetic Services, Inc, Sudbury, MA. The *dl-dVenus* BAC was injected into the fly line yw; VK33 (landing site: third chromosome 65B2) by Genetic Services, Inc, Sudbury, MA.

The plasmid carrying *FRT-stop-FRT hsp83> Toll 10b: bcd 3'UTR* was injected into fly line attP2 with a landing site at (3L) 68A4 by Genetivision, Inc. (Houston, TX). To remove the FRT-stop-FRT cassette, we crossed male flies carrying this construct to virgins carrying hsFLP on both X chromosomes (BS# 8862). Females were allowed to lay embryos for 2-3 days before they were removed to a new vial. Vials containing 3-5 day old larvae (F1 generation) were heat shocked at 37°C for 2 hours. Males with red eyes (F1 generation) were crossed to virgin yw flies. Flies from the F2 generation were crossed to virgin yw flies to create the F3 generation, which was screened for female sterility, used as an indication of removal of the FRT-stop-FRT cassette.

In order to ablate the native DV dl gradient, we generated a gd^7 line null for white. gd^7/*FM3* flies (BS# 3109) were crossed to *yw* and the progeny crossed into stable lines that were screened for white eyes and females that were homozygous sterile. These flies (gd^7w^- /*FM3*) were then crossed to males carrying $toll^{10b}$*: bcd 3'UTR*/+ (weak *bcd* promoter construct on the second chromosome, strong *hsp83* promoter on the third chromosome). Males from this cross with the phenotype gd^7/Y; $toll^{10b}$*: bcd 3'UTR*/+ were crossed again to gd^7w^-/*FM3* virgins, generating females that are homozygous null for *gd* (thus abolishing the wt dl gradient) and provide their embryos with only the AP dl gradient. We screened these females for the absence of bar (present on FM3) and the presence of *white* (present on *toll^{10b}: bcd 3'UTR*).

5.5.2 BAC Recombineering

We followed Protocol 3 of the NCI at Frederick Recombineering website (http://ncifrederick.cancer.gov/research/brb/recombineeringinformation.aspx) to generate dl-paGFP, dl-mGFP, and dl-dVenus in pACMAN (*36*). NEB's proofreading Q5 DNA polymerase was used to amplify sequences at a high level of authenticity. Using a GalK selection protocol (*37*), single amino acid mutations were introduced at residue 206 in previously established BACs (*5*) to generate dl-mGFP (A206K) and dl-dVenus (K206A). Residue 206 in GFP is actually residue 207 in the Venus protein as Venus has a Valine residue after the initial Methionine that is not present in the original GFP protein. For consistency, researchers refer to these residues by their location in GFP. dl-paGFP was created by adding the open reading frame of *paGFP* (Addgene plasmid #11911),(*18*) in frame to the 3' end of the *dl* open reading frame in a dl rescue construct (*5*) in pACMAN (*36*) using a 6x-Gly linker. See **Table 5.1** for a list of primers used.

Table 5.1: List of Primers Used for BAC Recombineering and Sequencing.

Name	Sequence	Notes
dl_galK_F	GCCTCAATTCGGAAGATCTGCAGATATCGAACCTGTCCATATCCACGTAA CCTGTTGACAATTAATCATCGGCA	50 bp homology arms with galK sites
dl_galK_R	CTACTGACTCCTCCGTTCTTGCTCTGCTCTGGTTCGTTGTGAAAAAGGTA TCAGCACTGTCCTGCTCCTT	http://ncifrederick.cancer.gov/Research/Brb/ protocol/Protocol3_SW102_galK_v2.pdf
paGFP_dl_R	CTACTGACTCCTCCGTTCTTGCTCTGCTCTGGTTCGTTGTGAAAAAGGTA ttacttgtacagctcgtcc	50 bp homology arm, paGFP
paGFP_dl_F2	TGCGCCTCAATTCGGAAGATCTGCAGATATCGAACCTGTCCATATCCACG GAAGGAGGCGGTGGGGGT atggtgagcaagggcgagg	50 bp homology arm, 6x gly linker, paGFP specific, no stop codon
GFP_206_galK_F	GCGACGGCCCTGTGCTCCTCCCAGACAACCATTACCTGTCCACCCAGTCT CCTGTTGACAATTAATCATCGGCA	dl-dGFP through codon 205 50 bp homology + galK site
GFP_206_galK_R	AACTCCAGCAGGACCATGTGGTCTCTCTTTTCGTTGGGATCTTTAGACAG TCAGCACTGTCCTGCTCCTT	dl-dGFP start at codon 207 50 bp homology + galK site

Table 5.1 Continued

GFP_A206K_oligo1	GACGGCCCTGTGCTCCTCCCAGACAACCATTACCTGTCCACCCAGTCT AAG CTGTCTAAAGATCCCAACGAAAAGAGAGACCACATGGTCCTGCTGGAGT	K optimal codon is AAG (http://www.biomedcentral.com/content/pdf/1471-2148-7-226.pdf), deleted 2 bp off the front homology arm and 1 off the back so it would be only 100 bp
GFP_A206K_oligo2	ACTCCAGCAGGACCATGTGGTCTCTCTTTTCGTTGGGATCTTTAGACAGCTT AGACTGGGTGGACAGGTAATGGTTGTCTGGGAGGAGCACAGGGCCGTC	reverse complement of oligo1
GFP_A206K_seq	CACAACATTGAGGATGGATCCG	sequencing primer for GFP A206K start at 591 in GFP-frt-kan-frt
dl_3'_seq	CAACGCTCAGCAATCTGCTT	sequencing primer for 3' end of dorsal start at 15591 of dorsal-rescue
dl_mid_seq	GTTGCTCCAGTTCTCGTACC	dorsal reverse mid for sequencing
ven_K206A_seq	AAG ATC CGC CAC AAC ATC G	sequencing for K206A in dl venus
ven_galK_F	GCGACGGCCCCGTGCTGCTGCCCGACAACCACTACCTGAGCTACCAGTCC CCTGTTGACAATTAATCATCGGCA	venus through codon 205 (206?) 50 bp homology + galK site

Table 5.1 Continued

ven_galK_R	AACTCCAGCAGGACCATGTGATCGCGCTTCTCGTTGGGGTCTTTGCTCAG TCAGCACTGTCCTGCTCCTT	venus after codon 206 (207?) 50 bp homology + galK
dl_ven_K206A_oligo1	GACGGCCCCGTGCTGCTGCCCGACAACCACTACCTGAGCTACCAGTCCGC CCTGAGCAAAGACCCCAACGAGAAGCGCGATCACATGGTCCTGCTGGAG T	A optimal codon is GCC (http://www.biomedcentral.com/content/pdf/1471-2148-7-226.pdf), deleted 2 bp off front homology arm and 1 off back so it would be only 100 bp
dl_ven_K206A_oligo2	ACTCCAGCAGGACCATGTGATCGCGCTTCTCGTTGGGGTCTTTGCTCAGG GCGGACTGGTAGCTCAGGTAGTGGTTGTCGGGCAGCAGCACGGGGCCG TC	reverse compliment of oligo 1
dl_tot_F	TTAAATCAGACGGCACTGGCT	for sequencing dl, blast pair 8
dl_tot_R	AACAATCATTTAGACGACGACCA	for sequencing dl, blast pair 8
dl_seq1	GCCACTTGTCAGAGATCAAC	starts at 391
dl_seq2	CCGTGTGGATCCGTTTAAG	starts at 1110
dl_seq3	CGCCAACGATTGAGGTTATC	starts at 1835
dl_seq4	TGGAGGATAGCTTCGATGAC	starts at 2588

Table 5.1 Continued

dl_seq5	CCTACCTGAATGCTGATGTG	starts at 3308
dl_seq6	GGGTCAAACCCAATGATTTG	starts at 4040
dl_seq7	CTACTCGTTTACATGCGAAG	starts at 4789
dl_seq8	CTTTGGGCTTTCTTATCGGG	starts at 5531
dl_seq9	CATGAAACCTTCCATCTTGCAGC	starts at 6188
hsp83_seq	AGTGGGCTTTGCTCAATCG	for sequencing bcd>Toll 10b plasmids beginning near hsp83 promoter

5.5.3 Fluorescent in situ Hybridization

All embryos were aged to 2-4 hours, except for “young” yw embryos, which were aged to 0-2 hours, then fixed in 37% formaldehyde according to standard protocols (*38*). A combination fluorescent *in situ* hybridization/fluorescent immnuostaining was performed according to standard protocols (*38*). Briefly, fixed embryos were washed in Tween/PBS buffer, then hybridized at 55 ^{o}C overnight with anti-sense *sna*-biotin or *sna*-fluorescin RNA probes, which were generated according to the standard protocol. The embryos were then washed and incubated with primary antibodies at 4 ^{o}C overnight. Next, the embryos were washed and incubated for 1-2 hrs with fluorescent secondary antibodies at room temperature. The embryos were then washed and stored in 70% glycerol at -20 ^{o}C. Embryos were imaged within one month of completing the protocol.

Antibodies used were anti-dorsal 7A4 (deposited to the DSHB by Ruth Steward (DSHB Hybridoma Product anti-dorsal 7A4)) (1:10), donkey anti-mouse- 488 (Invitrogen A21202, Lot 81493) (1:500), rabbit anti-histone (abcam ab1791, Lot 940487) (1:5000), donkey anti-rabbit-546 (Invitrogen A10040, Lot 107388) (1:500), goat anti-biotin (ImmunoReagents, Raleigh, NC, GtxOt-070-D, Lot 19-19-112311) (1:50,000), donkey anti-goat-647 (Invitrogen A21447, Lot 774898) ((1:500), goat anti-fluorescin (Rockland 600-101-096, Lot 19458) (1:500), rabbit anti-fluorescin (Life Technologies A889, Lot 1458646) (1:500), goat anti-histone (Abcam, ab12079, Lots GR6952-4 and GR129411-1) (1:100).

5.5.4 Mounting and Imaging of Fixed Samples

Embryos were cross sectioned and mounted in 70% glycerol as described previously (*39*). Briefly, a razor blade was used to remove the anterior and posterior thirds of the embryo, leaving a cross section roughly 200 µm long by 200 µm in diameter. These sections were then oriented such that the cut sides became the top and bottom. They were then imaged at 20x on a Zeiss LSM 710 microscope. 15 z-slices 1.5 µm apart were analyzed. Embryos with an AP Dorsal gradient were mounted laterally in 70% glycerol using one piece of double-sided tape (weak *bicoid* promoter) or two pieces of double-sided tape (strong *hsp83* promoter). Images were taken at 2.5 µm intervals from just above the top of the embryo to the depth at which the embryo reached maximal size in the xy plane, which was assumed to be the midsagittal section. Stacks ranged from 15-25 slices.

5.5.5 Data Analysis

Images of embryo cross sections were analyzed using previously derived code (*28*). Briefly, the border of the embryo was found computationally, then the nuclei were segmented using a local thresholding protocol. The intensity of dl in each segmented nucleus was calculated as the ratio between the intensity in the dl channel divided by the intensity in the nuclear channel. The intensity of mRNA expression was calculated as average intensity within an annulus roughly 18 µm wide around the perimeter of the embryo. A description of the image analysis of whole mount embryos can be found in the Supplemental Experimental Procedures.

All dl gradients were fit to a Gaussian, and these fits were used to determine the width parameter, σ. Normalized intensity plots were generated by fitting each embryo's data to its own Gaussian by subtracting the B value and 70% of the M value, then dividing by the A value. ($X = (x - B - 0.7M)/A)$). The average normalized intensity plot was generated by averaging the plots of all embryos in the specified genotype.

Statistical significance was calculated using two-tailed homoscedastic t-tests.

5.5.6 Activating paGFP in Live Embryos

Embryos were dechorionated by hand or for 30 s in 100% bleach. They were then mounted laterally on a slide coated with heptane glue. Deionized water was used as a mounting medium. Two pieces of double-sided tape were used to attach the coverslip. Images were taken using a 40x water immersion objective on an LSM 710 confocal microscope. Activation box: 9000 pixels (300 microns x 30 microns), number of activation passes: 10, rest time: 15 s, number of cycles: 40, laser power: 3% for embryo activated near ventral midline, 2.5% for embryo activated near dorsal midline. A 405 nm laser was used for activation and a 488 nm laser was used for excitation of the activated GFP.

5.5.7 Sequencing $dl^{1.2.5}$

Genomic DNA was extracted from males homozygous for $dl^{1.2.5}$ according to standard lab protocol. We PCR amplified the entire dl region, then used 9 different primers to ensure complete sequencing coverage. Sequencing was performed by GENEWIZ, RTP, NC. The resulting sequence was compared to the consensus sequence available at FlyBase. Each mismatched codon was investigated as a potential source of an altered or truncated sequence. We found that a mutation at nt 3256 (entire dl genomic sequence) from G->T results in a premature stop codon, which we presume is the source of the amorphic allele.

5.5.8 Image analysis of toll^{10b}: bcd 3'UTR embryos

The Dorsal gradient and *snail* expression in embryos from mothers carrying the *toll^{10b}: bcd 3'UTR* transgene and homozygous for the *gd^7* mutation were analyzed using the following procedures. First, the z-stack images (taken as described in Experimental Procedures) were background subtracted assuming the mode of the image corresponded to zero fluorescence levels. Next, a maximum intensity projection was created, and the intensities from the three color channels (dl, histone h3, and *snail*) were summed. The resulting image was Gaussian filtered in both the x and y directions using ten pixels as a kernel. This created an image I1 with the embryo as a single, bright object to facilitate discovery of the embryo boundary.

Next, the approximate center of the embryo was found by thresholding I1 using the graythresh algorithm in Matlab to create a single binary object. The first approximation of the boundary of the embryo was found by previously published methods (*6*,*28*). Briefly, we divided the image into 60 slices centered at the approximate center. The average intensity of each slice, as a function of the distance from the approximate center of the embryo, was found. The boundary within that slice was taken to be the location where the intensity dropped to 10% of the maximum value within that slice.

This approximate boundary defined a 60-point polygon, and the ellipse with the same first and second moments as the solid fill of that polygon was computed. The two foci of that ellipse then served as points about which the image I1 could be divided into four regions: two rectangular regions that each have one side as the line segment between the foci, and the other two rectangular regions as the remaining parts of the image.

In the first two regions, the boundary of the embryo was found by dividing the regions into 15 smaller rectangles (rather than slices as described above). This corresponded to the trunk region of the embryo. In the second two regions, the boundary was found by dividing the regions up into 15 slices centered at the ellipse focus.

Once this updated boundary was found, an inner boundary was constructed by moving the 60 updated boundary points inward by 30 pixels in the direction of the local normal. This defined 60 quadrilaterals that encompass the outer periphery of the embryo. These quadrilaterals were laid on top of the image slice corresponding to the mid sagittal plane of the embryo, and each of the three color channels were unrolled using a affine transformation on the 60 quadrilaterals to result in 60 rectangles (see (*6*,*28*) for more information). The nuclear channel was then segmented using a local thresholding (*28*). The Dorsal intensity in each nucleus was then computed as the intensity in the Dorsal channel, normalized by the intensity in the nuclear channel. The intensity of *sna* expression was found as the average intensity of the *sna* channel within this unrolled strip loosely bounded by the nuclei.

5.6 Acknowledgments

Thanks to Angela Stathopoulos and Leslie Dunipace for provision of dl-dGFP and dl-mVenus flies and BACs, *bcd> toll*^{10b}*: bcd 3' UTR* flies, and the DNA used to generate *hsp83> toll*^{10b}*: bcd 3' UTR*flies. Thanks to ImmunoReagents for providing their goat ant-biotin antibody. We are greatful to Alex Thomas for generating the *sna*-biotin probe. Thanks to Parv Gondalia for generating the *sna*-fitc probe. Thanks to David Stein for providing the cact-lacZ fly line. We are grateful to Shubba Govind for providing the dl-lacZ flies. During this work, SNC and GTR (partially) were supported by a CAREER award funded by the United States National Science Foundation (www.nsf.gov), grant number CBET-1254344; MDO was supported by a Graduate Assistance in Areas of National Need Fellowship in Computational Science from the United States Department of Education (www.ed.gov), grant number P200A120047.

5.7 References

(1) Reeves, G. T.; Stathopoulos, A. Graded Dorsal and Differential Gene Regulation in the Drosophila Embryo. *Cold Spring Harb. Perspect. Biol.* **2009**, *1* (4), a000836.

(2) Moussian, B.; Roth, S. Dorsoventral Axis Formation in the Drosophila Embryo--Shaping and Transducing a Morphogen Gradient. *Curr. Biol.* **2005**, *15* (21), R887–R899.

(3) Roth, S.; Stein, D.; Nüsslein-Volhard, C. A Gradient of Nuclear Localization of the Dorsal Protein Determines Dorsoventral Pattern in the Drosophila Embryo. *Cell* **1989**, *59* (6), 1189–1202.

(4) Goto, S.; Morigaki, R.; Okita, S.; Nagahiro, S.; Kaji, R. Development of a Highly Sensitive Immunohistochemical Method to Detect Neurochemical Molecules in Formalin-Fixed and Paraffin-Embedded Tissues from Autopsied Human Brains. *Front. Neuroanat.* **2015**, *9*, 22.

(5) Reeves, G. T.; Trisnadi, N.; Truong, T. V; Nahmad, M.; Katz, S.; Stathopoulos, A. Dorsal-Ventral Gene Expression in the Drosophila Embryo Reflects the Dynamics and Precision of the Dorsal Nuclear Gradient. *Dev. Cell* **2012**, *22* (3), 544–557.

(6) Liberman, L. M.; Reeves, G. T.; Stathopoulos, A. Quantitative Imaging of the Dorsal Nuclear Gradient Reveals Limitations to Threshold-Dependent Patterning in Drosophila. *Proc. Natl. Acad. Sci. U. S. A.* **2009**, *106* (52), 22317–22322.

(7) Roth, S.; Schüpbach, T. The Relationship between Ovarian and Embryonic Dorsoventral Patterning in Drosophila. *Development* **1994**, *120* (8), 2245–2257.

(8) Huang, A. M.; Rusch, J.; Levine, M. An Anteroposterior Dorsal Gradient in the Drosophila Embryo. *Genes Dev.* **1997**, *11*, 1963–1973.

(9) Eldar, A.; Dorfman, R.; Weiss, D.; Ashe, H.; Shilo, B.; Barkai, N. Robustness of the BMP Morphogen Gradient in Drosophila Embryonic Patterning. *Nature* **2002**, *419* (19 September 2002), 304–308.

(10) Mizutani, C. M.; Nie, Q.; Wan, F. Y. M.; Zhang, Y. T.; Vilmos, P.; Sousa-Neves, R.; Bier, E.; Marsh, J. L.; Lander, A. D. Formation of the BMP Activity Gradient in the Drosophila Embryo. *Dev. Cell* **2005**, *8* (6), 915–924.

(11) Ben-Zvi, D.; Shilo, B.-Z.; Fainsod, A.; Barkai, N. Scaling of the BMP Activation Gradient in Xenopus Embryos. *Nature* **2008**, *453* (7199), 1205–1211.

(12) Marqués, G.; Musacchio, M.; Shimell, M. J.; Wünnenberg-Stapleton, K.; Cho, K. W. .; O'Connor, M. B. Production of a DPP Activity Gradient in the Early Drosophila Embryo through the Opposing Actions of the SOG and TLD Proteins. *Cell* **1997**, *91* (3), 417–426.

(13) Shimmi, O.; Umulis, D.; Othmer, H.; O'Connor, M. B. Facilitated Transport of a Dpp/Scw Heterodimer by Sog/Tsg Leads to Robust Patterning of the Drosophila Blastoderm Embryo. *Cell* **2005**, *120* (3), 873–886.

(14) Haskel-Ittah, M.; Ben-Zvi, D.; Branski-Arieli, M.; Schejter, E. D.; Shilo, B. Z.; Barkai, N. Self-Organized Shuttling: Generating Sharp Dorsoventral Polarity in the Early Drosophila Embryo. *Cell* **2012**, *150* (5), 1016–1028.

(15) Shilo, B.-Z.; Haskel-Ittah, M.; Ben-Zvi, D.; Schejter, E. D.; Barkai, N. Creating Gradients by Morphogen Shuttling. *Trends Genet.* **2013**, *29* (6), 339–347.

(16) Kanodia, J. S.; Rikhy, R.; Kim, Y.; Lund, V. K.; DeLotto, R.; Lippincott-Schwartz, J.; Shvartsman, S. Y. Dynamics of the Dorsal Morphogen Gradient. *Proc. Natl. Acad. Sci. U. S. A.* **2009**, *106* (51), 21707–21712.

(17) Carrell, S. N.; O'Connell, M. D.; Allen, A. E.; Smith, S. M.; Reeves, G. A Facilitated Diffusion Mechanism Establishes the Drosophila Dorsal Gradient. *bioRxiv* **2016**.

(18) Patterson, G. H.; Lippincott-Schwartz, J. A Photoactivatable GFP for Selective Photolabeling of Proteins and Cells. *Science* **2002**, *297* (5588), 1873–1877.

(19) O'Connell, M. D.; Reeves, G. T. The Presence of Nuclear Cactus in the Early Drosophila Embryo May Extend the Dynamic Range of the Dorsal Gradient. *PLOS Comput. Biol.* **2015**, *11* (4), e1004159.

(20) DeLotto, R.; DeLotto, Y.; Steward, R.; Lippincott-Schwartz, J. Nucleocytoplasmic Shuttling Mediates the Dynamic Maintenance of Nuclear Dorsal Levels during Drosophila Embryogenesis. *Development* **2007**, *134* (23), 4233–4241.

(21) Zacharias, D. a; Violin, J. D.; Newton, A. C.; Tsien, R. Y. Partitioning of Lipid-Modified Monomeric GFPs into Membrane Microdomains of Live Cells. *Science* **2002**, *296* (5569), 913–916.

(22) Govind, S.; Whalen, A. M.; Steward, R. In Vivo Self-Association of the Drosophila Rel-Protein Dorsal. *Proc. Natl. Acad. Sci. U. S. A.* **1992**, *89* (17), 7861–7865.

(23) Govind, S.; Drier, E.; Huang, L. H.; Steward, R.; Steward, R. Regulated Nuclear Import of the Drosophila Rel Protein Dorsal: Structure-Function Analysis. *Mol. Cell. Biol.* **1996**, *16* (3).

(24) Fernandez, N. Q.; Grosshans, J.; Goltz, J. S.; Stein, D. Separable and Redundant Regulatory Determinants in Cactus Mediate Its Dorsal Group Dependent Degradation. *Development* **2001**, *128*, 2963–2974.

(25) Sen, J.; Goltz, J. S.; Stevens, L.; Stein, D. Spatially Restricted Expression of Pipe in the Drosophila Egg Chamber Defines Embryonic Dorsal–Ventral Polarity. *Cell* **1998**, *95* (4), 471–481.

(26) Schüpbach, T. Germ Line and Soma Cooperate during Oogenesis to Establish the Dorsoventral Pattern of Egg Shell and Embryo in Drosophila Melanogaster. *Cell* **1987**, *49* (5), 699–707.

(27) Meinhardt, H. Different Strategies for Midline Formation in Bilaterians. *Group* **2004**, *5* (June), 502–510.

(28) Trisnadi, N.; Altinok, A.; Stathopoulos, A.; Reeves, G. T. Image Analysis and Empirical Modeling of Gene and Protein Expression. *Methods* **2013**, *62* (1), 68–78.

(29) Mavrakis, M.; Rikhy, R.; Lippincott-Schwartz, J. Plasma Membrane Polarity and Compartmentalization Are Established before Cellularization in the Fly Embryo. *Dev. Cell* **2009**, *16* (1), 93–104.

(30) Garcia, M.; Nahmad, M.; Reeves, G. T.; Stathopoulos, A. Size-Dependent Regulation of Dorsal–ventral Patterning in the Early Drosophila Embryo. *Dev. Biol.* **2013**, *381* (1), 286–299.

(31) Umulis, D. M.; Serpe, M.; O'Connor, M. B.; Othmer, H. G. Robust, Bistable Patterning of the Dorsal Surface of the Drosophila Embryo. *Proc. Natl. Acad. Sci. U. S. A.* **2006**, *103* (31), 11613–11618.

(32) Ashe, H. L.; Levine, M. Local Inhibition and Long-Range Enhancement of Dpp Signal Transduction by Sog. *Nature* **1999**, *398* (6726), 427–431.

(33) Wang, Y.; Ferguson, E. L. Spatial Bistability of Dpp – Receptor Interactions during Drosophila Dorsal – Ventral Patterning. **2005**, *702* (December 2004), 601–604.

(34) Holley, S. A.; Neul, J. L.; Attisano, L.; Wrana, J. L.; Sasai, Y.; O'Connor, M. B.; De Robertis, E. M.; Ferguson, E. L. The Xenopus Dorsalizing Factor Noggin Ventralizes Drosophila Embryos by Preventing DPP from Activating Its Receptor. *Cell* **1996**, *86* (4), 607–617.

(35) Dorfman, R.; Shilo, B. Z. Biphasic Activation of the BMP Pathway Patterns the Drosophila Embryonic Dorsal Region. *Development* **2001**, *128* (6), 965–972.

(36) Venken, K. J. T.; He, Y.; Hoskins, R. a; Bellen, H. J. P[acman]: A BAC Transgenic Platform for Targeted Insertion of Large DNA Fragments in D. Melanogaster. *Science* **2006**, *314* (November), 1747–1751.

(37) Warming, S.; Costantino, N.; Court, D. L.; Jenkins, N. a.; Copeland, N. G. Simple and Highly Efficient BAC Recombineering Using galK Selection. *Nucleic Acids Res.* **2005**, *33* (4), 1–12.

(38) Kosman, D.; Mizutani, C. M.; Lemons, D.; Cox, W. G.; McGinnis, W.; Bier, E. Multiplex Detection of RNA Expression in Drosophila Embryos. *Science* **2004**, *305* (5685), 846.

(39) Carrell, S. N.; Reeves, G. T. Imaging the Dorsal-Ventral Axis of Live and Fixed Drosophila Melanogaster Embryos. In *Tissue Morphogenesis*; Nelson, C. M., Ed.; Methods in Molecular Biology; Springer New York: New York, NY, 2015; Vol. 1189, pp 63–78.

6 Conclusions and Future Work

6.1 Chapter 3: Effects of Dorsal and Cactus Dosage on the Dorsal Nuclear Gradient

While the downstream effects of the Dorsal gradient (patterning and tissue differentiation) are well understood, less is known about regulation of the gradient itself. By manipulating the maternal dose of *dl* and *cact*, we aimed to shed light on this important unanswered question. Using hypomorphic alleles and rescue constructs, we looked at embryos with 1 - 4 copies of the genes of interest. It would be beneficial to investigate *cactus* as thoroughly as we did *dorsal*; therefore, future researchers should investigate embryos from mothers with mixtures of endogenous and exogenous *cactus*. Additionally, we are curious to know what happens when levels of *cactus* and *dorsal* are manipulated simultaneously. Using a double-mutant (*1*), researchers could tackle this experiment.

Our results from dl heterozygotes confirmed those seen by previous researchers; essentially, the Dorsal gradient in these embryos is both shorter and wider than wild type, with a flat top instead of a sharply graded peak. Under our current analysis method, we find that the width of this gradient is significantly expanded; however, our metrics may not apply to the heterozygous gradient as it no longer resembles a Gaussian. Therefore, researchers should devise a new method of modeling the Dorsal gradient in instances when it no longer resembles the wild type in shape.

Embryos from mothers with one exogenous and one endogenous (two total) copies of Dorsal had gradients indistinguishable from wild type, while those with only two exogenous copies had wider gradients. With a sample number of 4, this finding may not be biologically relevant and the experiment should be repeated. Embryos with 3 or 4 copies of Dorsal also had wider gradients.

Similar to the *dl* heterozygotes, one of the *cact* heterozygotes (*cact*^{4}) had a wider gradient than wild type. The other allele had no statistical difference (as defined by $p<0.05$) in width from the wild type. However, the other metrics we investigated matched what was seen in the *cact*^{1} mutants, so we do not find this difference to be significant. With one exception, all gene borders followed the Dorsal gradient as expected; that is, a wider gradient let to dorsally shifted borders and a narrower one to ventrally shifted borders. The exception occurs in embryos from mothers with four copies of *cactus*; instead of shifting ventrally, the ventral *sog* border shifts dorsally. Further experiments should be conducted to determine the precise cause of this discrepancy; is it due to a dorsally expanded *sna* domain or another mechanism entirely?

Because we do not understand the exact feedback mechanisms that regulate the Dorsal gradient when the maternal doses of *dorsal* and *cactus* are varied, it would be beneficial to conduct several experiments to narrow down the potential contenders. First, we would like to use intronic *cactus* probes to determine whether zygotic *cactus* is regulated by Dorsal. Previous researchers have developed these probes and determined that they function in the early embryo (Alistair Boettiger, personal communication); therefore, this experiment makes an excellent starting point.

Due to the variance between experiments and researchers, it would be beneficial to repeat some of the fluorescent *in situ* hybridization (FISH) experiments presented to ensure as many variables are controlled as possible by staining all genotypes simultaneously. For the genotypes that only had *sog* data, it would be advisable to stain for *sna* to ensure that the conclusions drawn from the ventral border of *sog* indeed match the effect on the *sna* domain.

Finally, researchers should investigate the assumptions that mRNA levels and/or protein levels are compromised in heterozygotes and that they are raised when exogenous copies are added. Previous qPCR results have been inconclusive, so future researchers should generate new primers to conduct more careful and controlled experiments. Western blot experiments have been unsuccessful as well due to a lack of antibodies that function well in the assay; however, if researchers generated new antibodies that had high specificity and worked on a blot, they could use the results to quantify and compare the levels of protein between genotypes.

6.2 Chapter 4: Novel Interactions Between NF-kB and BMP Signaling Pathways in the Early *Drosophila* Embryo

Using the Gal4/UAS system, we were able to investigate the effects of changed BMP signaling on the Dorsal gradient. When BMP signaling was increased due to overexpression of MAD and Medea or expression of a constitutively active Thickveins receptor, we found that the Dorsal gradient widened, perhaps as the result of a mechanism to ensure proper scaling. When we downregulated BMP signaling using a dominant negative from of the Thickveins receptor, we also found that the Dorsal gradient widened. We propose that this effect is the result of Dorsal taking up the empty space left as the BMP signaling recedes. More experiments must be done to verify these hypotheses or develop new ones.

Our results clearly show that there is interplay between the Dorsal and BMP signaling pathways in the developing embryo. However, we have not been able to decisively determine what factors act in these proposed feedback loops. One possibility is Cactus, the inhibitory factor that prevents Dorsal from entering the nuclei. Previous research has shown that *cact* is downstream of BMP signaling at this stage (*2*). In order to determine whether or not Cactus is involved in the feedback between the two pathways, several experiments should be conducted. First, researchers should repeat the experiments presented here using a different maternal driver, nos-gal4. This driver is not as “leaky” as matα-gal4 and is likely to drive higher expression of UAS-linked genes. Results from other researchers in our lab have shown that GFP-linked transgenes which do not fluoresce using the matα-gal4 driver do so when expressed with nos-gal4. We would expect to see more pronounced phenotypic differences in these embryos. Second, researchers should use *cactus* intronic probes to determine whether or not the expression of *cact* varies when BMP signaling is changed. These results would be bolstered by using qPCR to quantify the differences. If these results are promising, researchers could use a quantitative Western blot to determine if the protein concentration changes with the RNA concentration.

6.3 Chapter 5: A Facilitated Diffusion Mechanism Establishes the *Drosophila* Dorsal Gradient

While the downstream effects of Dorsal signaling have been well documented, less is known about the global gradient formation. We proposed a mechanism by which the inhibitory factor Cactus shuttles Dorsal to the ventral midline, where Toll signaling acts as a sink. First, we dispelled the myth that there is a counter gradient of free Dorsal present in the cytoplasm, leading us to ask how Dorsal could collect at the ventral midline when Fickian diffusion states that it should diffuse outwards and away. This question brought us to the idea of shuttling, by which a carrier essentially causes a molecule to diffuse against its own concentration gradient. Through experiments with fluorescently-tagged Dorsal, we found that increased protein size widened the Dorsal gradient when Fickian diffusion would indicate a narrowing. We could exacerbate this effect by using GFP, which forms weak dimers. We also expanded the domain of Toll signaling, leading to a double peak of nuclear Dorsal. Again, this phenomenon seems contrary to what would be expected in a simple diffusion model; however, in the context of a shuttling model, it can be explained. Essentially, the dl/Cact complex sink is so expanded that free Dorsal never makes it all the way to the ventral midline, leading to two areas of accumulation instead of one. Finally, we expressed an ectopic anteroposterior gradient of Dorsal in both wild type and *dorsal* null backgrounds. In the first instance, we found a gap in the Dorsal gradient at the intersection of the two gradients, which would be expected in the case of competing sinks. This effect was borne out when the high-threshold target gene *sna* was analyzed. In the latter instance, we found that a wide anterior domain of Toll signaling led to the same double peak phenomenon seen when the Toll gradient expanded along the ventral midline. We concluded that our proposed shuttling mechanism explains several hitherto inexplicable phenomena in a simple, straightforward manner.

While the experiments already conducted prove the existence of a previously unknown shuttling mechanism working to form the Dorsal nuclear gradient, further work should be done to differentiate whether our mechanism alone is responsible for the results we have obtained, or whether an additional upstream shuttling mechanism also functions, such as the one proposed to regulate Toll signaling via Spz cleavage (*3*). Work has already been conducted to model our shuttling mechanism (*4*), but further modeling results, particularly looking at the experimental perturbations, would bolster our results. Furthermore, it would be useful to understand what happens in embryos from mothers carrying two amorphic *cact* alleles. These embryos would have a very small amount of maternal *cactus* supplied; however, there would not be enough to enable a wild type Dorsal gradient to form. In a non-shuttling model, these embryos would have high Dorsal nuclear concentration everywhere, as Cactus would not be able to prevent it from entering the nuclei. This effect could be confirmed by staining for a high-threshold gene such as *sna* and finding it expressed ubiquitously. However, in a shuttling mechanism, we would expect even a small amount of Cactus to allow accumulation of Dorsal at the ventral midline, which would theoretically cause a depletion at the dorsal midline, preventing *sna* expression there.

Additionally, we would like to investigate the effect of a decreased *cactus* dose on the diffusion of Dorsal in live embryos by using the already-generated photoactivatable GFP (paGFP). We would first need to develop a method for carefully determining the diffusion coefficient from fluorescent data. Once we can calculate the diffusion, we could compare the diffusion of Dorsal in wild type embryos to that in *cactus* heterozygotes. With less cactus, we would expect diffusion toward the ventral midline to slow. With the results from **Chapter 3** that show a widened Dorsal gradient in *cact* heterozygotes, we expect this hypothesis to be confirmed in live embryos.

6.4 References

(1) Roth, S.; Hiromi, Y.; Godt, D.; Nüsslein-Volhard, C. Cactus, a Maternal Gene Required for Proper Formation of the Dorsoventral Morphogen Gradient in Drosophila Embryos. *Development* **1991**, *112* (2), 371–388.

(2) Fontenele, M.; Carneiro, K.; Agrellos, R.; Oliveira, D.; Oliveira-Silva, A.; Vieira, V.; Negreiros, E.; Machado, E.; Araujo, H. The Ca2+-Dependent Protease Calpain A Regulates Cactus/IκB Levels during Drosophila Development in Response to Maternal Dpp Signals. *Mech. Dev.* **2009**, *126* (8-9), 737–751.

(3) Haskel-Ittah, M.; Ben-Zvi, D.; Branski-Arieli, M.; Schejter, E. D.; Shilo, B. Z.; Barkai, N. Self-Organized Shuttling: Generating Sharp Dorsoventral Polarity in the Early Drosophila Embryo. *Cell* **2012**, *150* (5), 1016–1028.

(4) Carrell, S. N.; O'Connell, M. D.; Allen, A. E.; Smith, S. M.; Reeves, G. A Facilitated Diffusion Mechanism Establishes the Drosophila Dorsal Gradient. *bioRxiv* **2016**.